THE UNIVERSITY of EDINBURGH

Investigating the role of protein stability on eEF1A2 function

Alejandra Fernández Álvarez

MScR Genomics and Experimental Medicine

University of Edinburgh

2022

Declaration

I declare that this thesis is my own work unless stated otherwise and any inclusions of contributions or publications from others have been clearly acknowledged. This thesis has not been submitted for any other degree or professional qualification.

Alejandra Fernández Álvarez

Acknowledgements

I would like to thank my supervisor Cathy Abbott for all the help and support I've received throughout my master's. I could not have asked for a better supervisor, and I've learned so much in such a short amount of time. I'd also like to thank Cavan, Heather, Grant, and Faith at the Abbott lab for teaching me essential lab skills and answering my endless questions. I would not have been able to progress without all your help!

To my friends and family, I thank you for your patience and support, and I would especially like to thank my partner Diego for his patience, kindness, and support since the day we met.

Contents:

Abstract

Spontaneous missense mutations, whereby a single nucleotide results in amino acid substitution, affect the normal functioning of the eukaryotic translation elongation factor eEF1A2. These mutations have varying disease severity causing neurodevelopmental disorders in children, including autism, intellectual disability, and epilepsy. Mutations D252H and E122K, located in binding hotspots of eEF1A2, have differing eEF1A2 expression levels across different tissues in mouse models. This thesis aims to compare the effect of D252H and E122K mutations on eEF1A2 protein stability and how differences in disease severity and tissue-specific expression arise by investigating eEF1A2 expression and changes in the interactome resulting from mutations. Molecular biology techniques, such as western blotting, conducted on mouse tissue and mutant transfected HEK293T cells were conducted to determine the expression levels of D252H.eEF1A2 and E122K.eEF1A2 mutants compared to wildtype. Moreover, co-immunoprecipitation and mass spectrometry was conducted to identify and compare the molecular binding partners of eEF1A2 mutants and revealed that proteins involved in translation were downregulated in D252H and E122K eEF1A2 mutants. Mass spectrometry was also performed in mouse brain tissue to conduct a differential expression analysis of the brain proteome, which found translation and ribosomal proteins' expression was significantly affected in E122K mutants.

In conclusion, D252H and E122K mutations result in differing expression patterns of eEF1A2 across mouse tissues and an altered eEF1A2 interactome. The E122K.eEF1A2 mouse brain proteomic analysis suggested reduced translation efficiency is one of the major biological processes affected. Therefore, mutations could be targeted by identifying and grouping altered proteins to their common functions and molecular pathways.

Lay summary

A protein called eEF1A2 is an essential molecule that functions in protein production and is needed for survival. Mutations in eEF1A2 cause disorders in children, such as autism, epilepsy, and intellectual disability. The children affected show varying degrees of disease severity, and it is currently unknown why this happens. This research project aims to identify how the mutations, known as E122K and D252H, affect eEF1A2 function. Molecular biology experiments were conducted and found different levels of mutant eEF1A2 abundance across different mouse tissues, such as the brain and heart. This indicated that there may be a specific interaction between the different mutations and tissue environment. As a result, more experiments were performed in a human cell model to look at all the interactions between mutant eEF1A2 and other proteins found in the cell's environment. The results found altered interactions between mutant eEF1A2, and other proteins involved in protein production, suggesting that mutations affect eEF1A2's interactions with its environment. Another experiment identified which proteins in the mutant E122K mouse brain showed significant differences in protein abundance. Several proteins involved in protein production had reduced abundance, whereas other structural proteins showed increased abundance. By grouping affected proteins with similar functions, research may be able to better target and treat the most affected proteins caused by mutations.

List of abbreviations

aa-tRNA	Amino acetylated transfer ribonucleic acid
AMP	Ampicilllin
AP-MS	Affinity Purified Mass Spectrometry
ANOVA	Analysis of variance
ASD	Autism spectrum disorder
CMV	Cytomegalovirus promoter
CNS	Central nervous system
dH$_2$O	Distilled water
DMSO	Dimethyl sulfoxide
DNA	Deoxyribonucleic acid
DTT	Dithiothreitol
EDTA	Ethylenediaminetetraacetic acid
EEF1A2	Eukaryotic elongation factor 1A2 (human gene)
eEF1A2	Eukaryotic elongation factor 1A2 (protein)
Eef1a2	Eukaryotic elongation factor 1A2 (mouse gene)
EEF1A1	Eukaryotic elongation factor 1A1 (human gene)
eEF1A1	Eukaryotic elongation factor 1A1 (protein)
eEF1A	Eukaryotic elongation factor 1A (protein)
FCS	Fetal calf serum
GDP	Guanine diphosphate
GEF	Guanosine exchange factor
GO	Gene Ontology

GTP	Guanine triphosphate
HEK293T	Human embryonic kidney 293 cells with large-T antigen
kDa	Kilodalton
KO	Knockdown
LC-MS/MS	Liquid chromatography tandem mass spectrometry
mRNA	Messenger ribonucleic acid
mTOR	Mammalian target of rapamycin
PNC	Perinucleolar compartment
PTM	Post-translation modification
qPCR	Quantitative polymerase chain reaction
Q-Q	Quantile-Quantile
RIPA	Radioimmunoprecipitation assay buffer
RNA	Ribonucleic acid
RT	Room temperature
SDS	Sodium dodecyl sulfate
TBS	Tris buffered saline
TBS-T	Tris buffered saline plus TWEEN 20
TEMED	Tetramethylethylenediamine
TPS	Total protein stain
Tris	Tris(hydroxymethyl)aminomethane
ValRS	Valyl-tRNA synthetase
Wst	Wasted
WT	Wild-type

Chapter 1: Introduction

1.1 The role of eEF1A in translation

Eukaryotic elongation factor 1A (eEF1A) functions in the delivery of amino acetylated tRNAs (aa-tRNAs) to the A-site of the 80S ribosome during the elongation phase and has two independently encoded isoforms, eEF1A1 and eEF1A2, that are 92% identical (Soares et al., 2009). The delivery of acetylated tRNAs is a GTP dependent process, whereby eEF1A is initially bound to GDP and then exchanged to GTP when bound to the guanosine exchange factor (GEF) eEF1B complex, forming a ternary complex. Both eEF1A isoforms have different binding affinities for GDP and GTP, with eEF1A2 exhibiting a higher affinity for GDP whereas eEF1A1 has a higher affinity for GTP (Kahns et al., 1998). The eEF1B complex consists of the subunits eEF1B, eEF1D, and eEF1G, also known as eEF1Bα, eEF1Bβ, and eEF1Bγ, respectively. The subunits assemble into a complex by eEF1G binding to eEF1D, which forms a stable homotrimer, and both eEF1D and eEF1B have GEF activity (Bondarchuk et al., 2022). The eEF1B and aa-tRNA binding sites overlap and compete for eEF1A binding, but the function of the eEF1D homotrimer is unknown (Andersen et al., 2001). It's been suggested that these two subunits have GEF activity because they might have differing functions when the enzyme valyl-tRNA synthetase (ValRS) is bound to the eEF1B complex, as ValRS has been found to interact with eEF1D (Bec et al., 1994). The eEF1B-ValRS complex catalyzes the amino acylation of tRNAs, and the ValRS enzymatic activity is only activated when eEF1A is bound to GTP. Once eEF1A-GTP bound to aa-tRNA reaches the A-site of the 80S ribosome, a codon-anticodon match elongates the polypeptide chain and releases the deacetylated tRNA. The eEF1A-GTP is recycled back to eEF1A-GDP via hydrolysis and exits the ribosome (*Figure 1*).
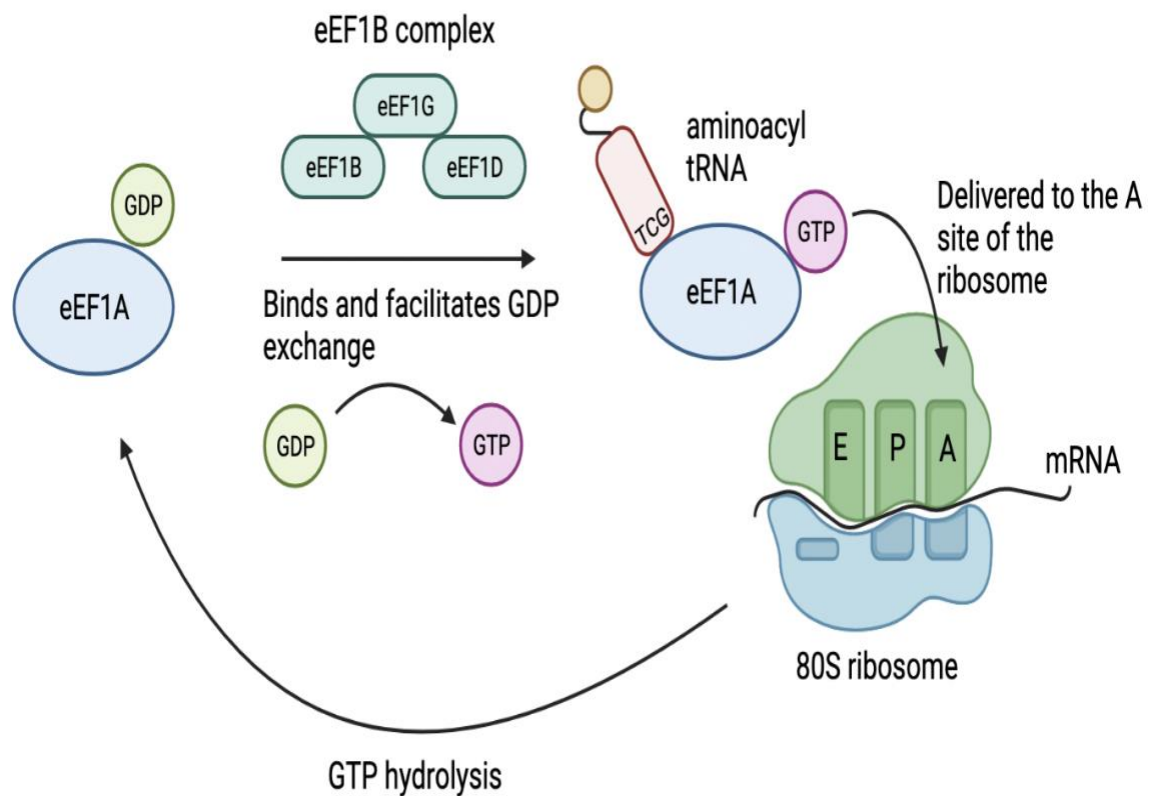
Figure 1: Overview of eEF1A's role in protein translation. *eEF1A has two isoforms, eEF1A1 and eEF1A2, which deliver aminoacyl tRNAs to the A site of the ribosome. The eEF1B complex consists of subunits eEF1G, eEF1B, and eEF1D, and functions as a GEF for the GTP-dependent delivery of aminoacyl tRNAs. Diagram: Author's own.*

1.2 The non-canonical functions of eEF1A isoforms

Despite the high degree of similarity in eEF1A isoforms, they have distinct tissue-specific and development-specific expression patterns. eEF1A1 is expressed ubiquitously, whereas eEF1A2 is only expressed in skeletal muscle, heart, brain, and spinal cord. eEF1A1 and eEF1A2 expression is mutually exclusive, and a switch occurs during development in which eEF1A1 expression is replaced by eEF1A2 in neurons and muscle (Knudsen et al., 1993). It is unknown what causes the switch from eEF1A1 to eEF1A2 expression and why there is tissue-specific expression, but one hypothesis is eEF1A1 and eEF1A2 have different non-canonical functions,

such as modifying the cytoskeleton, apoptosis, and different post-translational modifications (PTMs) have been identified (Soares et al., 2009; Soares and Abbott, 2013). Mutagenesis experiments in yeast also mapped protein turnover and nuclear transport to eEF1A structure in *Saccharomyces cerevisiae*. The mutations E286K and E291K were located on the aa-tRNA-binding domain of eEF1A and showed an accumulation of tRNAs in the nucleus indicating defects in nuclear export of aa-tRNA. Protein turnover was another potential noncanonical function of eEF1A as eEF1A interacts with 26S proteosome and the D156N mutation, located on the GTP binding site of eEF1A, was resistant to canavanine, which induces protein misfolding and degradation. No altered translation was observed in D156N.eEF1A mutants, but an altered rate of ubiquitin-dependent degradation of misfolded proteins, further suggested a noncanonical role of eEF1A in protein turnover (*Figure 2*)(Chuang et al., 2005; Sasikumar et al., 2012).

In vitro experiments revealed that eEF1A can bundle and bind to actin if aminoacyl tRNAs aren't present, and genetic screening in yeast revealed mutations N305S and N329S disrupt actin dynamics but do not alter the rates of translation, suggesting translation and actin cytoskeleton dynamics are independent eEF1A functions. However, the mutations F308L, and S405P in yeast eEF1A altered the actin cytoskeleton and reduced translation rates. One potential reason for reduced translation in these mutants could be due to the mutation sites overlapping the aa-tRNA binding site on eEF1A (Gross and Kinzy, 2007). The structure of eEF1A in yeast has three binding site domains; the actin binding site is suggested to be in domains II and III of eEF1A, and domain II is also the binding site of tRNAs and eEF1B (Gross and Kinzy, 2005; Soares et al., 2009)(*Figure 2*).

Mammalian eEF1A isoforms have been suggested to induce actin bundling by dimerization. The actin formed by both eEF1A isoforms exhibited a different morphology; eEF1A2 formed bundles that were thicker, shorter, and appeared denser than eEF1A1 actin bundles (Novosylna et al., 2017). A study found that phosphorylation of eEF1A2 regulates its ability to dimerize and is linked to actin dynamics in dendritic spines. Four conserved phosphorylation serine residues were identified in domain III of eEF1A2 but were not present in eEF1A1. These conserved residues were replaced to create phospho-null and phosphomimetic mutants and an interactome analysis revealed that significant enrichment of proteins involved in the actin

cytoskeleton were present in phosphomimetic mutants, whereas translation-associated proteins were enriched in phospho-null mutants. Moreover, eEF1A2 phosphorylation regulated translation by the eEF1A interaction with the GEF eEF1B (Mendoza et al., 2021). These findings suggest that regulation of the actin cytoskeleton is a non-canonical function in eEF1A that is linked to translation and regulated by phosphorylation. Furthermore, differences were found in the regulation of the actin cytoskeleton between eEF1A isoforms could highlight their functional differences.

Apoptosis was also linked to both eEF1A isoforms in a study on myotube cell differentiation in rodent myoblast cell lines that express endogenous eEF1A2. The eEF1A2 isoform was upregulated during differentiation, whereas eEF1A1 was downregulated. Following serum deprivation to induce apoptosis, eEF1A2 myotube cells survived longer than eEF1A1-transfected myotubes, suggesting eEF1A2 is anti-apoptotic in comparison to eEF1A1 (Ruest et al., 2002). Another difference found in eEF1A isoforms is that eEF1A2 is a putative oncogene overexpressed in breast cancer tumours whilst eEF1A1 expression remains unchanged (Tomlinson et al., 2005). The same expression pattern of eEF1A isoforms in ovarian tumours was observed, with eEF1A2 significantly overexpressed in tumours. However, eEF1A1 was found upregulated in colorectal cancer (CRC) patients, and higher eEF1A1 expression in affected CRC tissues correlated with poorer prognosis (Fan et al., 2022). Therefore, the exact mechanisms of how eEF1A isoforms display oncogenic properties are unknown, but it could be linked to apoptosis. The eEF1A isoforms share several noncanonical functions but have underlying functional differences.
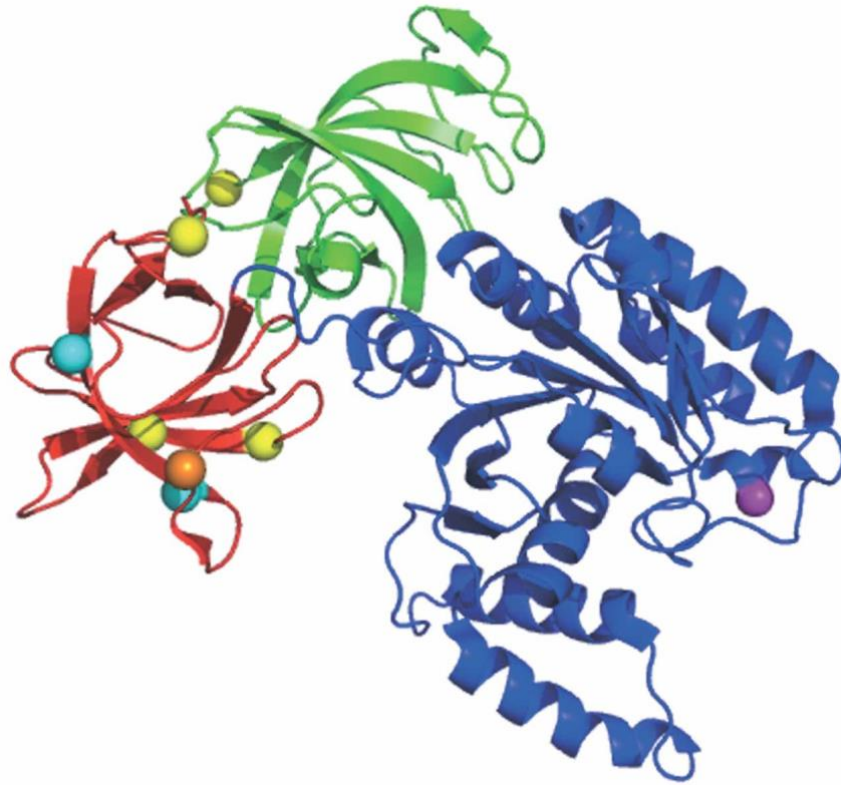
Figure 2: Domains identified in the structure of eEF1A in Saccharomyces cerevisiae yeast and mutations that alter its noncanonical functions. Domain I (blue) is where GTP binding occurs, and aa-tRNAs bind in domain II (red). Domains II and III have been identified as the sites of actin binding and bundling. The spheres represent mutations that affect eEF1A noncanonical functions. In domain I, the mutation Asp156Asn (purple) altered protein turnover. In domain II, Glu286Lys and Glu291Lys (cyan) mutations affect nuclear transport. The mutations Asn305Ser, Asn329Ser, Phe308Lys, and Ser405Pro (yellow) are shown in domains II and III and affected actin dynamics. Phosphorylation of Glu298 in yeast (orange) revealed downregulation of translation. Image taken from Sasikumar et al. (2009).

1.3 Missense mutations in eEF1A2

The *EEF1A2* gene encodes for a neuromuscular specific translation elongation factor, eEF1A2, and over 50 *de novo* heterozygous missense mutations were identified by whole exome sequencing as disease-causing in patients with neurological issues, such as epilepsy, autism, and intellectual disability, and in some cases cardiomyopathy and/or facial dysmorphia. These mutations also result in a broad range in disease severity and symptoms observed in patients, though severity frequently correlates with the precise mutation. The eEF1A2 missense mutations occur in highly conserved amino acid regions, therefore, the functional consequences of these mutations are severe (Inui et al., 2016; Lam et al., 2016). No EEF1A1 mutant variants have been reported to cause similar neurodevelopmental disorders in humans as it is presumed that any deleterious mutations would be embryonic lethal due to the ubiquitous expression of EEF1A1. To determine the effect of missense mutations on eEF1A2 function, missense mutations expressed in plasmids were transformed in the MC214 yeast strain, a double knockout of the eEF1A-expressing orthologous genes *TEF1* and *TEF2*. Mutant yeast showed impaired growth, except for the P333L mutant, suggesting protein synthesis was impaired in mutants with growth defects. The P333L mutant was considered an outlier as heterozygotes are unaffected but homozygotes are lethal, causing cardiomyopathy (Cao et al., 2017). The mapping of the missense mutations on eEF1A2 structure showed several mutations cluster in adjacent or inside eEF1A2 binding domains, suggesting mutants may disrupt EEF1 complex formation, dimerization, and/or GTP/GDP recycling (Carvill et al., 2020). Interestingly, molecular modelling of the P333L mutation wasn't mapped on any eEF1A2 binding site but was located on the back side of eEF1A2 on the loop linking domains II and III (Cao et al., 2017). The P333L mutant is predicted to induce a conformational change that may affect functional binding in domains II and III. This project will focus on mutations E122K and D252H located in eEF1A2 binding domains I and II, respectively (*Figure 2*). Therefore, studies have found eEF1A2 missense mutations affect protein synthesis and are predicted to alter eEF1A2 binding by computational modelling.
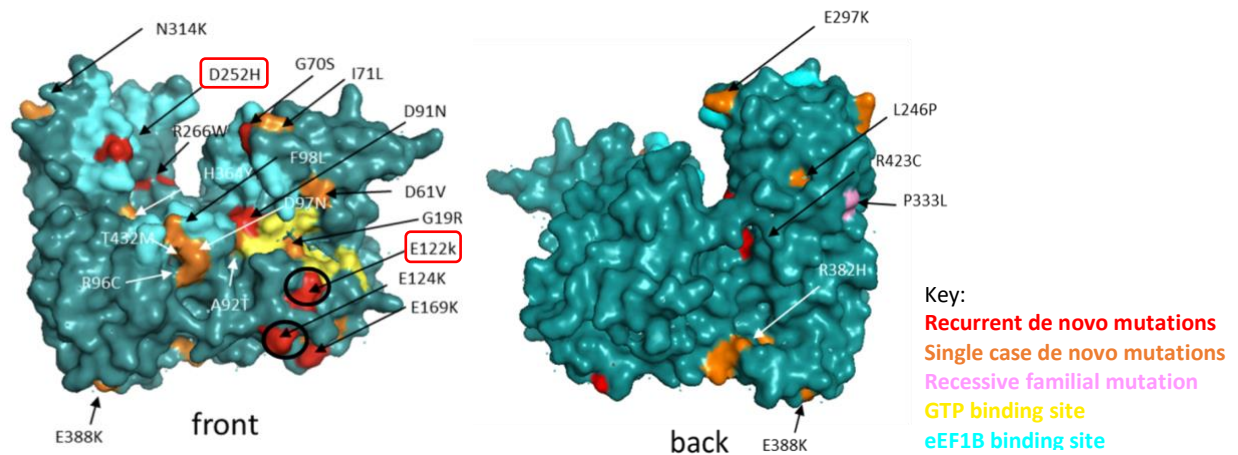
Figure 2: The location of missense mutations on the eEF1A2's molecular structure. *The molecular structure of eEF1A2 in yeast shows where some identified missense mutations are predicted to be located on eEF1A2. This project is focusing on the mutations D252H and E122K (highlighted in red), which are located on the eEF1B and GTP binding site, respectively. Image was created on PyMol software and taken from: Cathy Abbott (Principal Investigator at the University of Edinburgh).*

1.4 Disease progression

As mentioned above, patients with missense mutations in eEF1A2 have a broad disease severity with some patients exhibiting both neurological, behavioural and/or morphological features, such as autism and facial dysmorphic features. For example, the severity of epilepsy ranges from mild to severe whereby mild cases can be controlled by antiepileptic drugs (*Table 1)*. Clinical reports and whole exome sequencing of affected patients, reported that parents were healthy and unaffected, indicating missense mutations are *de novo* autosomal dominant. (Carvill et al., 2020; De Rinaldis et al., 2020; Inui et al., 2016; Lam et al., 2016; Nakajima et al., 2015). However, the P333L missense mutation was an exception and was first identified in siblings suffering from cardiomyopathy in addition to other common symptoms in eEF1A2, including epilepsy and motor defects. Whole exome sequencing revealed that the siblings' parents were heterozygotes and, therefore, P333L was a recessive familial mutation. As mentioned above, P333L is homozygous lethal, and the affected siblings' condition progressively deteriorated, leading to an early death (Cao et al., 2017). A more recent study reported the first case of the P16L mutation, which is dominantly inherited. The patient exhibited a broad phenotype spectrum, such as epilepsy, severe intellectual disability, and

cardiomyopathy, as well as other symptoms not apparent in neurodevelopmental disorders, including diabetes insipidus. Interestingly, in comparison to P333L mutants, heart function improved with age in the P16L mutant (Kaneko et al., 2021). Therefore, the exact mechanism of how eEF1A2 missense mutations are inherited is unknown, but recessively inherited eEF1A2 missense mutations may be more detrimental than autosomal dominant mutations. A study by Long et al. (2020) revealed the most damaging mutations, predicted by a series of algorithms from the databases VarCards, ReVe, Grantham, and SNAP2, were located in the functional binding domains of eEF1A2, suggesting the location of mutation correlates with disease severity (De Rinaldis et al., 2020; Long et al., 2020). However, this observation could just be a correlation, and no molecular mechanism has been proposed.

It is largely unknown how these destabilizing mutations affect different tissues and whether the affected interactome and proteome have a significant role in determining disease severity. Therefore, an understanding of the molecular mechanisms in which missense mutations affect eEF1A2 function is crucial.

Table 1: Summary of reported patient symptoms and predicted mutant pathogenicity in multiple eEF1A2 mutations

Mutation	No. of cases reported	Inheritance	Epilepsy (type and onset)	Developmental delay	ID	Facial Dysmorphism	ASD	DCM	Predicted pathogenicity scores (Long et al., 2020)	Reference
E122K	5	Dominant de novo	4m Infantile spasms	Motor delay	+	+	+	NR	25	Nakajima et al. 2015 (II)
		Dominant de novo	2m Controlled infantile spasms	Non-verbal, gross motor delay	+	+	–	NR		Lam et al. 2016 (5)
		Dominant de novo	8m Myoclonic seizures, Myoclonic-atonic	Non-verbal, developmental delay	+	+	–	NR		Inui et al. 2016 (2)
		Dominant de novo	10m Myoclonic seizures, atypical absences	Non-verbal, developmental delay	+	+	–	NR		Inui et al. 2016 (1)
		Dominant de novo	4yr Myoclonic absences	Global developmental delay	+	+	+	NR		De Rinaldis et al.
D252H	2	Dominant de novo	8yr Generalised tonic seizure	Developmental delay	+	+	+	NR	35	Nakajima et al. 2015 (I)
		Dominant de novo	NR	Global developmental delay	NR	+	+	NR		DDD

Table 2 shows a summary of multiple missense mutations to show the heterogeneity of eEF1A2 missense mutations. ID = Intellectual disability, ASD = Autism Spectrum Disorder, DCM = Dilated Cardiomyopathy. Key: (+) reported (–) absent NR = Not Reported. The parenthesis under "References" notes the patient or case number reported in the study. Note: there may be a higher number of cases that haven't yet been described in studies.

Mutation	No. of cases reported	Inheritance	Epilepsy (type and onset)	Developmental delay	ID	Facial Dysmorphism	ASD	DCM	Predicted pathogenicity scores (Long et al., 2020)	Reference
G70S	5	Dominant de novo	2m Myoclonic; tonic-clonic; absence seizures	Global developmental delay, non-verbal	+	+	NR	NR	36	Lam et al. 2016 (1)
		Dominant de novo	4m Myoclonic seizures, grand mal insults, absences	Global developmental delay	Severe +	–	+	NR		de Ligt et al. 2012
		Dominant de novo	Infant	Non-verbal	+	NR	NR	NR		Veeramah et al. 2013
		Dominant de novo	Early infantile Epileptic encephalopathy	NR	NR	NR	NR	NR		de Kovel et al. 2016
		Dominant de novo	Childhood Epileptic encephalopathy	NR	+	+	NR	NR		Helbig et al. (34)
P333L	2	Familial recessive	7m Absences; tonic-clonic; febrile	Global developmental delay	+	+	NR	+ Progressive	20	Cao et al., 2017 (II.1)
		Familial recessive	12m Febrile, tonic-clonic	Global developmental delay	+	+	NR	+ Progressive		Cao et al., 2017 (II.2)
P16L	1	Dominant de novo	5 days, Infantile spasms, intractable epilepsy	Severe; non-ambulatory; non-verbal	+	+	NR	+ Mild	NR	Kaneko et al., 2021
E124K	1	Dominant de novo	3m, Controlled myoclonic seizures, absences	Delays in language but verbal	–	+	–	NR	17	Lam et al. 2016 (6)

Table 2 shows a summary of multiple missense mutations to show the heterogeneity of eEF1A2 missense mutations. ID = Intellectual disability, ASD = Autism Spectrum Disorder, DCM = Dilated Cardiomyopathy. Key: (+) reported (-) absent NR = Not Reported. The parenthesis under "References" notes the patient or case number reported in the study. Note: there may be a higher number of cases that haven't yet been described in studies.

1.5 The different characteristics of eEF1A2 missense mutations E122K and D252H

Two of the identified *de novo* missense mutations, E122K and D252H, may have different tissue-specific expression levels in the mouse brain and muscle. In the D252H mutant mouse brain, a gradual decrease in eEF1A2 expression was observed relative to WT, with heterozygotes showing ~20% decrease and homozygote expression levels that were ~40% lower than WT. In comparison, eEF1A2 expression levels in muscle were not changed in heterozygotes but were 1.6 times higher in D252H homozygotes mice relative to WT. The changes in expression were averaged across male and female mutant mice as no statistically significant differences were observed across sex (Davies et al., 2020). In contrast, male E122K mutant mice displayed larger differences in eEF1A2 expression compared to female E122K mutant mice. In the mouse brain, no significant changes in eEF1A2 expression were observed across heterozygote and homozygote female mice relative to WT. In contrast, male E122K homozygotes showed a 42% decrease in eEF1A2 expression relative to the WT brain. In the muscle, no significant changes in eEF1A2 expression were observed in female mouse heterozygotes, but males exhibited a 46% decrease compared to WT. In comparison to the increased eEF1A2 expression observed in muscle D252H homozygotes, E122K homozygotes showed an 83% and 49% decrease in expression relative to WT in males and females, respectively *(Table 2)*(Marshall, 2022). The changes in eEF1A2 expression across D252H and E122K mutants occur at the protein level as qPCR experiments revealed that RNA transcript levels were stable and not significantly altered in D252H mutants and were only increased in E122K homozygotes, suggesting mutations D252H and E122K mostly likely induce decreased eEF1A2 stability (Davies et al., 2020; Marshall, 2022).These mutations are located at eEF1A2 sites of dimerization and/or binding sites to other molecules. The D252H mutation is located in domain II of eEF1A2, the binding site of aa-tRNAs and the eEF1B complex (Carriles et al., 2021; Lam et al., 2016). A paper by Davies *et al. (2020)* reported a 500-fold decrease in the binding of eEF1B complex subunits eEF1D, eEF1G, eEF1B2, and VARS in a label-free mass spectrometry quantification of the altered interactome in D252H.eEF1A2-transfected SH-SY5Y cells. Furthermore, validation by co-immunoprecipitation found D252H missense mutation abolishes all binding of eEF1A2 to the eEF1B complex (Davies et al., 2020). The E122K mutation is located in domain I, the GDP/GTP binding site of eEF1A2, and, therefore, likely affects the GTP-dependent delivery of aminoacyl tRNAs to the ribosome (Nakajima et

al., 2015). A study predicted that the mutations E122K and D252H are more pathogenic, with Polyphen-2 prediction scores of 1.000/0.999 and 0.962/0.980, respectively, than other mutations, including E124K, which has a much lower pathogenicity score of 0.101/0.072 (Lam et al., 2016). Interestingly, the E124K mutation is much milder than D252H or E122K and its location doesn't overlap any eEF1A2 binding sites (*Table 1*). Therefore, mutations D252H and E122K are similarly pathogenic but have different properties and are located in different regions of eEF1A2, which may be linked to the mutations' effects on eEF1A2 function.

Table 2: Comparing eEF1A2 expression in D252H and E122K mutant mouse tissue

Genotype	Change in eEF1A2 expression (relative to WT = 1)	
	Brain	**Muscle**
E122K/+	NS (M + F)	0.54 (M) NS (F)
E122K/E122K	0.58 (M) NS (F)	0.17 (M) 0.51 (F)
D252H/+	0.80 (M + F)	NS (M + F)
D252H/D252H	0.60 (M + F)	1.6 (M + F)

All mouse tissue samples had the C57BL/6JCrl genetic background. Changes in eEF1A2 expression were considered significant if p<0.05. NS = No significant change relative to wildtype eEF1A2 expression. (M) represents the eEF1A2 change in expression in male mouse mutants and (F) in female mouse mutants. Note: results not labelled (M + F) are averaged across both sexes and no statistically significant difference across sex was found. These results were reported by (Davies et al., 2020) and (Marshall, 2022).

1.6 Modelling eEF1A2-mutant epileptic encephalopathies in mice

In comparison to species lower than vertebrates, mammals, such as rodents, express both eEF1A1 and eEF1A2 isoforms. Mouse eEF1A2 is encoded by Eef1a2 and only differs from human eEF1A2 by one amino acid (Mills and Gago, 2021). Rodents have the same developmental switch as humans that results in tissue-specific expression of eEF1A1 and eEF1A2, which is only expressed in neurons, cardiac and skeletal muscle. The developmental switch is complete after 21 days in humans, and wst/wst mice only start to show a neurodegenerative phenotype after 21 days that progresses for approximately one week until they die (Khalyfa et al., 2001). Therefore, mice exhibit a high degree of homology that make them appropriate models for studies on eEF1A2 function.

Mouse modelling of the D252H missense mutation were created using CRISPR/Cas9 technology. Initially, heterozygotes showed a similar growth trend to WT mice until postnatal day 21. The phenotype observed in D252H heterozygotes had significantly impaired motor function, with worse neuroscores, reduced grip strength, and rotarod performance relative to WT mice. However, no behavioural abnormalities were detected in heterozygotes, which were observed in affected children with the D252H.eEF1A2 mutation. In comparison, homozygotes resembled the wst/wst phenotype, exhibiting abnormal pathology in spinal cords. Neither heterozygote nor homozygote D252H mice exhibited spontaneous seizures throughout their one-year lifespan (Davies et al., 2020). However, this might not be a lack of face validity as only one patient with the D252H mutation developed epilepsy with a late age of onset at 8 years (Nakajima et al., 2015). Another potential reason that D252H mutant mice didn't develop spontaneous seizures could be due to their much shorter lifespan.

In E122K missense mutant mouse models also created using CRISPR/Cas9, heterozygotes lived into adult life with motor delays but no significant impairments in behavioural phenotype. Homozygous E122K mice displayed a more severe motor defects than heterozygotes but didn't display spinal cord degeneration and outlived null mice by about a week, indicating that E122K.eEF1A2 was not sufficient to keep the mice alive. In addition, homozygotes displayed a more severe neurological phenotype than null mice, suggestive of

a toxic gain-of-function and/or dominant negative effect. Similar to D252H mouse models, no spontaneous seizures were observed in heterozygote or homozygote mice. However, in this case, every E122K affected patient developed epilepsy, with the age of onset was ranging from 10 weeks to 4 years. Based on these findings, it is suggested that E122K mouse models lack face validity in the modelling of epilepsy (De Rinaldis et al., 2020; Marshall, 2022).

Overall, modelling eEF1A2 missense mutations in mice has provided insight into the motor deficits, which are also observed in patients. These genetic models of single missense mutations are relatively easy to create using CRISPR/Cas9 technology. However, eEF1A2 missense mutations resulting in complex epileptic encephalopathies are difficult to model in mice as it was revealed that neither D252H and E122K mouse models exhibited spontaneous seizures (Marshall, 2022; Marshall et al., 2021).

1.7 Are missense mutations loss- or gain-of-function?

Missense mutations in eEF1A2 are predicted to be damaging since it's evolutionarily conserved in distant species, with yeast orthologues bearing 80% similarity to human eEF1A2, and under high selective constraint (Samocha et al., 2014). One of the first instances of the damaging effects of eEF1A2 mutations was found in wasted syndrome (*wst*), a neurodegenerative disease arising spontaneously in homozygous mice and caused by a 15.8 kb deletion in Eef1a2 stopping transcription and resulting in no eEF1A2 production and motor neuron degeneration. Ultimately, complete loss of eEF1A2 in homozygous wst/wst mice resulted in death after approximately 4 weeks (Chambers et al., 1998). However, eEF1A2 mutant heterozygous (*wst/+*) mice survived until 21 months with no significant motor defects or spinal cord pathology compared to WT mice, suggesting loss-of-function may be present in humans with an unaffected phenotype and, therefore, eEF1A2 missense mutations may cause a gain of function or dominant negative effect (Griffiths et al., 2012). Another study by *Cao et al.* (2017) induced a morpholino eEF1A2 knockdown in zebrafish and found that P333L EEF1A2 mRNA cannot rescue the mutant phenotype, suggesting loss-of-function. As described above, humans heterozygous for P333L show no apparent clinical phenotype, suggesting haploinsufficiency in humans is not lethal (McLachlan et al., 2019). However, a study on the D252H mutation by *Davies et al. (2020)* compared the neurodegenerative

phenotype in D252H/D252H and null mice and found neurological function in homozygous missense mice was more severely affected. Therefore, the D252H mutation could be a gain-of-function that induces eEF1A2 toxicity (Davies et al., 2020). These findings suggest eEF1A2 mutations have unusual distinct properties and a wide allelic heterogeneity. Therefore, an understanding of the properties of these mutations is important for determining their effect on eEF1A2 function. This project will be investigating protein stability and eEF1A2 binding to give insight into the effects of different mutations on eEF1A2 function.

1.8 Aims

This project conducted a series of molecular biology experiments, such as western blotting, to assess the impact of missense mutations on eEF1A2 expression. High-throughput proteomics experiments by AP-MS were also performed to identify changes in the E122K.eEF1A2 interactome that could further elucidate how missense mutations alter eEF1A2 function. A comparative analysis of the E122K and previously reported D252H altered eEF1A2 interactomes was then conducted to identify differences that may be specific to the mutation, as eEF1A2 missense mutations have differing functional properties. A differential expression analysis in the mouse brain proteome was then performed by comparing E122K homozygotes to WT to identify altered proteins that could give insight into potential biomarkers for targeting eEF1A2-related neurodevelopmental disorders. To summarize, the aims discussed in the next section, are to:

- Compare eEF1A2 expression across mutations, E122K and D252H, to determine how different mutations affect eEF1A2 stability in different tissues/cell types.
- Analyze and compare the mutant eEF1A2 interactome in E122K mutant transfected HEK293T cells to identify significantly altered proteins.
- Conduct a differential expression analysis to identify proteins altered in the mouse brain proteome of E122K homozygous mice compared to WT littermates.

Chapter 2: Materials & Methods

2.1 Materials

2.1.1 Mouse tissue

Brain and heart tissue from the mouse strain *C57BL/6JCrl* was used in this project. Mouse lines were bred by Grant Marshall (postdoctoral researcher). The mouse brain samples used for mass spectrometry and western blotting validation of the differential expression analysis are detailed in *Table 3*. Wildtype mouse muscle was used as a negative control for eEF1A1 expression and wasted mouse brain (wst/wst) was the negative control for eEF1A2 expression (Chambers et al., 1998).

Table 3: Description of mouse samples used for mass spectrometry and western blot validation of mass spectrometry

Sex	Genotype	Age
M	+/+	P28
M	+/+	P29
M	+/+	P30
F	+/+	P28
F	+/+	P30
M	E122K/E122K	P28
M	E122K/E122K	P28
M	E122K/E122K	P29
F	E122K/E122K	P28
F	E122K/E122K	P29

Each sample is one half of a mouse brain hemisphere to reduce heterogeneity across samples and prevent heterogeneity that might be caused by removal/inclusion of specific parts of the brain.

2.1.2 Cell culture

HEK293T cells were cultured in Dulbecco's modified Eagle's medium (DMEM) supplemented with 10% (v/v) fetal calf serum (FCS) and 5% penicillin streptomycin (P/S), whereas SH-SY5Y cells were cultured in DMEM supplemented with 15% FCS and 1% P/S. Both cell lines were incubated at 37 °C with 5 % CO_2. HEK293T and SH-SY5Y cells were passaged by adding TrypLE to cells and incubating for 1-2 minutes. To stop the TrypLE reaction, DMEM was added with twice the volume of TrypLE previously added. The cell suspension was then spun in a centrifuge at 1200 rpm for 3 mins to cause pellet formation. HEK293T and SH-SY5Y cells were seeded at the appropriate density in DMEM (supplemented with 10% FCS and 5% P/S or 15% FCS and 1% P/S). Cells were maintained below passage (P)18.

Table 4: Cell lines used in this project.

Cell line	Species	Cell type	eEF1A isoform expression
HEK293T	Human	Embryonic kidney	eEF1A1
SH-SY5Y	Human	Neuroblastoma	eEF1A1 + eEF1A2

Table 5: List of reagents made for sample preparation and western blotting

10% separating gel	13.4 ml dH_2O, 1.5M Tris pH 8.8, 10.4 ml 30% Acrylamide, 160 μl 20% SDS, 20 μl TEMED, 80 μl 25% AMPS.
4.3% stacking gel	11.9 ml dH_2O, 5 ml 0.5 M Tris-HCl pH 6.8, 2.9 ml 30% Acrylamide, 100 μl 20% SDS, 10 μl TEMED, 100 μl 25% AMPS
Invitrogen transfer buffer	750 ml dH_2O, 50 ml 20x NuPAGE Transfer Buffer, 200 ml Methanol
RIPA buffer	50 mM Tris pH 7.5, 150 mM NaCl, 0.5% (w/v) Sodium Deoxycholate, 1% (v/v) NP-40, 0.1% (v/v) SDS

Laemmli loading buffer (2x)	0.95 g 60mM Tris-HCl pH 6.8, 0.1 g 0.1 % Bromophenol blue, 10 ml 10% Glycerol, 2 % SDS, 100 ml dH_2O
TBS-T	10x TBS with 0.1% Tween20. Diluted in distilled water to 1x.
Wash solution	6.7 % (v/v) Glacial Acetic Acid and 30% (v/v) Methanol. Diluted in distilled water.
Reversal solution	0.1% (w/v) Sodium Hydroxide, 30% (v/v) Methanol. Diluted in distilled water.

2.1.3 Antibodies

Table 6: List of primary antibodies.

Antibody	Host species	Dilution	kDa	Primary/Secondary antibody	Company
eEF1A1	Sheep	1:1000	~52	Primary	Abbott Lab Homemade (Newberry et al., 2007)
eEF1A2	Rabbit	1:5000	52	Primary	ProteinTech custom
anti-mCherry	Mouse	1:2000	28	Primary	Abcam
anti-mCherry	Goat	1:2000	29	Primary	OriGene
ZPR1	Rabbit	1:1000	~51	Primary	Sigma Aldrich
FKBP3	Rabbit	1:1000	25-30	Primary	ProteinTech
EEF2	Rabbit	1:1000	95	Primary	ProteinTech

Shootin 1	Rabbit	1:1000	60-75	Primary	ProteinTech
Phospho-EEF2	Rabbit	1:1000	95	Primary	ProteinTech
KIF5A	Rabbit	1:1000	118-120	Primary	ProteinTech
EEF1D	Rabbit	1:1000	~32	Primary	GeneTex
EEF1B2	Rabbit	1:1000	34	Primary	ProteinTech
V5	Rabbit	1:5000	~95	Primary	Genetex

Table 7: List of Secondary antibodies.

Name	Target species	Species raised	Dilution	Conjugate	Company
IR Dye 680RD Anti-rabbit	Rabbit	Goat	1: 20000	Fluorescent	LICOR
RDye 800CW Anti-rabbit	Rabbit	Donkey	1:15000	Fluorescent	LICOR
RDye 800CW Anti-mouse	Mouse	Donkey	1: 15000	Fluorescent	LICOR
RDye 800CW Anti-goat	Goat	Donkey	1:15000	Fluorescent	LICOR

2.1.4 Co-immunoprecipitation (co-IP) and mass spectrometry solutions and buffers

2x Laemmli

Chemicals	Amount (volume/grams)
120 mM tris-HCl	12 ml of 1 M tris (pH 6.8)
20% glycerol	20 ml
4% SDS	20ml of 20% SDS
0.04% bromophenol blue	0.04 g

Note: Adjust to pH 6.8.

co-IP lysis buffer (pH 7.5)

Final concentration of solution	Volume required
10 mM tris-HCL	1 ml of 1 M tris
150 mM NaCl	15 ml of 1 M NaCl
0.5 mM EDTA	0.1 ml of 0.5 M EDTA
0.5% IGEPAL	0.5 ml

Note: Adjust pH to 7.5.

co-IP wash buffer

Final concentration of solution	Volume required
10 mM tris-HCL	1ml of 1 M tris
150 mM NaCl	15 ml of 1 M NaCl
0.5 mM EDTA	0.1 ml of 0.5 M EDTA

Note: Adjust pH to 7.5.

Mass spectrometry sample preparation lysis buffer

Chemicals	Amount (volume/grams)
6 M guanidinium hydrochloride (GuHCl)	1 ml
Chloroacetamide (CAA)	1 mg
Tris(2-carboxyethyl)phosphine (TCEP)	1.5 mg

2.2 Methods

2.2.1 Transformation of DH5a *Escherichia coli* (E.Coli)

Transformation E122K.eEF1A2 mCherry constructs into DH5a E.Coli was achieved by heat shock at 42°C and then incubated for one hour at 37°C (200 rpm) in super optimal broth with catabolite repression (SOC) medium before plating the plasmid-E.Coli mixture onto ampicillin (AMP) agar plates. The plates were incubated overnight at 37 °C to allow the formation of transformed E.Coli colonies. For the transformation of E122K.eEF1A2-V5 tagged constructs, the same protocol was followed but zeocin agar plates were used instead of AMP.

Mini-Prep

Plasmids were isolated from DH5a E.Coli. Bacterial culture was prepared overnight by picking a single transformed colony into 5 mL of L-broth containing 100 ug/ mL AMP or 100 mg/ml of zeocin. The next day, the same protocol described in the Monarch® Plasmid Miniprep Kit was followed.

Midi-Prep

Bacterial culture was prepared by inserting a small amount of desired plasmid into 5 ml of L-Broth and 10 μl of AMP followed by an incubation period of 6 hours. After incubation, the broth mixture was added to 50 ml of L-Broth and 100 μl of AMP and left in the incubator overnight. The following day, the plasmid isolation steps followed were those described in the ZymoPURE Express Plasmid Midiprep Kit.

2.2.2 Transfections in HEK293T and SH-SY5Y cells

Transfections in HEK293T cells

At 24-48 hours prior to transfection, HEK-293T cells with a final concentration of 0.075×10^6 cells/ml were seeded in a 12-well plate overnight. The following day, cells were treated with 1 µg of either wildtype, empty vector, or mutant plasmid DNA. The protocol described in Invitrogen Lipofectamine® 3000 Kit was followed; then, cells were incubated for 48 hours at 37°C. After 48 hrs, cells were treated with 1ul of 10,000um stock for every ml of proteasome inhibitor MG132 or DMSO for a final concentration of 10 µM and incubated at 37°C for 4-6 hours. 0.5ml TryplE was added to each well and incubated for 2-3 minutes. Then, 1ml of DMEM/media was added to each well and centrifuged at 22°C 1200 rpm for 3 mins. Protein lysates were prepared in 70 ul of ice-cold lysis buffer (RIPA buffer with cOmplete™ Mini protease inhibitors added). Cells were vortexed and leave on ice for 30 minutes followed by centrifugation at 4°C, max speed for 10 minutes.

Transfections in SH-SY5Y cells

At 48 hours prior to transfection, SH-SY5Y cells were seeded into 6-well plates with a final concentration of 5×10^5 cells/ml overnight. The following day, cells were treated with 1 µg of either wildtype, empty vector, or mutant plasmid DNA. The protocol described in the Invitrogen Lipofectamine® 3000 Kit was followed, and then cells were incubated for 48 hours at 37°C. After 6 hours, the media was changed for fresh, prewarmed DMEM (supplemented with 15% FCS and 1% P/S). Following 48 hours after plasmid transfection, cells were lysed in co-IP lysis buffer (*see Materials section*) containing protease (cOmplete™ Mini, Roche) and phosphatase inhibitors (Thermo Scientific™ A32957). The protein collected was then used for co-immunoprecipitation (*see Co-immunoprecipitation (co-IP)*).

2.2.3 Western blotting

Protein lysates from cell transfections were prepared in radioimmunoprecipitation assay buffer (RIPA buffer) with protease inhibitor (cOmplete™ Mini, Roche) whereas protein lysates from mouse tissue were prepared in 0.32 M sucrose with protease inhibitor. A bicinchoninic acid (BCA) assay was then conducted to calculate protein concentration (Pierce BCA Protein Assay Kit). Then, 5 ul of reference ladder (New England Biolabs Color Prestained Protein Standard) and 10 ug of protein was separated on 4-12 % bis-tris gels at 100-150 V and transferred to polyvinylidene (PDVF) membrane. Immediately after transfer, PDVF membranes were incubated in Revert Total Protein Stain (TPS) (Li-Cor) for 5 min at room temperature (RT) and washed in reversal solution. The membranes were left to dry overnight at RT. The next day, the membranes were blocked in PBS blocking buffer (Li-Cor) for 1-2 hours at room temperature After blocking, the membranes were incubated in the appropriate antibodies for 1 hour, and then washed 4 x 5 minutes with TBS-Tween at RT. The appropriate secondary antibodies were then added and incubated for 1 hour at RT. Membranes were washed 4 x 5 mins in TBS-Tween and air-dried. Images were acquired on an Odyssey CLX laser-based scanning system (Li-Cor).

Image Studio Lite

Western blot images were imported into Image Studio Lite for western blot quantification. The brightness and contrast of the images were adjusted to enhance the visibility of the blots and reference ladder for correct identification of the desired protein bands. Under the "Analysis" section, the "add rectangle" was selected to draw a rectangle surrounding a single protein band. The same rectangle size was used across the desired protein bands, ensuring that the rectangles were not overlapping each other or multiple protein bands. Each rectangle quantified a fluorescent signal, and a "user defined" background was selected to prevent quantifying overlapping bands and remove outlier pixel intensities in the background surrounding the rectangles. Spots representing overexposed signal were excluded to prevent inaccurate quantification. TPS was used to normalize each protein band. TPS stains all the proteins in the sample and provides a visual image after the transfer of proteins. For the TPS blots, "add rectangle" was selected to create a large rectangle placed along the same area

and approximate position of each column. Each rectangle was the same size and non-overlapping across each TPS blot. A signal ratio was used as a measure of normalized protein expression, which was calculated by dividing the protein signal by the total signal value of the desired TPS blot. Western blots probed for mCherry in addition to eEF1A2 were also normalized to mCherry protein signal following TPS normalization by dividing the calculated signal ratio by the quantified mCherry protein signal. Normalizing samples to mCherry controlled for changes in transfection efficiency. In co-IP validation western blots, (*Figures 24 and 25*) samples were normalized to eEF1A2-V5 instead of TPS total signal to also normalize for changes in transfection efficiency and eEF1A2-V5 protein stability, which was expected to be lower in E122K.eEF1A2-V5 samples. A statistical comparison to the average wildtype signal ratio was performed to determine statistically significant differences in protein expression and account for small sample sizes where normal distribution cannot be assumed (*section: Statistical Tests*).

$$Signal\ ratio = \frac{Protein\ signal}{TPS\ total\ signal}$$

2.2.4 Co-Immunoprecipitation (co-IP)

Samples of eEF1A2$^{E122K/E122K}$ transfected HEK293 cells were seeded onto 6-well plates, transfected, and protein collected (see "*Transfections in HEK293T cells*"). Each treatment (i.e., WT, EV, and mutant) had three replicates. The samples were prepared for the robot co-IP by extracting the protein by lysis, and then eluting the samples with the help of Roopesh Krisnankutty (postdoctoral researcher) for the robot co-IP and mass spectrometry quantification.

Co-immunoprecipitation experiments for the validation of the interactome analysis were performed with the help of Grant Marshall (postdoctoral researcher). Cells were seeded onto 6-well plates and transfected by following the Invitrogen Lipofectamine® 3000 protocol. Wildtype and mutant constructs were transfected in triplicates, and the empty vector constructs were transfected in two replicates. At 48 hours after transfection, cells were lysed

in co-IP lysis buffer containing protease (cOmplete^{TM} Mini, Roche) and phosphatase inhibitors (Thermo Scientific™ A32957) for 30 minutes. Then, the cell mixture was centrifuged at 17,000 x g for 10 minutes to collect the supernatant. The supernatants were diluted in dilution buffer to make 500μl of lysate. Magnetic beads (ProteinTech ChromoTek V5-Trap™ Magnetic Agarose) were equilibrated in co-IP washing buffer and added to the lysate to incubate for 1 hour at 4 °C. Input, elute, and wash fractions were made and prepared for western blotting by adding 2x Laemmli buffer, 10% (v/v) DTT, and boiled for 5 minutes at 95 °C.

2.2.5 Affinity-purified mass spectrometry (AP-MS)

Mass spectrometry is a highly sensitive and high-throughput technique used for the identification and quantification of proteins in complex mixtures, such as tissue and cells. Affinity-purified mass spectrometry (AP-MS) was used to identify significantly altered eEF1A2 binding proteins in the mutant E122K.eEF1A2 interactome. In AP-MS, samples undergo co-immunoprecipitation prior to quantification by mass spectrometry. Prior to AP-MS, HEK293T cells were transfected with eEF1A2-V5 constructs to express the bait protein for co-IP (see *Transfections in HEK293T cells*). Cells were then lysed with RIPA buffer containing protease inhibitor (cOmplete^{TM} Mini, Roche) to extract proteins from the cell lysate. The bait (target protein) was eEF1A2, which was immobilized by V5-tagged magnetic agarose beads (ProteinTech ChromoTek V5-Trap™ Magnetic Agarose), and captures eEF1A2 molecular binding proteins (Dunham et al., 2012). Proteins were then purified and digested by the protease trypsin, which cleaved the proteins into peptides (Gingras et al., 2007). The peptides were then separated by liquid chromatography and identified by mass spectrometry (Dunham et al., 2012). The raw data was analysed of the software pipeline Fragpipe for normalisation and interpretation of the MS data (*Figure 4*). Roopesh Krishnankutty (postdoctoral researcher) conducted the co-immunoprecipitation in a robot co-IP followed by mass spectrometry.
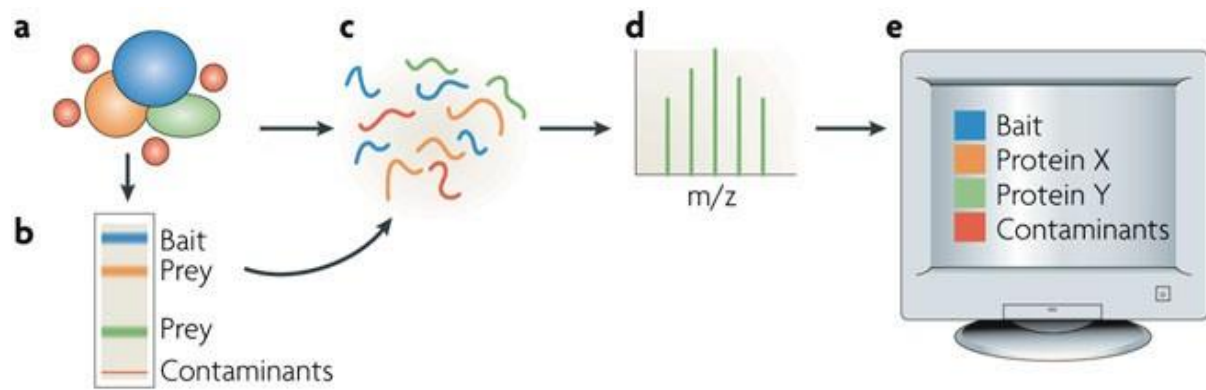
Figure 4: An overview of Affinity Purified Mass Spectrometry (AP-MS). *(a) Proteins were purified from the transfected HEK293T cell lysate. (b) The purified proteins included consisted of the bait (eEF1A2-V5), protein binding partners (prey), and contaminants. (c) The addition of trypsin lysed the proteins into peptides. (d) Analysis of the peptides by mass spectrometry separated ionized peptides by their mass to charge (m/z) ratio for peptide identification. (e) Statistical analysis using software, such as Fragpipe, of the MS data generated list of identified binding proteins, the bait, and contaminants. Further statistical analysis was conducted on Rstudio to identify only the statistically significant proteins with altered binding. Image taken from: Gingras et al. (2007).*

2.2.6 Liquid Chromatography Mass Spectrometry (LC-MS/MS) with label-free quantification

Mouse brain homozygous eEF1A2$^{E122K/E122K}$ and WT samples were analysed by applying bottom-up proteomics, in which proteins are digested into peptides that are then separated by liquid chromatography, ionized, and analysed by tandem mass spectrometry (MS/MS) (*Figure 4*) (Zhu et al., 2010).

Mouse brain tissue samples were prepared for the mass spectrometer by homogenizing the tissue in RIPA buffer, containing protease and phosphatase inhibitors, in a Precellys® homogenizer. The tissue was then centrifuged at 4°C, 16000 x g for 15 minutes. Then, tissue samples were diluted 1 in 10, and a BCA assay was performed to calculate the protein concentration needed for the mass spectrometer. Samples were washed in ice-cold acetone to precipitate the proteins, then suspended in lysis buffer (*see "Lysis buffer for mass spectrometry"*) at 95 celsius for 5 mins. Proteins were then denatured in urea and alkylated

using TCEP followed by addition of IAA. Proteins also underwent double digestion by the addition of Lys-C protease and trypsin, resulting in peptides. The peptides were acidified in 100% trifluoroacetic acid (TFA) and then eluted with 50% acetonitrile (ACN) before placing in the LC-MS/MS. Samples were prepared with the help of Grant Marshall and Roopesh Krishnankutty (postdoctoral researchers).

Liquid chromatography then separated peptides by differences in the size, adsorption, and partitioning, and ionized peptides to analyse changes in ion intensity and peak heights. Mass spectrometry analysed differences in the mass to charge ratio (m/z) of ionized peptides for peptide identification. A reference database linked identified peptides to their corresponding proteins. Identified proteins were then quantified by comparing peak heights and spectral counting (Zhu et al., 2017). Following peptide identification, proteins were mapped based on peptides, and the raw data was processed and normalized in the proteomics pipeline DIA/NN for further statistical and bioinformatics analyses.
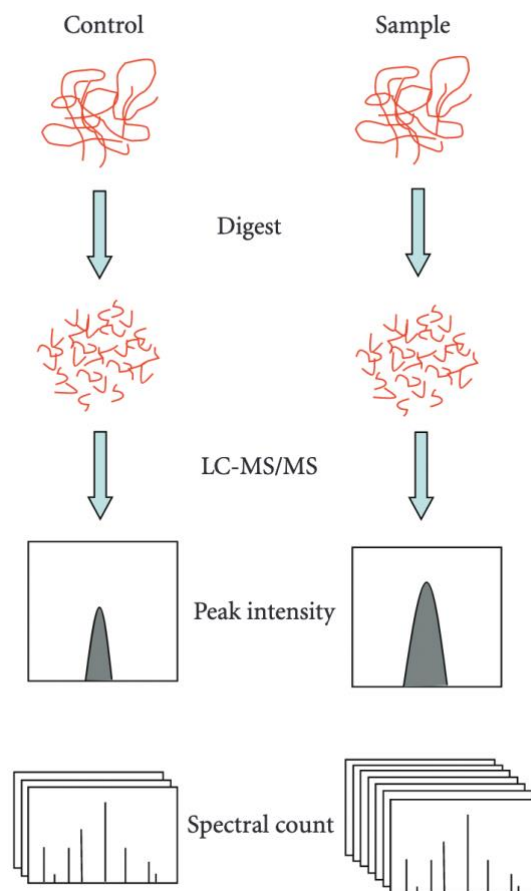

Figure 5: An overview of label-free quantification mass spectrometry (LC-MS/MS). *Different samples undergo digestion separately. Then, proteins were separated by liquid*

chromatography, and mass spectrometry analyses the mass to charge ratios (m/z) of ionized peptides. Proteins were quantified by a comparison of peak intensity and spectral count. This technique was applied for differential expression analysis of the eEF1A2$^{E122K/E122K}$ mouse brain proteome. Image taken from: (Zhu et al., 2010).

2.2.7 Proteomics pipelines

For the interactome analysis in HEK293 cells, the AP-MS raw data was run on Fragpipe with integrated software, such as Philosopher, for the post-processing of results. The Uniprot human proteome was uploaded as a reference for peptide identification and quantification of MS/MS data. Fragpipe is open access and can be downloaded for free at https://fragpipe.nesvilab.org/.

For the differential expression analysis on mouse tissue, the software pipeline DIA/NN performed normalization, protein quantification, and PTM identification. The mouse proteome downloaded from Uniprot was uploaded as a reference for peptide identification (Wang et al., 2021). Roopesh Krishnankutty (postdoctoral researcher) ran the PTM analysis on DIA/NN. Identified PTMs were assigned an identifier from the UNIMOD database, which is free and accessible at: https://www.ebi.ac.uk/ols/ontologies/unimod. DIA/NN is free and accessible to download at https://github.com/vdemichev/DiaNN/releases/tag/1.8.1.

2.2.8 Bioinformatics analyses

The Gene Ontology (GO) analysis was performed on R studio using packages biomaRt and enrichplot to analyse and visualize enriched biological pathways using the biomaRt database. The STRING analysis was conducted by selecting the statistically significant genes for analysis against a reference gene list, which consisted of all the proteins detected by mass spectrometry. STRING is free and accessible at: string-db.org/.

2.2.9 Statistical tests

All statistics and bioinformatics analyses were performed in R studio using packages tidyverse, plotly, htmlwidgets, clusterProfiler, limma, rstatix, ggpubr, biomaRt, ggrepel, enrichplot, and

DOSE. A Wilcoxon-Rank sum test was conducted to compare the medians of non-parametric data, with the null hypothesis stating both datasets have equal medians. A Kruskal Wallis test was another non-parametric test performed to test whether there was a statistically significant difference between the medians of three or more independent treatment groups. Welch's one-way ANOVA was used to compare the medians of heteroscedastic data, whereas a one-way ANOVA compared the means of homoscedastic data with a normal distribution. The Games-Howell post-hoc test was conducted on heteroscedastic data with a normal distribution. The Games-Howell test calculates confidence intervals for the differences between group means and whether the differences are statistically significant. For the analysis of mass spectrometry data, a 2-sample t-test was performed to calculate the mean differences in expression between mutant and WT for each protein. A p-value of >0.05 was considered statistically significant.

Chapter 3: Results

3.1 Mutations D252H and E122K have different eEF1A2 tissue-specific expression levels in mouse tissue

One of the aims of this project is to investigate how different mutations affect eEF1A2 expression levels in different tissues, following in from results in the lab that suggested that E122K and D252H had different effects on protein levels in different tissues. First, eEF1A2 expression in mouse heart tissue was compared in D252H and E122K mutants to WT. No P333L mutant mouse tissue was available for western blotting, which is one of the reasons for conducting transfections in HEK293T cells (*Figures 6-9*). Heart and brain tissue were chosen to be analysed on western blotting because eEF1A2 is only expressed postnatally in heart tissue, whereas brain tissue expresses both eEF1A1 and eEF1A2. Therefore, comparing eEF1A2 expression in both tissues could highlight tissue-specific differences suggestive of an interaction between the mutant and tissue. The results show increased eEF1A2 expression in homozygous D252H mutants compared to WT mouse heart tissue, and a trend suggests a slight increase in eEF1A1 expression, but no statistical significance was found (*Figures 6 and 9*). Initial western blots comparing E122K.eEF1A2 expression in heterozygous mouse heart

tissue showed no significant difference in expression relative to wildtype (*Figure 7*). However, eEF1A2 expression was significantly decreased in E122K homozygote mouse heart tissue highlighting the different eEF1A2 expression patterns in E122K and D252H mutant heart tissue (*Figure 8*; *Table 8*). Moreover, eEF1A1 expression was not significantly altered across both mutants, suggesting that differences in expression patterns are specific to eEF1A2, and the mutations, D252H and E122K, do not compromise the developmental switch from eEF1A to tissue-specific expression of eEF1A1 and eEF1A2. Previous results found E122K.eEF1A2 expression relative to WT is lower in the brain and skeletal muscle (*Table 2*), whereas D252H.eEF1A2 expression was lower in the brain and higher in muscle, suggesting protein stability is not solely attributed to a specific mutation. Similarly, this project found mouse heart tissue displayed decreased E122K.eEF1A2 expression in mouse homozygotes and increased D252H.eEF1A2 expression like in the mutant mouse skeletal muscle, indicating mutant eEF1A2 may display a tissue-specific interaction. As mentioned above, Marshall et al. (2022) found sex-specific differences in eEF1A2 expression across E122K mutants; however, this thesis reports no statistically significant sex-specific differences in E122K.eEF1A2 expression across mutants, which could be partly due to low sample sizes (*Table 8*).
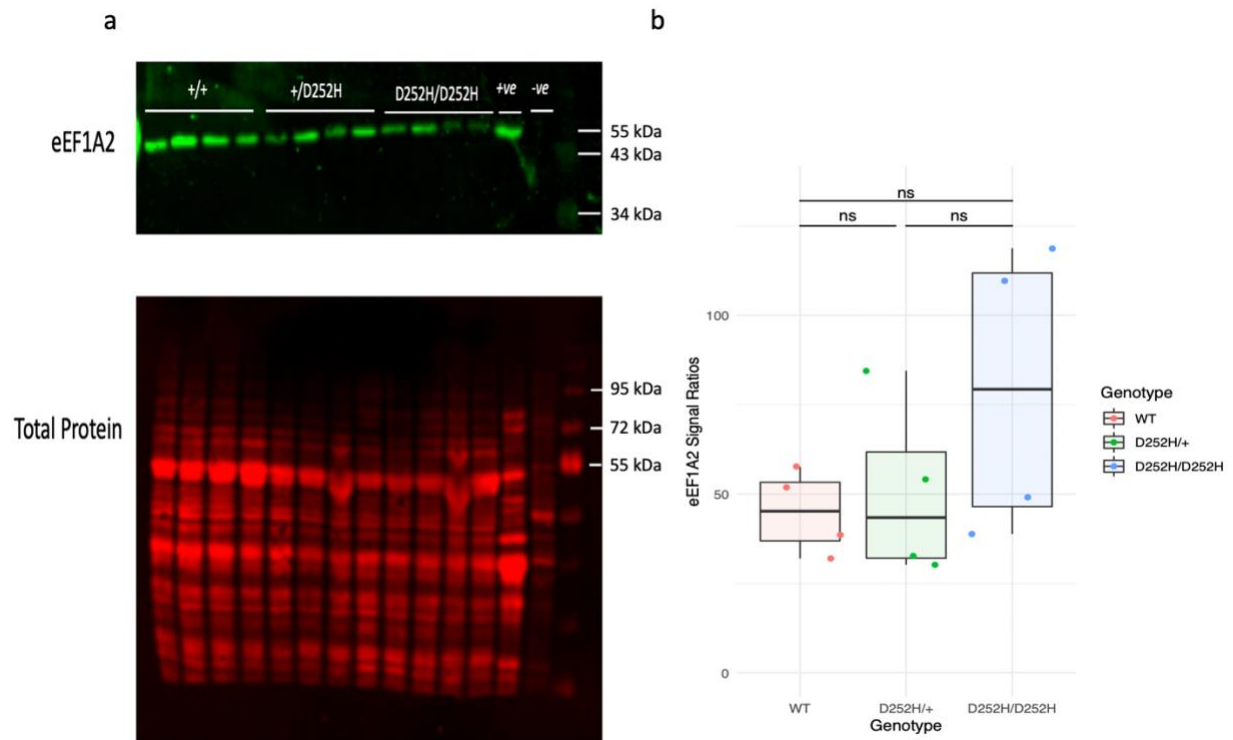
Figure 6: eEF1A2 expression in mouse D252H mutant heart tissue. *(a) Quantification of eEF1A2 was normalised to total protein stain. (b) Quantified eEF1A2 expression was not significantly different across D252H mutants compared to wildtype (Kruskal-Wallis: chi-squared = 11, df = 11, p-value = 0.4433). Wildtype muscle was used as a positive control, and the negative control is wasted mouse brain. Sample size (n): 12 (4 per genotype). Statistical significance: ns = non-significant, * p ≤ 0.05. Samples were from P22 mice.*
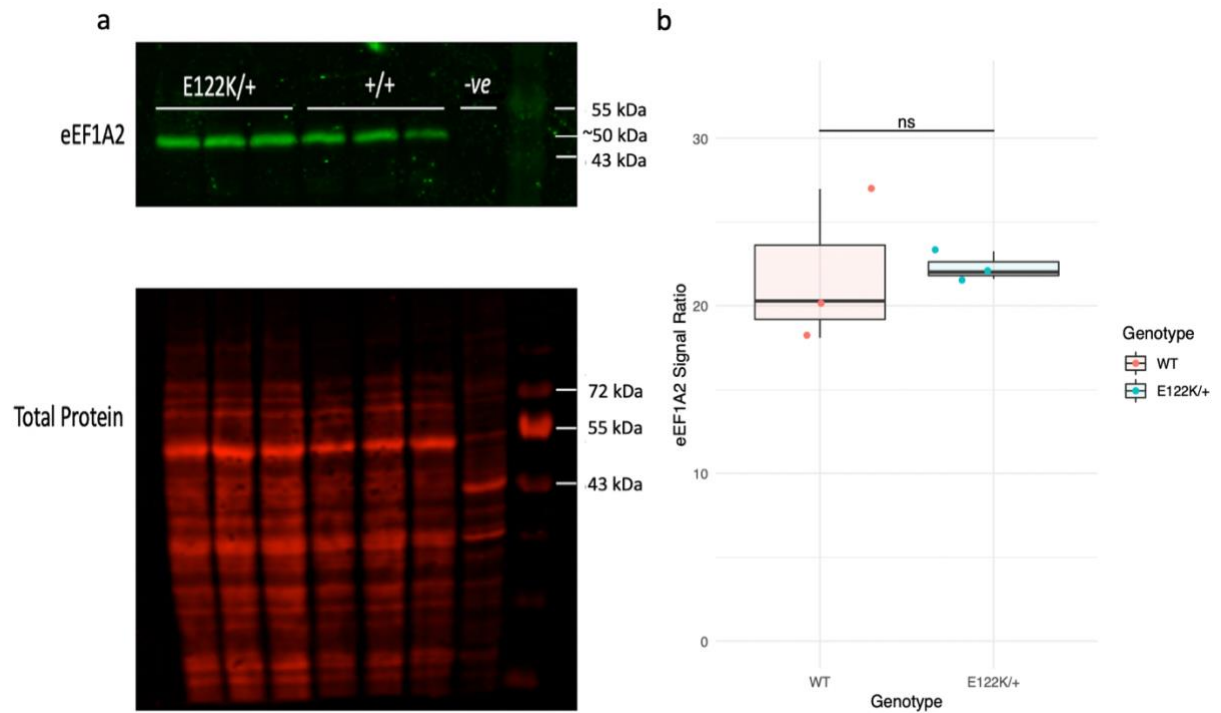
Figure 7: eEF1A2 expression in E122K mutant heterozygote mouse heart tissue. *(a) Quantification of eEF1A2 was normalised to total protein stain. (b) E122K heterozygotes did not show a statistically significant difference in eEF1A2 expression compared to wildtypes (Wilcoxon rank-sum test: W = 6, p-value = 0.7). Wasted mouse brain was used as the negative control (-ve). Sample size (n): 7. Statistical significance: ns = non-significant, * p ≤ 0.05. Samples are from P30 mice.*
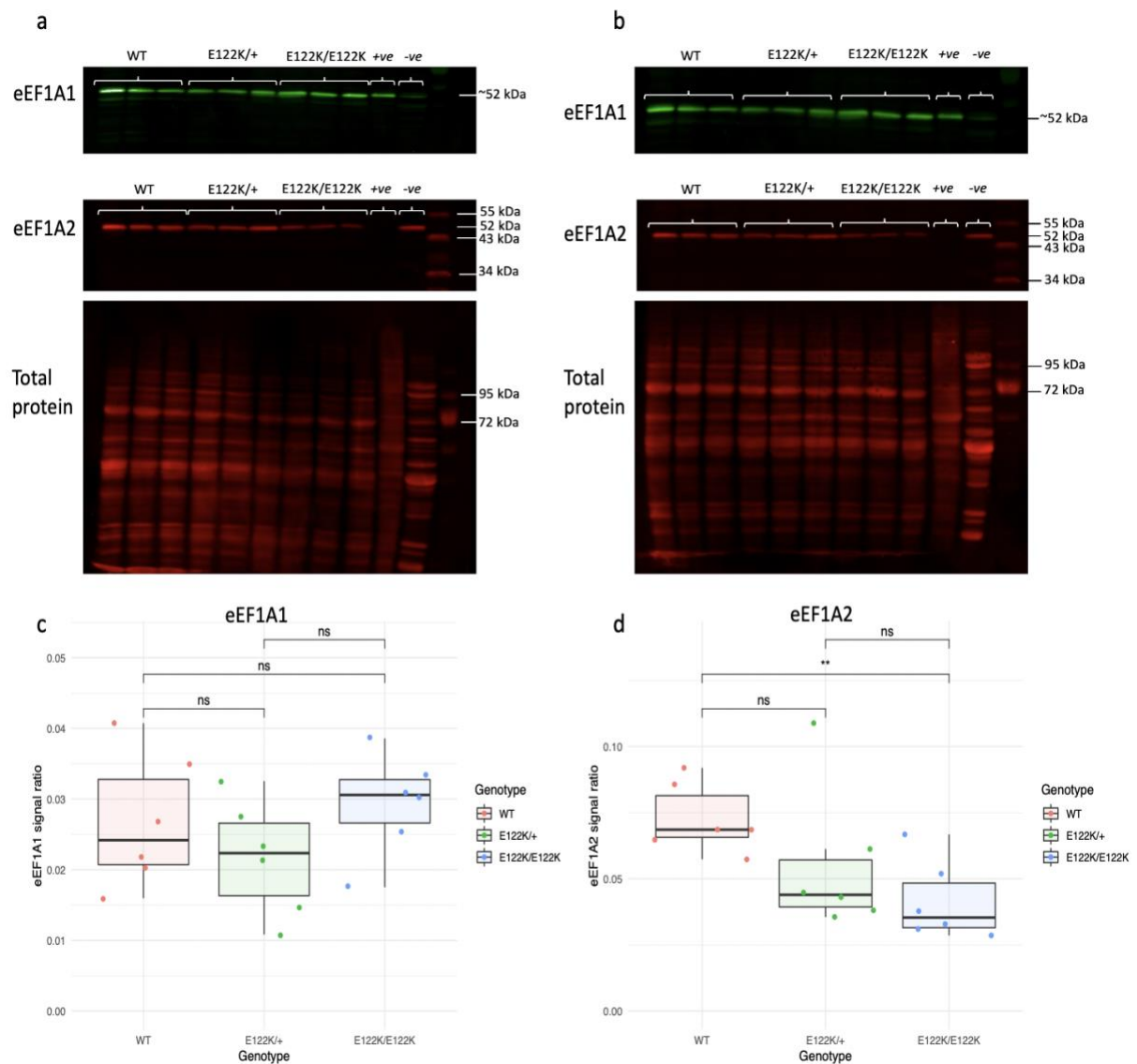
Figure 8: eEF1A2 expression in E122K heterozygote and homozygote mutant mouse heart tissue. *eEF1A2 (shown in red) and eEF1A1 (shown in green) expression in male (a) and female (b) mice was quantified and normalized to TPS. (c) No significant differences in eEF1A1 expression were found across E122K mutants (Kruskal-Wallis: chi-squared = 2.33, df = 2, p-value = 0.31). (d) eEF1A2 expression was significantly lower in homozygotes compared to wildtype mice (Kruskal-Wallis: chi-squared = 7.68, df = 2, p-value = 0.02). Wasted mouse brain was used as the negative control (-ve) for eEF1A2, whereas wildtype muscle was a positive control for (+ve) eEF1A1 expression. Sample size (n): 3 per genotype in each sex (total: 18). Statistical significance: ns = non-significant, * p ≤ 0.05, ** p ≤ 0.01. Samples are from P24 mice.*
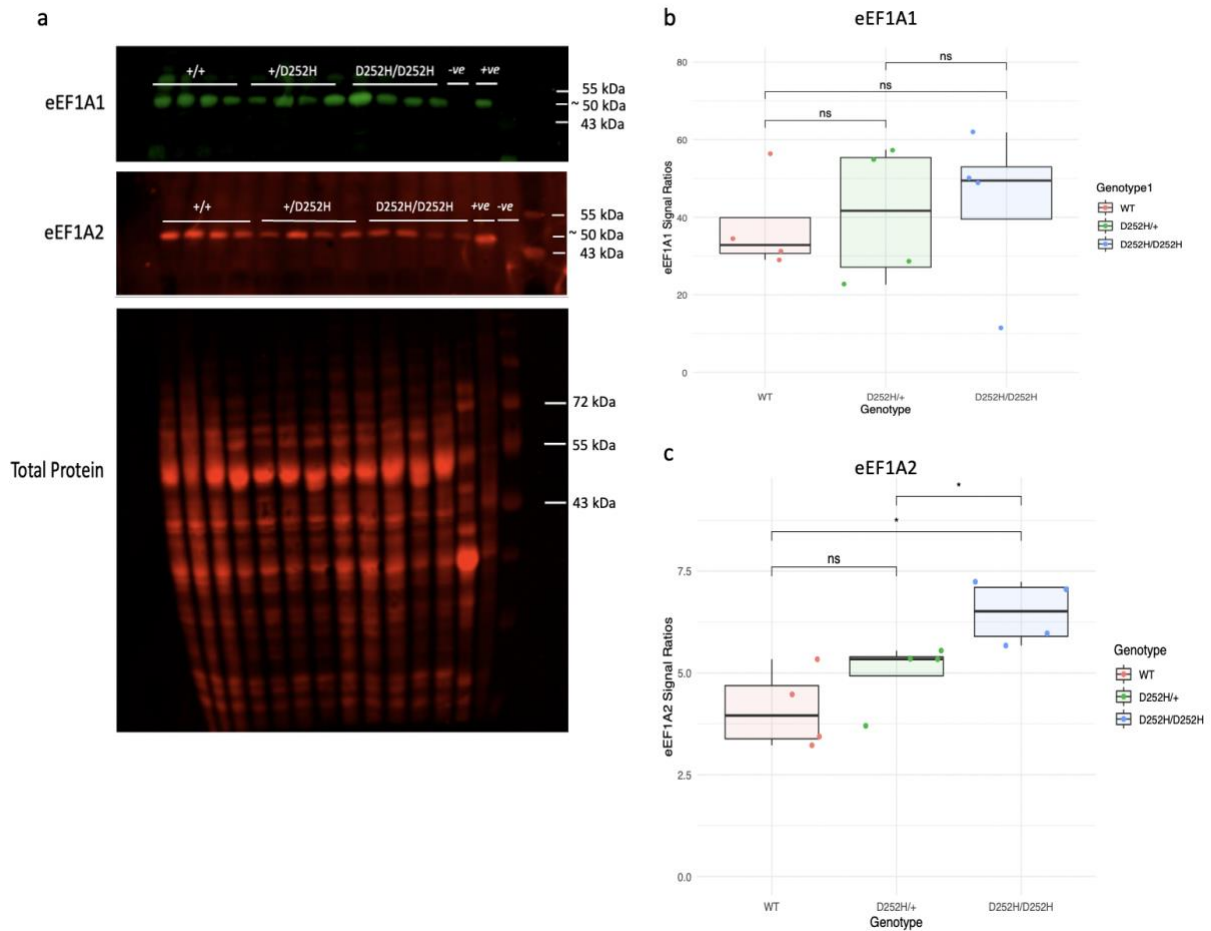
Figure 9: Probing for eEF1A1 and eEF1A2 expression in D252H mutant mouse heart tissue.
(a) eEF1A1 and eEF1A2 expression was analysed on western blotting to observe any differences in expression in eEF1A2 mutant heart tissue compared to wildtype. Quantification of eEF1A1 and eEF1A2 was normalised to total protein stain. (b) eEF1A1 expression did not show a statistically significant difference across genotypes (Kruskal-Wallis: chi-squared = 11, df = 11, p-value = 0.44). (c) Increased eEF1A2 expression was found in D252H/D252H relative to wildtype (Wilcoxon rank-sum test: W = 16, p-value = 0.03) and D252H/+ relative to D252H/D252H (Wilcoxon rank-sum test: W = 0, p-value = 0.03). Wildtype muscle was a negative control for eEF1A1 expression and wasted mouse brain was the negative control for eEF1A2 expression. Sample size (n): 12 per boxplot (4 per genotype). Statistical significance: ns = non-significant, * p ≤ 0.05. Samples are from P22 mice.

Table 8: A comparison of eEF1A2 expression patterns affected by the mutations D252H and E122K

Genotype	Change in eEF1A2 expression (relative to WT = 1)		
	Brain	**Muscle**	**Heart Muscle**
E122K/+	NS (M + F)	0.54 (M) NS (F)	NS (M+F)
E122K/E122K	0.58 (M) NS (F)	0.17 (M) 0.51 (F)	0.57 (M+F)
D252H/+	0.80	NS	NS (M+F)
D252H/D252H	0.60	1.6	1.27 (M+F)

This table is a modified version of table 1 that includes a summary of the results found in *Figures 6-9*. The opposing eEF1A2 expression patterns in mutant mouse tissue might suggest an interaction between the mutant eEF1A2 and tissue environment. This project didn't find any significant sex-specific differences in eEF1A2 mutant expression in the mouse heart. NS = Not significant. (M) = male, (F) = female.

3.2 Comparing eEF1A2 expression and stability across mutant eEF1A2 transfected HEK293T cells

In this section, the results of transfections in HEK293T cells and MG132 treatment will be discussed. Previous studies found that mRNA transcripts and RNA levels were stable in E122K.eEF1A2 and D252H.eEF1A2 mutant mouse brain, respectively, compared to WT mice (Davies *et al.*, 2020; Marshall 2022). Therefore, it's likely that missense mutations cause unstable eEF1A2. The aim of the transfections was to compare eEF1A2 expression in E122K, D252H, and P333L mutants to WT, whereas the aim of treating cells with MG132 proteasome inhibitor was to determine if missense mutations result in reduced eEF1A2 stability by comparing eEF1A2 expression to WT across mutants. MG132 inhibits ubiquitin-proteasome degradation of abnormal cytosolic proteins, such as eEF1A2, by interfering with the transition state analogue and affecting protease activity (*Figure 10*)(Kjaer et al., 2001; Lee and Goldberg, 1998). A study revealed that MG132 treatment stabilized the expression of homozygous mutant TRAPPC6A protein, attributed to a neurodevelopmental syndrome, by transfecting HEK293T cells with the mutant protein. Moreover, another study investigated global protein stability by treating HEK293T cells with MG132 (Mohamoud et al., 2018; Yen et al., 2008). Therefore, it was reasoned that MG132 could potentially have a similar effect on eEF1A2

mutants. Both experiments studying eEF1A2 expression across mutant transfected cells and the effects of MG132 on eEF1A2 protein stability were conducted at the same time to maximize time efficiency.
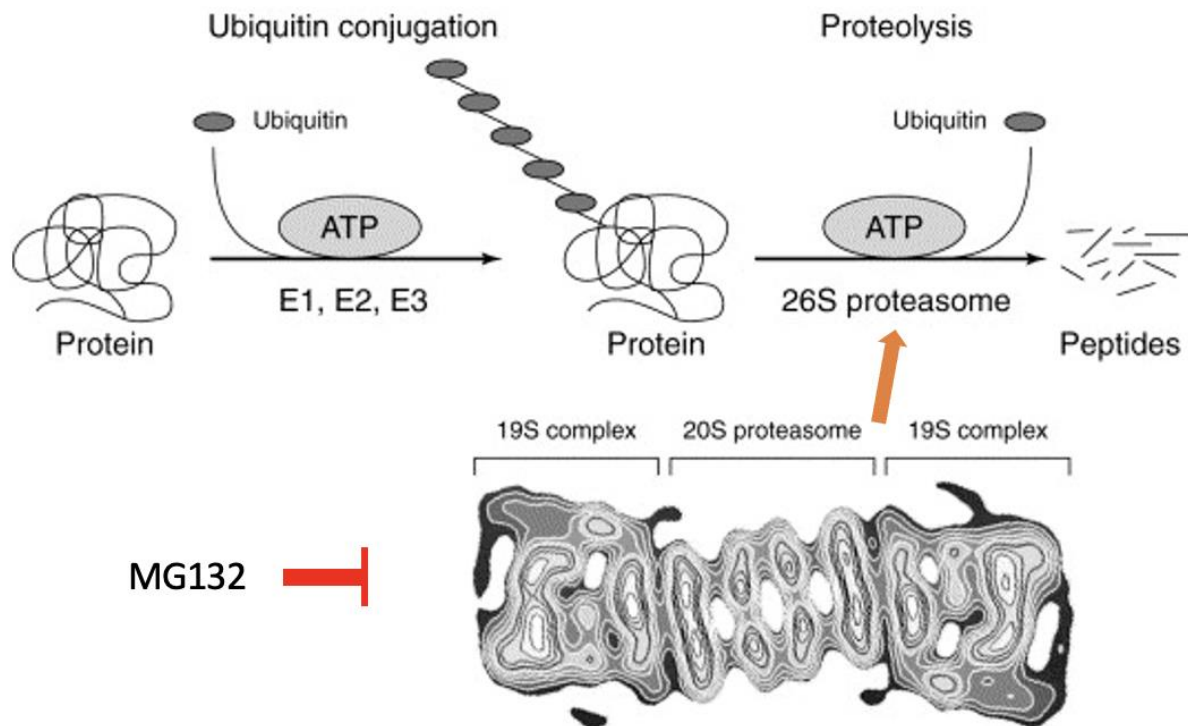
Figure 10: An overview of ubiquitin-proteasome mediated degradation. *In mammals, proteins are tagged for degradation by ubiquitin conjugation, an ATP-dependent reaction catalysed by the enzymes* ubiquitin-activating enzyme (E1), ubiquitin carrier protein (E2) and ubiquitin–protein ligase (E3)*. Then, a series of proteolytic reactions in the 26S proteasome, composed of the 19S complexes and 20S proteasome, cleaves the proteins into peptides. MG132 inhibits the 26S proteasome by the formation of a transition state analogue. Image adapted from: Lee and Goldberg (1998).*

3.2.1 eEF1A2 expression is lower in E122K, D252H, and P333L mutants relative to WT

Following the findings of different eEF1A2 expression patterns in D252H and E122K mutated eEF1A2, transfections were conducted on HEK293T cells with expression vectors containing E122K, D252H, and P333L mutant full-length eEF1A2. The HEK293T cell line was chosen because of its easy maintenance in the laboratory, high transfection efficiencies in comparison to other cell lines, and do not express endogenous eEF1A2 that could confound results studying the effects of the synthetic eEF1A2 variant (Thomas and Smart, 2005). The synthetic eEF1A2 variant was expressed in HEK293T cells under the cytomegalovirus (CMV) promoter, which hijacks the HEK293T cell's protein synthesis machinery to force the translation of the synthetic eEF1A2 variant in cells. T2A, derived from the *Thoseaasigna* virus, forms part of a class of self-cleaving 2A peptides that enable the simultaneous expression of multiple genes in mammalian cell lines and was used in this project to express mCherry and eEF1A2 (*Figure 11*)(Kim et al., 2011). During translation in transfected HEK293T cells, mCherry and eEF1A2 are in the same transcript but are cleaved due to the self-cleaving peptide T2A producing separate proteins that appear as separate bands in western blotting. The fluorescent protein mCherry was used across all transfections as its immunofluorescence can assess the transfection efficiency in cells. Experimental controls included wildtype muscle as a positive control of eEF1A2, wasted brain as a negative control of eEF1A2 to ensure eEF1A2 antibody specificity; and empty vectors to ensure eEF1A2 expression was the result of transfection with plasmids containing eEF1A2 mutant DNA (i.e., a negative control).
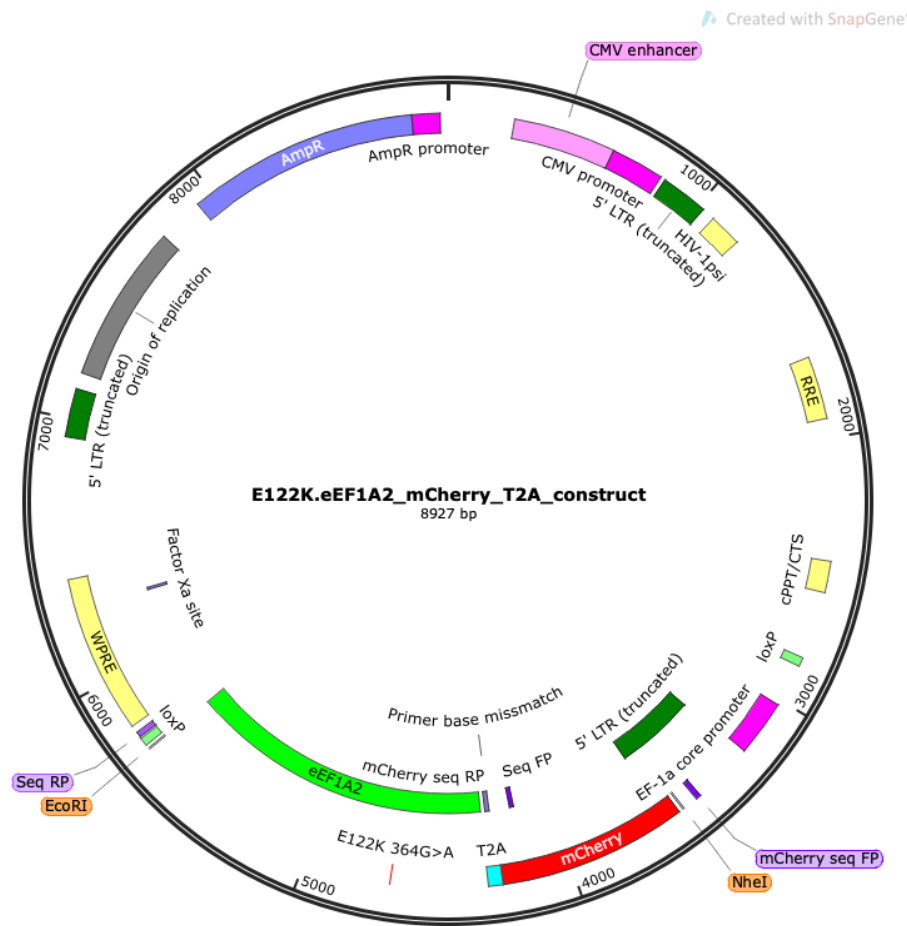
*Figure 11: Map of the E122K.eEF1A2 mCherry construct. Full length eEF1A2 cDNA containing the E122K missense mutation (364G>A). The self-cleaving peptide T2A is located between mCherry and eEF1A2, so they are translated into two separate proteins under the CMV promoter. The same constructs were used for P333L and D252H transfections, except the location and mutation differed to E122K. Image created on SnapGene (*www.snapgene.com).

Following transfections in HEK293T cells, the expression of eEF1A2 was quantified by western blotting comparing mutants to wildtype transfected cells. Faint bands were observed in EV controls, which may be the result of eEF1A2 antibody cross reactivity with eEF1A1 due to their high sequence similarity and structure (*Figures 12-14*). The mCherry signal was weak, particularly in blots probed for eEF1A2 and mCherry antibodies on the same channel that had a strong background signal (*Figure 12*). Therefore, subsequent western blots had mCherry and eEF1A2 antibodies probed on separate channels. Every replicate western blot showed an mCherry signal indicative of successful transfection in HEK293T cells, but a few western blots still showed relatively weak mCherry band signals, which may be the result of low antibody concentration or poorer efficiency of transfer (*Figures 12-14*). The expression of eEF1A2 was visibly lower in mutants compared to wildtype; however, small sample sizes and outliers

found no statistical significance except for P333L (*Figures 15-17*). In figures 11-13, each replicate transfection is colour-coded to better interpret the data, and the third replicate (shown in red) might be an outlier skewing the statistical significance in E122K and P333L transfections. However, the second and third replicates in D252H transfections (shown as green and red, respectively) have very similar expression levels (*Figure 15*), which is consistent with the western blot images. Therefore, more significant differences in E122K.eEF1A2 and P333L.eEF1A2 expression relative to wildtype are suggested.

A more qualitative comparison (*Table 9*) was included to further analyse the differences in eEF1A2 expression levels across mutants relative to wildtype. Like the previous results discussed in figures 15-17, the largest differences in eEF1A2 expression between wildtype and mutants were observed in E122K and P333L western blots with a 61.5% and 42.1% difference, respectively (*Figures 12-14; Table 9*). In comparison, there's a much smaller difference in D252H.eEF1A2 expression relative to wildtype. The decreased eEF1A2 expression in E122K and D252H transfections in HEK293 cells resembled the decreased expression observed in muscle and brain tissue, respectively (*Table 2*). Therefore, E122K and D252H have a similar decreasing pattern of eEF1A2 expression in HEK293 transfections but have differing expressions in mouse brain tissue, which may suggest that the tissue environment influences the expression of mutant eEF1A2.

Table 9: The percentage difference in eEF1A2 expression between mutant and wildtype transfected HEK293 cells.

Mutation	Mutant average signal ratio	Wildtype average signal ratio	Percentage difference (%)
E122K	0.15	0.39	61.5%
D252H	0.18	0.21	14.3%
P333L	0.11	0.19	42.1%

The signal ratio was used as a measure of expression and was calculated on western blot images in Image Studio Lite and normalized to total protein stain. Sample size (n): 4 wildtype per transfection replicate; 4 per E122K transfection replicate; 4 per D252H transfection replicate, and 4 per 2 P333L transfection replicates. The results from the first P333L transfection were excluded because MG132 treatment visibly rescued P333L.eEF1A2 expression. All other groups were included as MG132 treatment showed no difference in eEF1A2 expression; therefore, it was not considered a confounding factor.

3.2.2 MG132 treatment had no effect on eEF1A2 protein stability

Following the transfections in HEK293T, cells were treated with DMSO (control) and proteasome inhibitor MG132 to determine if missense mutations reduce eEF1A2 stability. Since MG132 inhibits ubiquitin-proteasome degradation of unstable and/or misfolded proteins, an increase in stability seen after cells treated with MG132 could suggest that the mutation has a destabilizing effect on eEF1A2. In western blotting, increased fluorescence in transfected mutant HEK293T cells following MG132 treatment, indicating higher eEF1A2 expression compared to DMSO-treated cells, would indicate altered eEF1A2 stability. The western blot results initially suggested that mutations D252H and E122K may be more stable than P333L because eEF1A2 expression was higher in P333L.eEF1A2 cells treated with MG132 compared to control (DMSO) P333L.eEF1A2. However, no statistical significance was found (*Figure 17*) as this observation wasn't consistent across all P333L.eEF1A2 transfections. Overall, MG132 treatment didn't significantly rescue eEF1A2 expression in mutants, which could be due to low concentrations of MG132 in addition to small sample sizes.
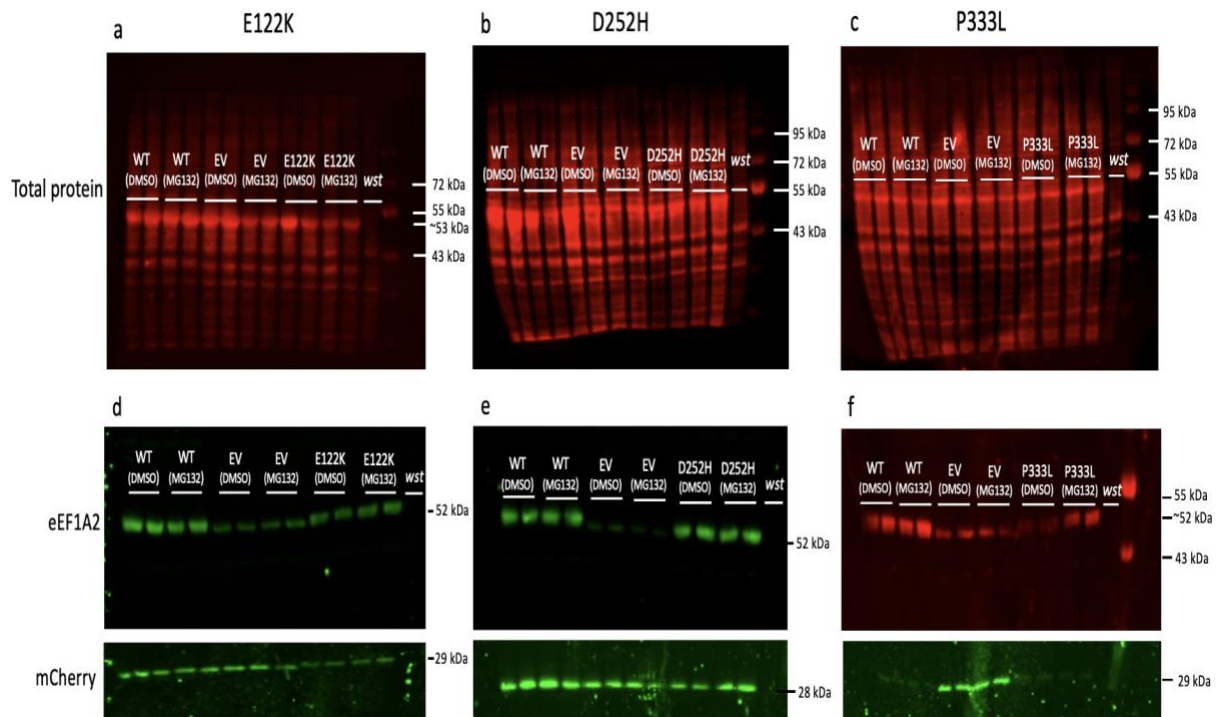
Figure 12: First HEK293 cell transfections with E122K, D252H, and P333L mutant plasmids. *(a-c) shows the total protein stain (TPS) of each transfection with E122K, D252H, and P333L mutant plasmids. Quantification of eEF1A2 was normalized to TPS. (d-f) eEF1A2 expression across genotype and treatment groups is shown by a green or red fluorescent signal. The bottom bands are mCherry signal (green). Empty plasmids (EV) were transfected in cells as a negative control for eEF1A2 expression and wasted brain (wst) was another negative control for eEF1A2 expression* to ensure eEF1A2 antibody specificity. *Cells transfected with either wildtype (WT), EV, or P333L plasmids were treated with DMSO as a control to cells treated with proteasome inhibitor MG132.*
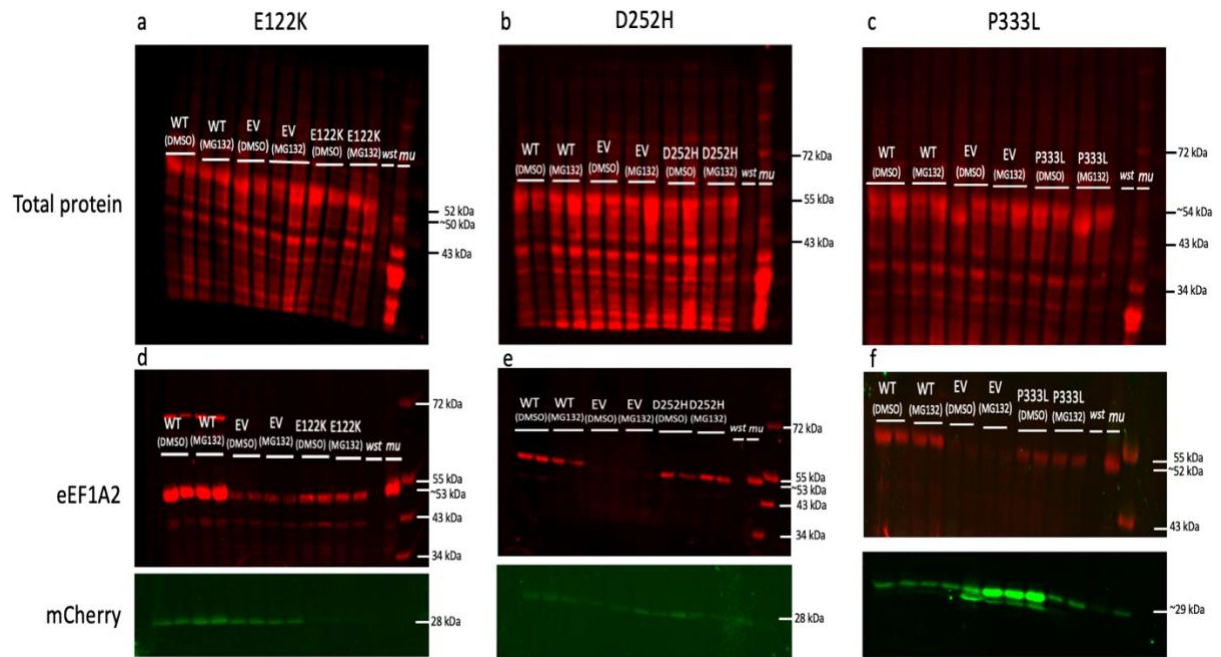
Figure 13: Second set of HEK293 transfections with E122K, D252H, and P333L mutant plasmids. *(a-c) Quantification of eEF1A2 was normalized to TPS. (d-f) eEF1A2 expression across genotype and treatment groups is shown by a red fluorescent signal. The bottom bands are mCherry signal (green). Empty plasmids (EV) were transfected in cells as a negative control for eEF1A2 expression, and wildtype muscle (mu) was a positive control for eEF1A2 expression. Wasted brain (wst) was used as another negative control for eEF1A2 expression, although it was not necessary to include as the EV samples also control for eEF1A2 expression.*
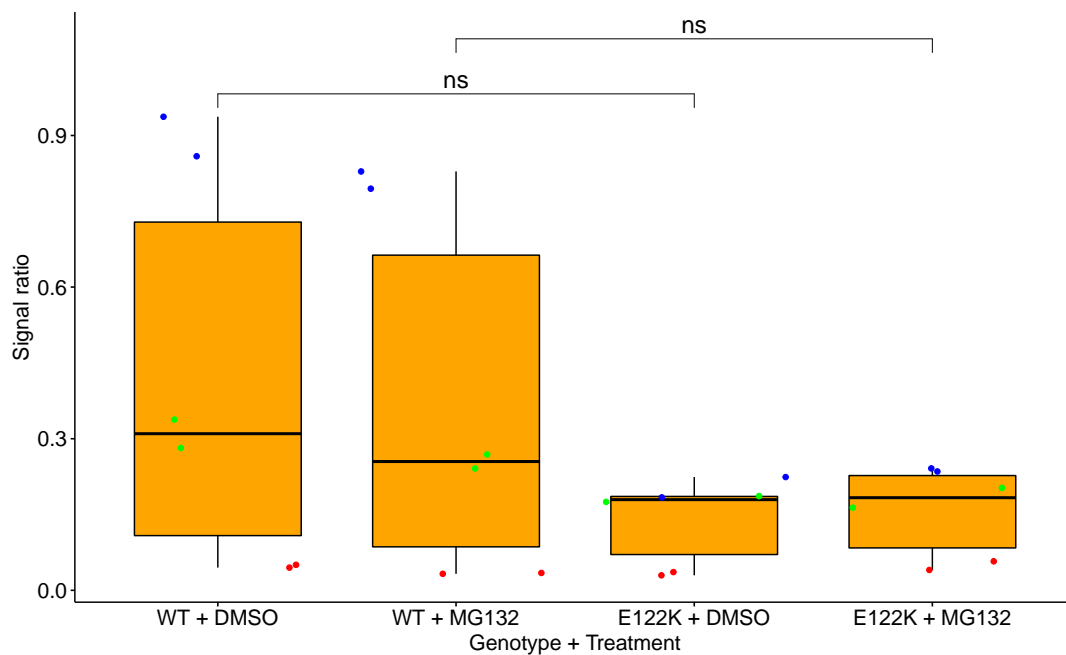
Figure 15: Comparing E122K.eEF1A2 expression to wildtype. eEF1A2 expression appears to be higher in wildtype transfected cells compared to E122K transfected cells but no statistical significance was found (Welch's one-way ANOVA: F = 1.472, p = 0.28). Sample size (n): 6 per boxplot (total = 24). Total no. of experimental replicates = 3. Each experimental replicate is distinguished by colour. Blue = first transfection, green = second replicate, and red = third replicate. Statistical significance: ns = non-significant, * p ≤ 0.05. Samples are from HEK293 transfected cells.
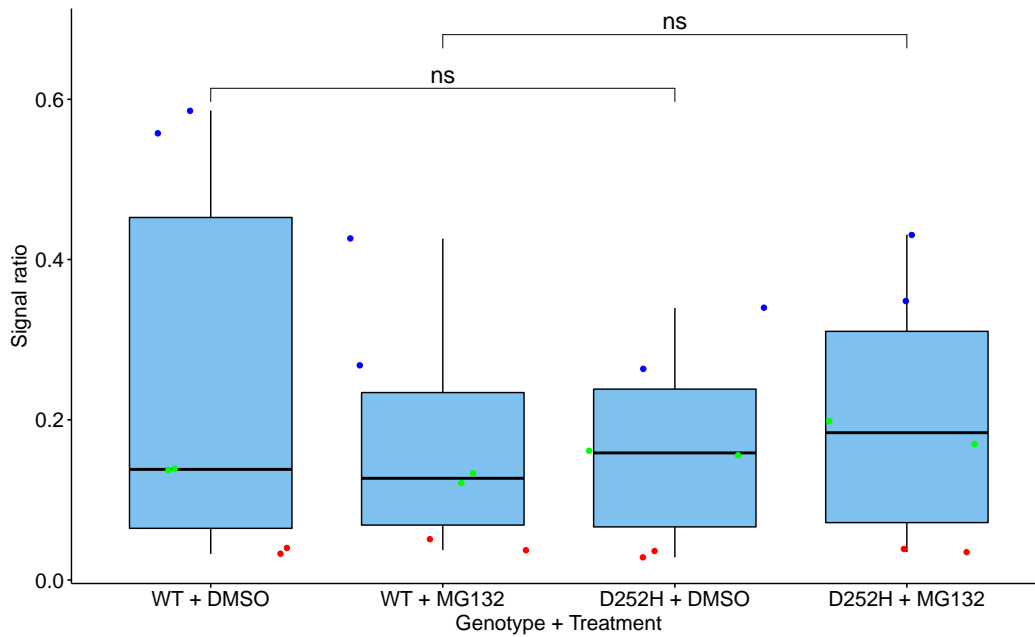
Figure 16: Comparing D252H.eEF1A2 expression to wildtype*. Wildtype control cells (WT +
DMSO) have a slightly higher eEF1A2 expression but isn't statistically significant compared to
the other treatment groups (Welch's one-way ANOVA: F = 0.197, p = 0.896). Sample size (n):
6 per boxplot (total = 24). Total no. of experimental replicates = 3. Each experimental replicate
is distinguished by colour. Blue = first transfection, green = second replicate, and red = third
replicate. Statistical significance: ns = non-significant, * p ≤ 0.05. Samples are from HEK293
transfected cells.*
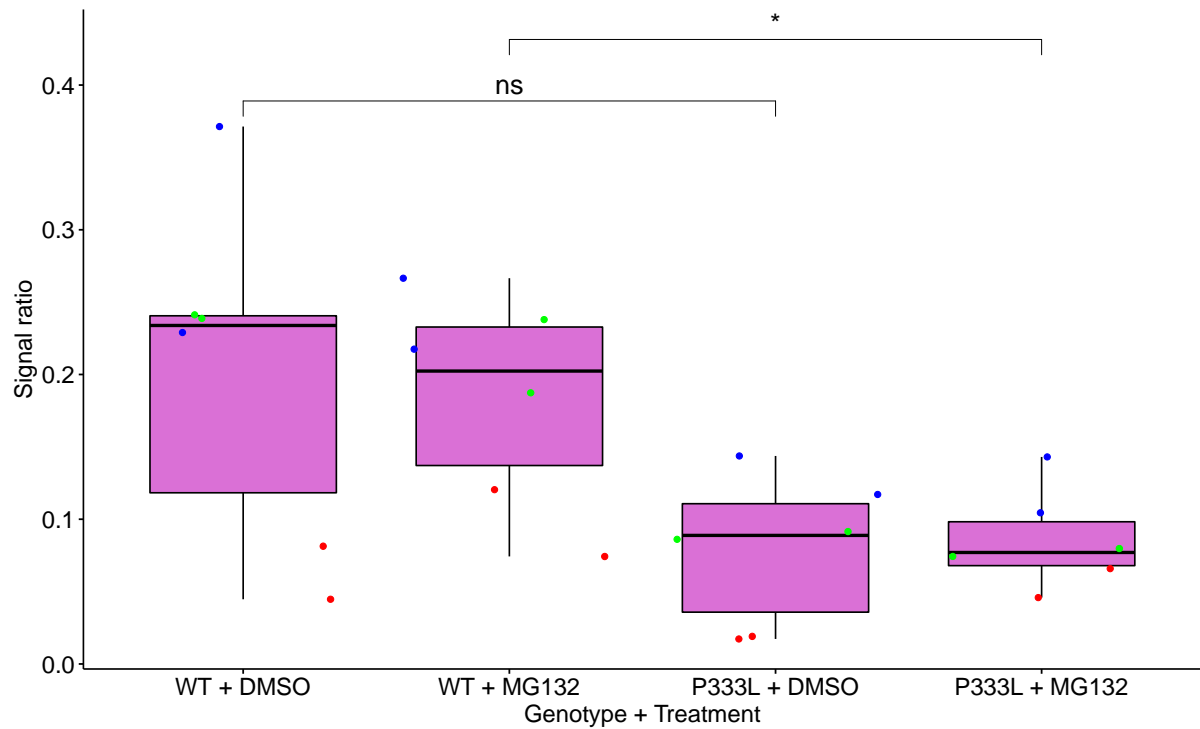
Figure 17: Comparing P333L.eEF1A2 expression to wildtype. *eEF1A2 expression is slightly higher in wildtype transfected cells with expression in WT + MG132 cells being significantly higher than P333L + MG132 treated transfected cells (p = 0.041) (One-way ANOVA: F= 4.19, p=0.019). Sample size (n): 6 per boxplot (total = 24). Total no. of experimental replicates = 3. Each experimental replicate is distinguished by colour. Blue = first transfection, green = second replicate, and red = third replicate. Statistical significance: ns = non-significant, * p ≤ 0.05. Samples are from HEK293 transfected cells.*

3.3 Identifying differences in the E122K.eEF1A2 mutant interactome

The western blot results showed that HEK293 cells, which don't express endogenous eEF1A2, can be successfully transfected with eEF1A2 DNA-containing plasmids, which was performed for E122K.eEF1A2 interactome analysis in affinity purified mass spectrometry (AP-MS). However, the P333L.eEF1A2 interactome could not be analysed because the mutation was found to be too unstable in transfections despite increasing the amount of P333L.eEF1A2 DNA transfected in HEK293T cells. An interactome analysis was conducted to analyze and identify all the proteins in a cell that interact with eEF1A2 and are altered by the presence of the E122K mutation since previous studies had already demonstrated that D252H alters the eEF1A2 interactome. For example, D252H was found to prevent binding of the eEF1B complex, which functions in the GTP exchange that is needed for the delivery of acetylated tRNAs to the ribosome (McLachlan, Sires, and Abbott, 2019; Davies et al., 2020). Comparing different mutations in eEF1A2 to the WT interactome can give insight into molecular disturbances in the microenvironment and its molecular pathways. This strategy was tested as a potential method for grouping mutations to better understand and target their effects on eEF1A2. To identify any changes in the E122K.eEF1A2 interactome, HEK293T cells transfected with eEF1A2^{E122K} expression vectors were analyzed by AP-MS (conducted by Roopesh Krishnankutty (postdoctoral researcher)) and bioinformatics analysis. The V5 tag was used for co-immunoprecipitation instead of mCherry because a cleavage site is translated in mCherry, leaving eEF1A2 untagged, whereas V5 will remain tagged to eEF1A2 and can, therefore, be used to pull down interacting proteins specifically. The eEF1A2-V5 construct was created by cloning the eEF1A2 cDNA sequence into the backbone of the pcDNA3.1-V5 vector (*Figure 18*). This method was effective in identifying the eEF1A2 molecular binding partners.
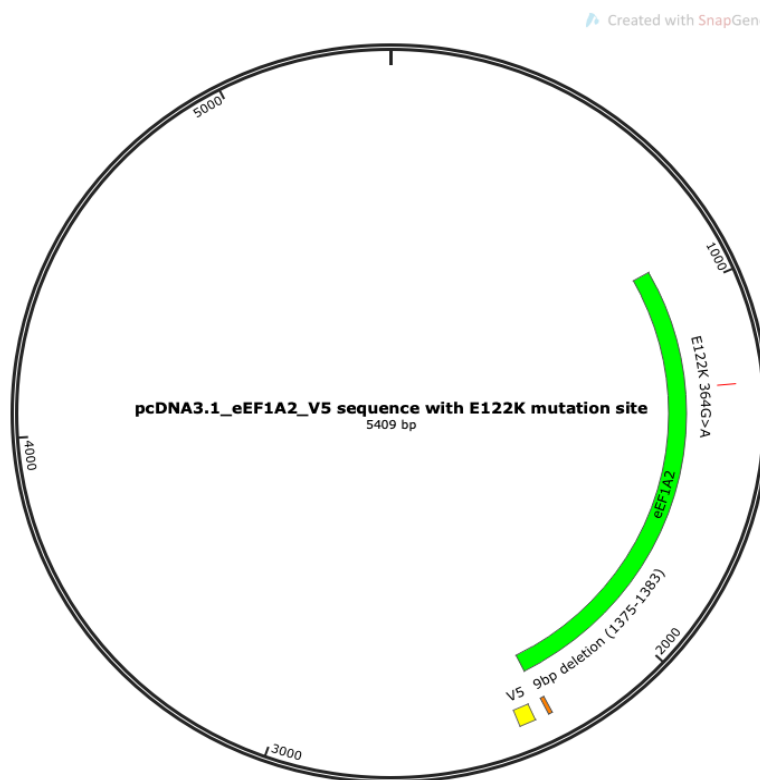
*Figure 18: Map of the eEF1A2-V5 construct transfected into HEK293 cells. The pc.DNA3.1-V5 vector cloned with full-length eEF1A2 cDNA containing the E122K missense mutation. Image created on SnapGene (*www.snapgene.com*).*

Following normalization conducted on the software pipeline Fragpipe, statistically significantly altered proteins were identified by conducting a two-sample t-test comparing the average MaxLFQ values of E122K and WT samples. MaxLFQ is the maximal peptide ratio extraction, an algorithm for the normalized quantification of label free mass spectrometry, which was generated from the software pipeline Fragpipe. A 2-sample t-test of the average MaxLFQ values across E122K and WT replicates was conducted to identify significantly altered eEF1A2-interacting proteins as the data met the 2-sample t-test statistical assumptions of random sampling, independence, normality, and homogeneity of variances. Random sampling and independence of mouse samples were handled by Grant Marshall (postdoctoral researcher). A quantile-quantile (Q-Q) plot found that both WT and E122K protein quantification groups' data distribution appeared relatively normal. A Q-Q-plot is a probability plot of the quantiles of sample data versus the theoretical quantile values from a normal distribution. However, a Shapiro-Wilk test for normality revealed that only the average WT MaxLFQ values were normally distributed, and no statistical significance was found in the

average E122K MaxLFQ values, which didn't appear obvious in the Q-Q plot. Therefore, there may have been outliers in the E122K group shown in the Q-Q plot, which altered the Shapiro-Wilk test's results. Potential outliers were expected in E122K mutants, however, as altered E122K proteins indicate the eEF1A2 interactome is altered. Despite the violation of normality in the E122K group, a two-sample t-test is robust to small violations in normality in larger sample sizes with no extreme outliers, which was observed in the Q-Q plot for E122K (*Figure 19*)(le Cessie et al., 2020; Sedgwick, 2015). Studies have recommended non-parametric tests for analyzing smaller datasets with sample sizes as the calculated p-values are smaller than those calculated by parametric tests, and this disparity increases with sample size (Fagerland, 2012; le Cessie et al., 2020). An F-test was also conducted to determine whether the variances of the average WT and E122K protein expression groups were equal and found the data was homoscedastic (F = 1.261, df = 159, p-value = 0.145). Thus, a 2-sample t-test was deemed an appropriate statistical test. A volcano plot was then created by applying the negative decadic logarithm ($-\log_{10}$) of the p-values and calculating the binary logarithm (log2) of the fold change, which is the log2 difference between mutant and WT MaxLFQ averages across replicates.
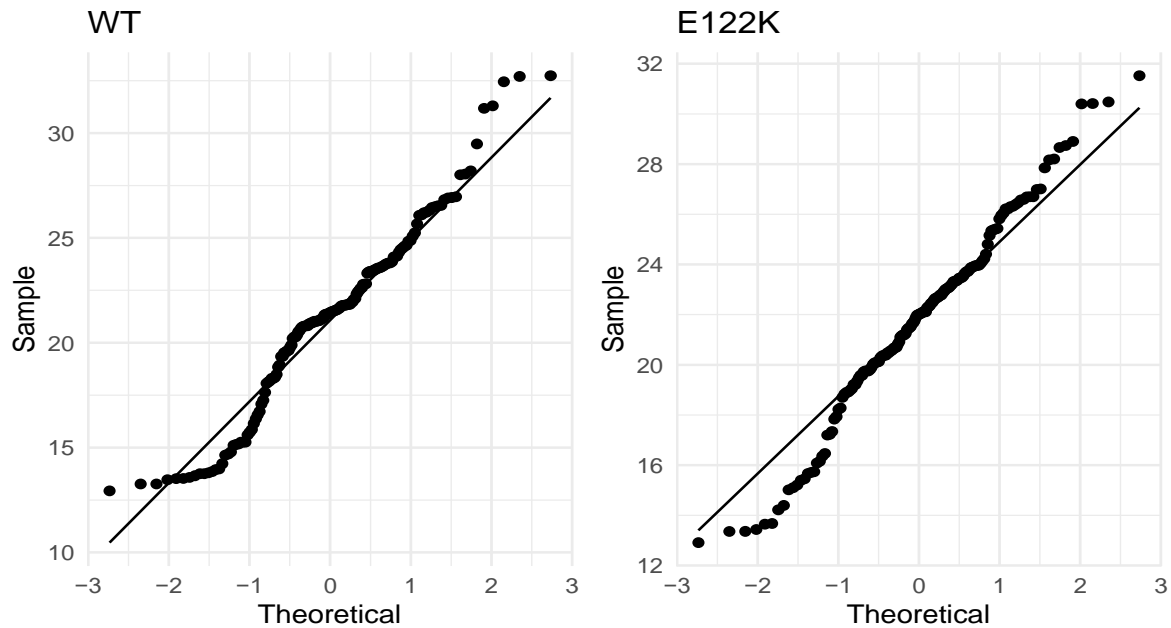
Figure 19: Q-Q-plots normality plots predict the data distribution. *A Shapiro-Wilk test for normality also confirmed WT protein expression was normally distributed (Shapiro-Wilk: W = 0.96821, p-value = 0.0001). However, the E122K protein expression was not significantly normally distributed (Shapiro-Wilk: W = 0.98591, p-value = 0.105). Sample size (n)= 160 per sample group (WT and E122K). Image is author's own and created on R studio.*

3.3.1 A cluster of proteins involved in translation elongation are downregulated in the E122K.eEF1A2 interactome

The interactome analysis results found that most proteins showing decreased binding are subunits of the eEF1B-ValRS complex comprising the subunits eEF1Bα, eEF1Bδ, eEF1Bγ, and valyl-tRNA synthetase, which are encoded by the genes *EEF1B2, EEF1D, EEF1G* and *VARS1*, respectively. The *EEF1D* gene is located on chromosome 8 and gives rise to four isoforms through alternative splicing, which were all found significantly downregulated (*Figure 20*) (Kaitsuka and Matsushita, 2015). Three out of the four eEF1D isoforms are involved in translation elongation, referred to as short isoforms 2,4, and 5, and the other isoform, known as isoform 1 or eEF1BδL, functions as a transcription factor. The three short eEF1D isoforms assemble into a homotrimer in the eEF1B complex, which acts as a GEF for eEF1A during translation elongation (Kaitsuka and Matsushita, 2015). The most significantly downregulated eEF1D isoform was the short isoform 4, which forms part of the eEF1D homotrimer in the

eEF1B complex. These findings support previous studies that found eEF1A2 binds to the eEF1B complex (Bondarchuk et al., 2022; Cao et al., 2014).

Figure 20: Volcano plot of E122K.eEF1A2 molecular partners. *The labelled proteins (shown in blue) are eEF1A2 binding partners that have significantly altered binding caused by the E122K mutation. The repeating datapoints of EEF1D protein represent different isoforms. Statistical significance: $p \leq -\log_{10}(0.05)$ and fold change > +/- 1.5.*

3.3.2 A Gene Ontology (GO) analysis highlighted the importance of protein translation regulation and quality control

To gain a deeper understanding of which biological pathways are likely altered in the E122K.eEF1A2 interactome, a GO analysis was conducted on RStudio to identify the 10 most enriched biological pathways (*Figure 21*). GO is a computational tool that can cluster large datasets consisting of genes and proteins generated from high-throughput experiments into their consequent overrepresented biological pathways, molecular function, or cellular components. Therefore, GO analyses are an effective strategy for grouping proteins by common molecular functions for efficient targeting in research.

As expected, translation elongation was one of the most enriched biological pathways as subunits of the eEF1B-ValRS complex were significantly downregulated. Another group of significantly altered proteins in the E122K.eEF1A2 interactome were ribosomal proteins, RPL6, 11, 12, 23, 30, and 34. Among the group of significant ribosomal proteins, some were found upregulated and others were downregulated (*Figure 21*). These ribosomal protein subunits form part of the 60S ribosome. The upregulated proteins RPS3 and RPS15A are also ribosomal proteins, which encode protein subunits of the 40S complex. The 60S ribosome binds to the 40S subunit to form the 80S ribosome, which functions in the elongation of the polypeptide chain (Thornton et al., 2003). The GO enrichment analysis focusing on the 10 most significantly altered biological pathways found cytoplasmic translation was enriched in all ribosomal proteins, and RPL23 was particularly associated with the formation of DNA-protein complexes and protein quality control processes. These findings could be indicative of reduced protein translation efficiency and regulation of protein synthesis E122K.eEF1A2 interactome.

Some altered proteins in the E122K.eEF1A2 interactome, such as SUPT16H, have been linked to neurodevelopmental disorders. A clinical report on *de novo* mutations identified in SUPT16H, a subunit of the FACT (facilitates chromatin transcription) complex, described patients with symptoms of epilepsy, autism, and corpus callosum abnormalities (Bina et al., 2020). Surprisingly, SUPT16H was found to be one of the most upregulated proteins with the largest fold change in the E122K.eEF1A2 interactome, but no studies have found a link to

eEF1A2. The GO analysis results also found enriched biological pathways involving nucleosome organization, which may be indirectly linked or not relevant to eEF1A2 because it is localized in the cytoplasm (*Figure 21*).
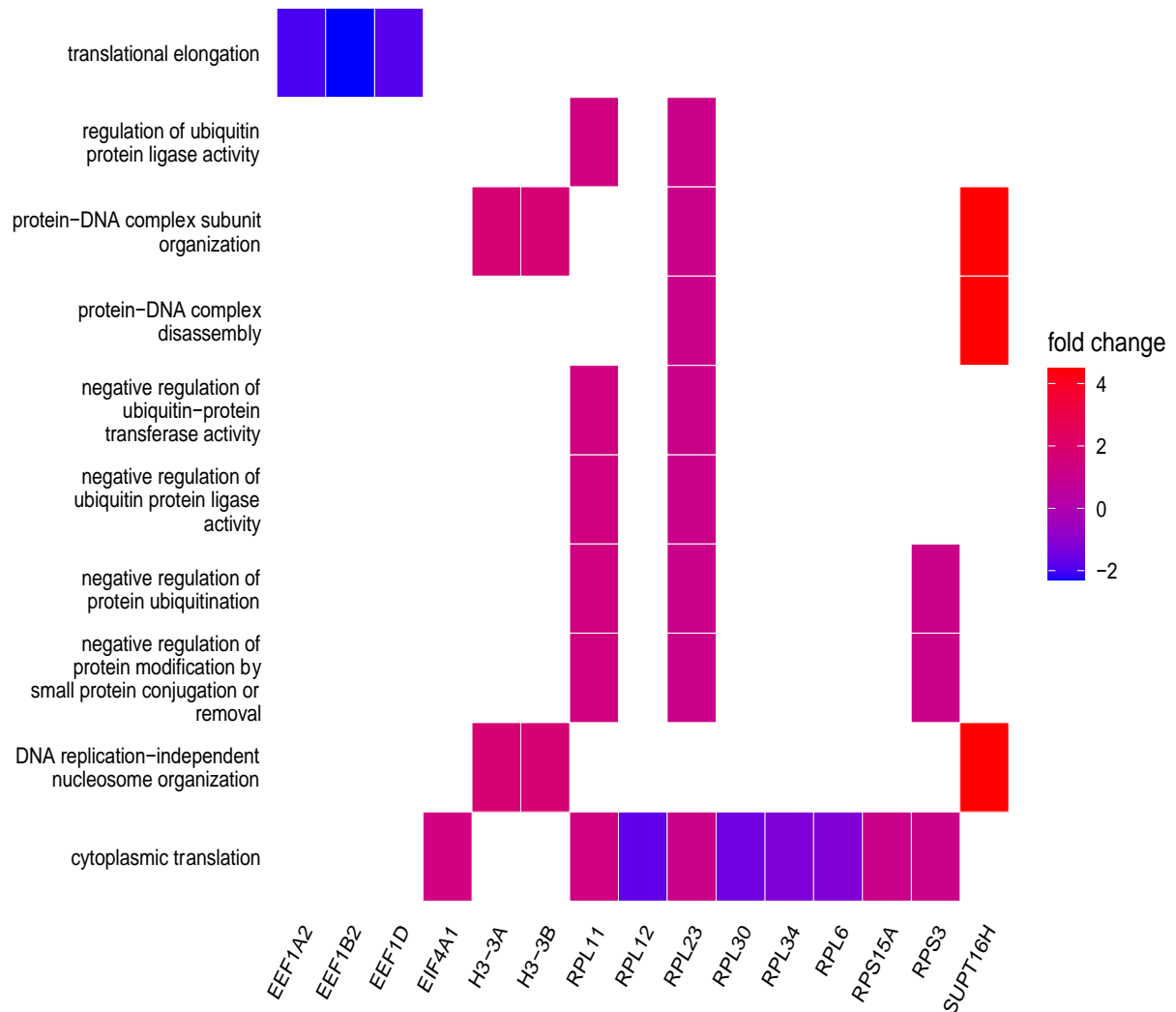

Figure 21: Gene ontology (GO) analysis of the 10 most prominent biological pathways in E122K.eEF1A2 and their altered proteins. *The heatmap was created on R using the package enrichplot. The fold change was used a quantitative measure showing whether proteins in the E122K.eEF1A2 were upregulated or downregulated.*

3.3.3 STRING predicts potential molecular networks in the E122K.eEF1A2 interactome

The GO analysis grouped proteins into enriched biological pathways, but the next question was whether the eEF1A2 molecular binding partners significantly altered in the E122K.eEF1A2 interactome formed protein-protein interaction networks that could give insight into eEF1A2 function. A network was generated from the STRING database by selecting all the significantly altered proteins identified by AP-MS against a reference dataset, which in this case, were all the proteins detected in the E122K.eEF1A2 interactome, irrespective of statistical significance. The STRING database forms predicted protein-protein interactions from many sources, including studies, experimental data, and computational prediction tools. The predicted protein interactions are not all necessarily physical interactions, as they could be functional associations (Szklarczyk et al., 2021). A functional association network could give insight into how the significantly altered proteins in the E122K.eEF1A2 interactome may be connected by common molecular pathways (*Figure 22*). Figure 22 shows a large cluster of closely interconnected proteins, including ribosomal proteins and translation elongation factors, which all have a role in protein translation. Therefore, the E122K mutation might trigger a chain reaction in the protein translation pathway rather than solely affect a few specific proteins, causing reduced translation regulation and efficiency.

Protein translation is said to be interlinked with cytoskeletal arrangement and actin bundling as studies found that phosphorylation of eEF1A2 increases dimerization, which stabilizes actin bundling (Carriles et al., 2021; Negrutskii et al., 2018). Moreover, sites of phosphorylation have been identified in highly conserved regions of eEF1A2, and eEF1A2 has been shown to directly bind to actin (Mendoza et al., 2021). However, the E122K.eEF1A2 interactome hasn't identified actin as an altered molecular binding partner of eEF1A2, despite the evidence of eEF1A2 mutations altering actin dynamics (*Figure 20*). Therefore, eEF1A2's non-canonical function in actin dynamics may not be altered by the E122K missense mutation. Alternatively, eEF1A2 may also regulate actin dynamics indirectly via tubulin or other proteins that interact with actin. The STRING network shows a small cluster of interacting cytoskeletal proteins, such as tubulin, cofilin, and vimentin. Tubulin proteins, TUBB, TUBA1B, and TUBB4B, were found to interact with cofilin 1 (CFL1) and eEF1G, a subunit of the eEF1B complex. Cofilin 1 is an actin-binding protein that regulates the neuronal actin cytoskeleton, and undergoes cycles

of inactivation by phosphorylation, resulting in actin disassembly and activation by dephosphorylation (Sarmiere and Bamburg, 2004). Cofilin was found to compete with tau protein for direct binding to tubulin in mouse primary neurons. Tau proteins function in microtubule assembly and can undergo pathological PTMs, causing misfolded protein aggregates found in tauopathies, including Alzheimer's disease. Active cofilin was found to disrupt microtubule stability, which disrupts tau, and is implicated in promoting tauopathy. Thus, cofilin directly interacts with tubulin and is associated with neurodegenerative diseases (Woo et al., 2019; Zilka et al., 2009). The interaction of eEF1G in actin dynamics is unknown as further studies are needed to elucidate its function.

Interestingly, GPC4 was the most significantly downregulated protein in the E122K.eEF1A2 interactome, but no functional association to other proteins in the interactome was found in the STRING predicted interaction network. GPC4 is a heparan sulfate proteoglycan that is involved in Keipert syndrome, an X-linked disorder characterized by craniofacial abnormalities and intellectual disability (Amor et al., 2019). Similar to SUPTH-related disorders, there is overlapping pathology with eEF1A2-related neurodevelopmental disorders; however, no link has been found to eEF1A2 other than its role as molecular binding partners. Overall, STRING networks are an effective strategy for clustering proteins by their functional associations to highlight which proteins in common biological pathways are altered in the E122K.eEF1A2 interactome.
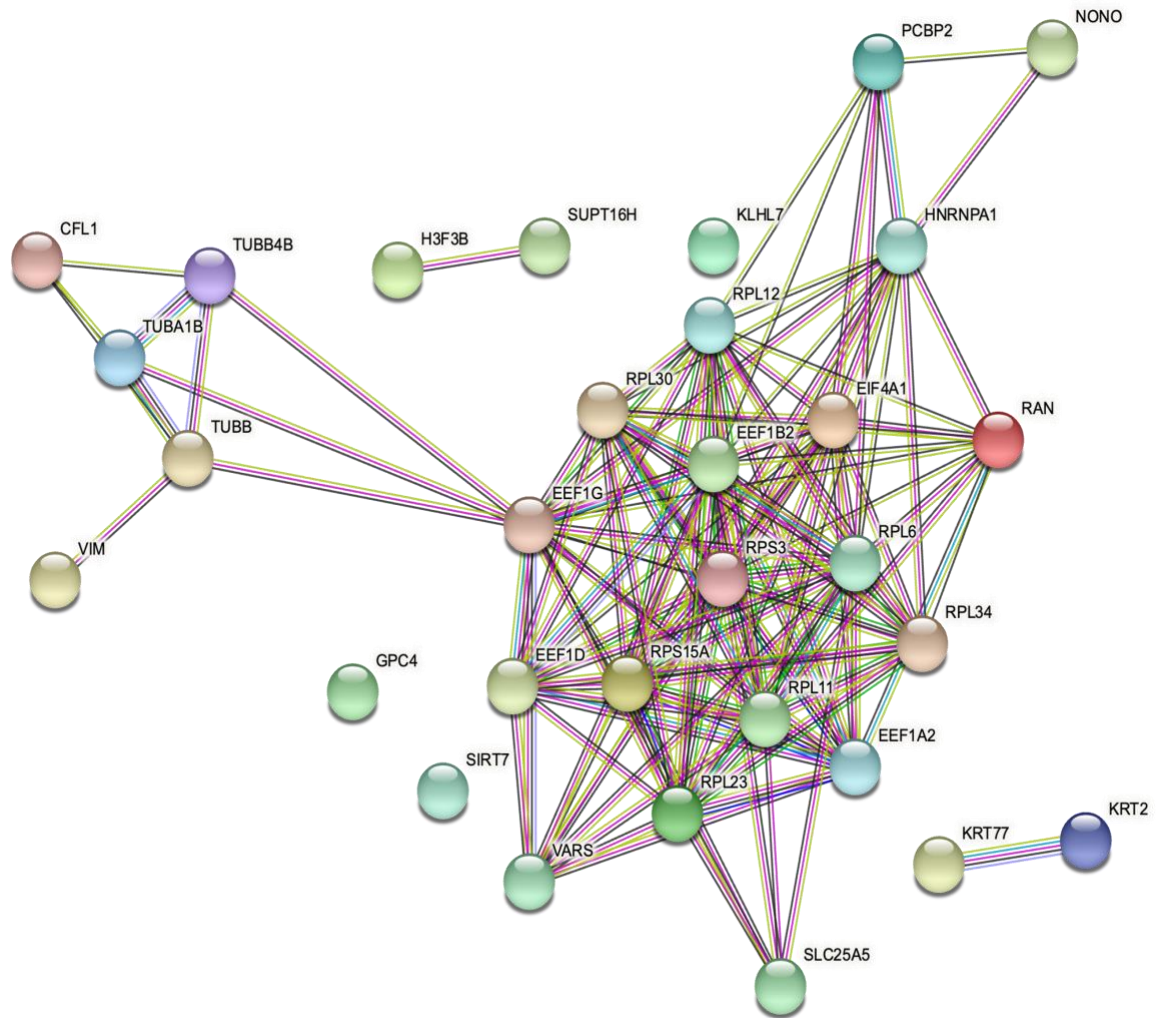
Figure 22: STRING generated protein interaction network of the significantly altered binding partners in the E122K.eEF1A2 interactome. *The functional interactions in the network may be direct or indirect (Szklarczyk et al., 2011). The colour-coded connectors represent how the functional association between proteins was determined. Dark green = gene neighbourhood, light green = textmining, red = gene fusions, dark blue = gene co-occurrence, black = co-expression, pink = experimentally determined, light blue = from curated databases, and violet = protein homology. Imagen created on STRING: https://string-db.org/.*

3.3.4 A comparison of the E122K.eEF1A2 and D252H.eEF1A2 interactome highlights the mutations' detrimental effects on protein translation machinery

A comparative analysis was then conducted on a previous lab member's (Fiona McLachlan's) data, which investigated the D252H.eEF1A2 mutant interactome by AP-MS on transfected neuronal progenitor SH-SY5Y cells. The D252H mutation was introduced into the cloned eEF1A2 cDNA sequence in the backbone of the pcDNA3.1-V5 vector (McLachlan, 2020) prior to transfection in SH-SY5Y cells. This comparative analysis was conducted to identify any similarities and differences to the E122K.eEF1A2 interactome. Figure 23 compares the proteins that were found to be significantly altered in the D252H.eEF1A2 and E122K.eEF1A2 interactomes. Surprisingly, few proteins converged between both interactomes and it's unknown whether the different cell backgrounds confounded these results. The converging proteins altered in both interactomes are downregulated subunits of the EEF1B-ValRS complex, suggesting that these proteins are likely to be altered in the interactomes of other missense mutations. However, when comparing the differences between both interactome datasets, E122K.eEF1A2 has considerably more altered ribosomal proteins.
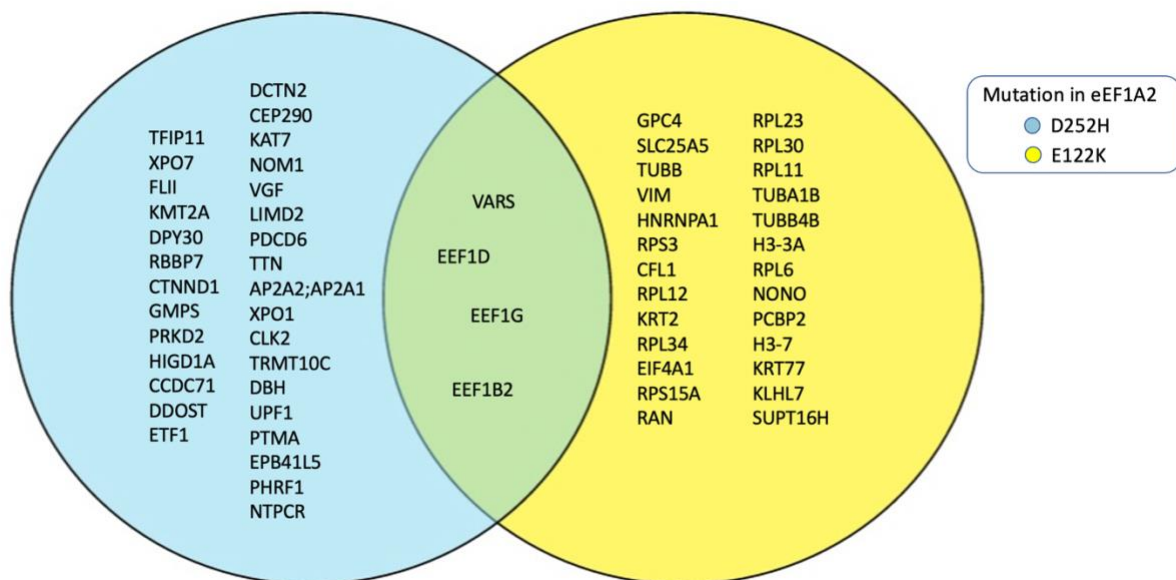
Figure 23: Venn diagram comparing the significantly altered proteins identified in the eEF1A2^{D252H} and eEF1A2^{E122K} interactome. The significantly altered proteins shown were either upregulated or downregulated. The converging section of the Venn diagram shows VARS, EEF1D, EEF1G, and EEF1B2 proteins are altered in both D252H and E122K mutant eEF1A2 interactomes. These proteins form part of the EEF1B-ValRS complex and have

important functions in protein translation elongation. The D252H.eEF1A2 data was taken from: Fiona McLachlan (McLachlan, 2020).

3.3.5 Validating the interactome analysis in eEF1A2[E122K] transfected HEK293T and SH-SY5Y cells

The results of the interactome analysis were then validated by co-immunoprecipitation followed by western blotting to confirm that the same binding strength in molecular binding partners was observed in independent experiments using HEK293T and SH-SY5Y cells transfected with E122K.eEF1A2-V5 constructs. There were some issues with antibody specificity and protein detection, which limited the number of proteins that could be validated by western blotting. Therefore, both this project's results, and the previous results of a lab member (Grant Marshall, postdoctoral researcher) are reported in *Figures 24 and 25,* respectively. EEF1D and EEF1B2 binding were analyzed in co-immunoprecipitated eEF1A2[E122K] transfected HEK293T cells, and EEF1D binding was analyzed in undifferentiated eEF1A2[E122K] transfected SHS-Y5Y cells. Protein signal bands observed in western blotting were normalized to the eEF1A2-V5 signal, the bait in the co-IP experiment, to also normalize for changes in transfection efficiency and protein stability (*Figures 24 and 25*). The results found that eEF1D and eEF1B2 binding appears slightly weaker in eEF1A2[E122K] transfected HEK293T mutants; however, the difference in binding was not statistically significant (*Figure 25*). No difference in eEF1D binding was observed in SH-SY5Y transfected cells, although input fractions on western blotting were much weaker, suggestive of less protein in samples than inputs in transfected HEK293T samples. Moreover, two bands were detected for eEF1D across E122K mutant and WT co-IP samples from HEK293T transfected cells (*Figure 25b*). Other than the possibility of antibody cross reactivity, the antibody may have detected another eEF1D isoform. As mentioned above, there are four eEF1D protein isoforms, of which three are involved in translation elongation, referred to as short isoforms 2,4, and 5, and the other isoform, known as isoform 1 or eEF1BδL, functions as a transcription factor. According to the UNIPROT database and a study investigating the effect of eEF1BδL KO in mice, it's likely that two short eEF1Bδ isoforms were detected in western blotting because they have similar molecular weights (~28-32 kDa), whereas eEF1BδL has a much higher molecular weight reported (~72 kDa(Kaitsuka et al., 2018; Wang et al., 2021). Validation of the interactome

analysis was performed in the SH-SY5Y cells because it is a neuronal cell line that is more physiologically relevant to the mouse brain than HEK293T cells. The human neuroblastoma SH-SY5Y cells express endogenous eEF1A2 and exhibit neuronal properties, which could be more physiologically relevant as eEF1A2 is expressed in most neurons in the brain (Newbery et al., 2007). Despite these differences, the validation results found no obvious differences across cell lines. The HEK293T human embryonic kidney cell line was chosen because it can be easily manipulated to express eEF1A2, has higher transfection efficiencies, and is easier to maintain in the lab compared to SH-SY5Y cells. Despite the lack of statistical significance found in the western blot quantification, there are visibly weaker bands in the eEF1D and eEF1B2 mutant-transfected SH-SY5Y and HEK293T samples, respectively. Thus, the validation results found some results resembled those of the high-throughput co-immunoprecipitation and mass spectrometry experiments.
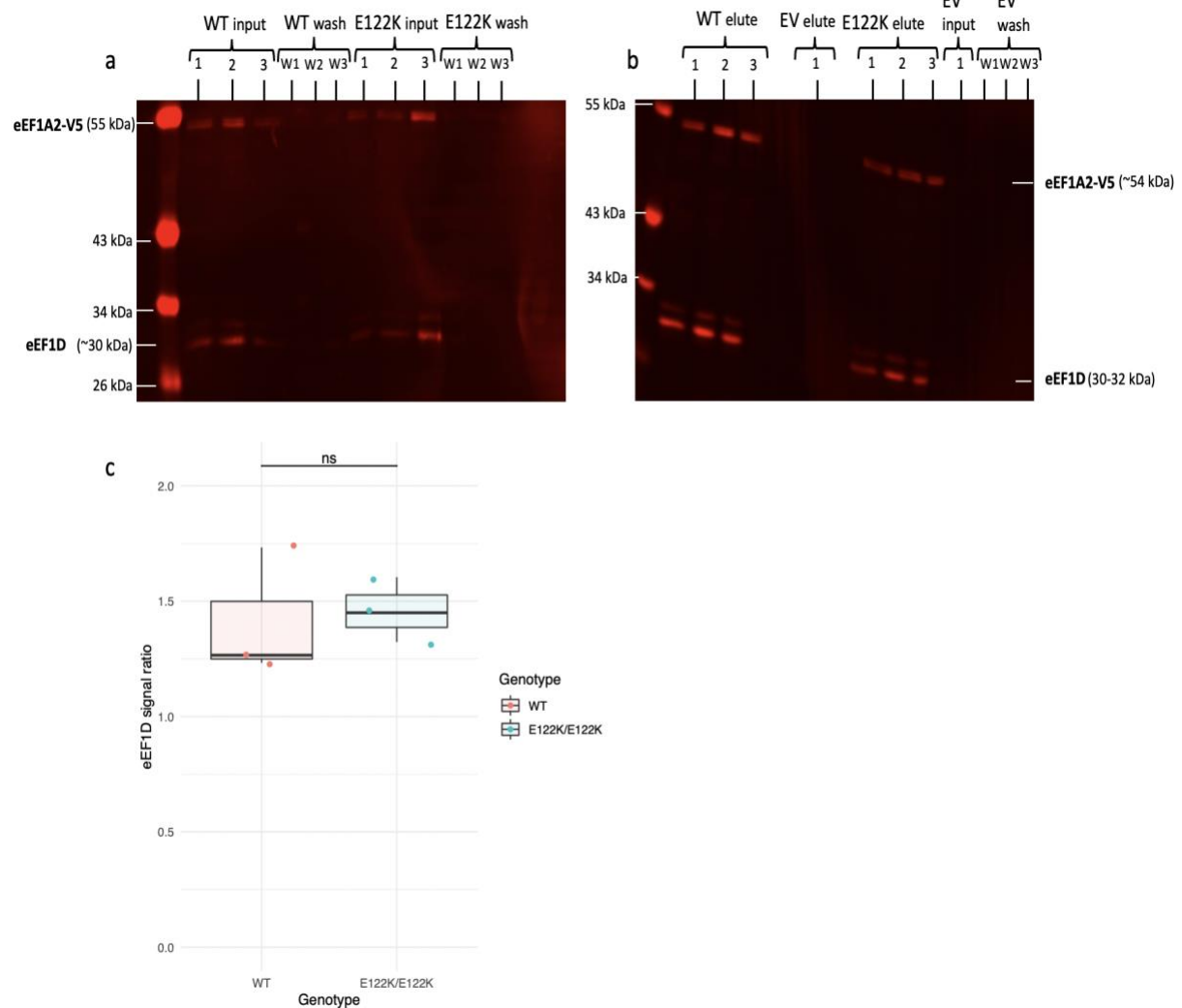
Figure 24: Validating eEF1D binding by co-immunoprecipitation in eEF1A2^{E122K} transfected SH-SY5Y cells. *(a) shows the elute western blot that was used as a control for co-immunoprecipitation to ensure that enough protein was present in samples. (b) co-immunoprecipitated samples of eEF1A2^{E122K} transfected SH-SY5Y cells were analyzed on western blotting. Note: Both V5 (GeneTex) and eEF1D (GeneTex, GTX102292) antibodies were reprobed and imaged on the red channel due to high background fluorescence on the green channel. (c) western blot quantification of eEF1D normalized to eEF1A2-V5 found no statistically significant difference in eEF1D binding (Wilcoxon: W = 3, p-value = 0.7). Empty vector (EV) was used as a negative control for transfection. Upper bands on both western blots are eEF1A2-V5, whereas lower bands are eEF1D. Sample size (n): 6 (3 per genotype). Statistical significance: p ≤ 0.05. Experiment was performed by the author of this project.*
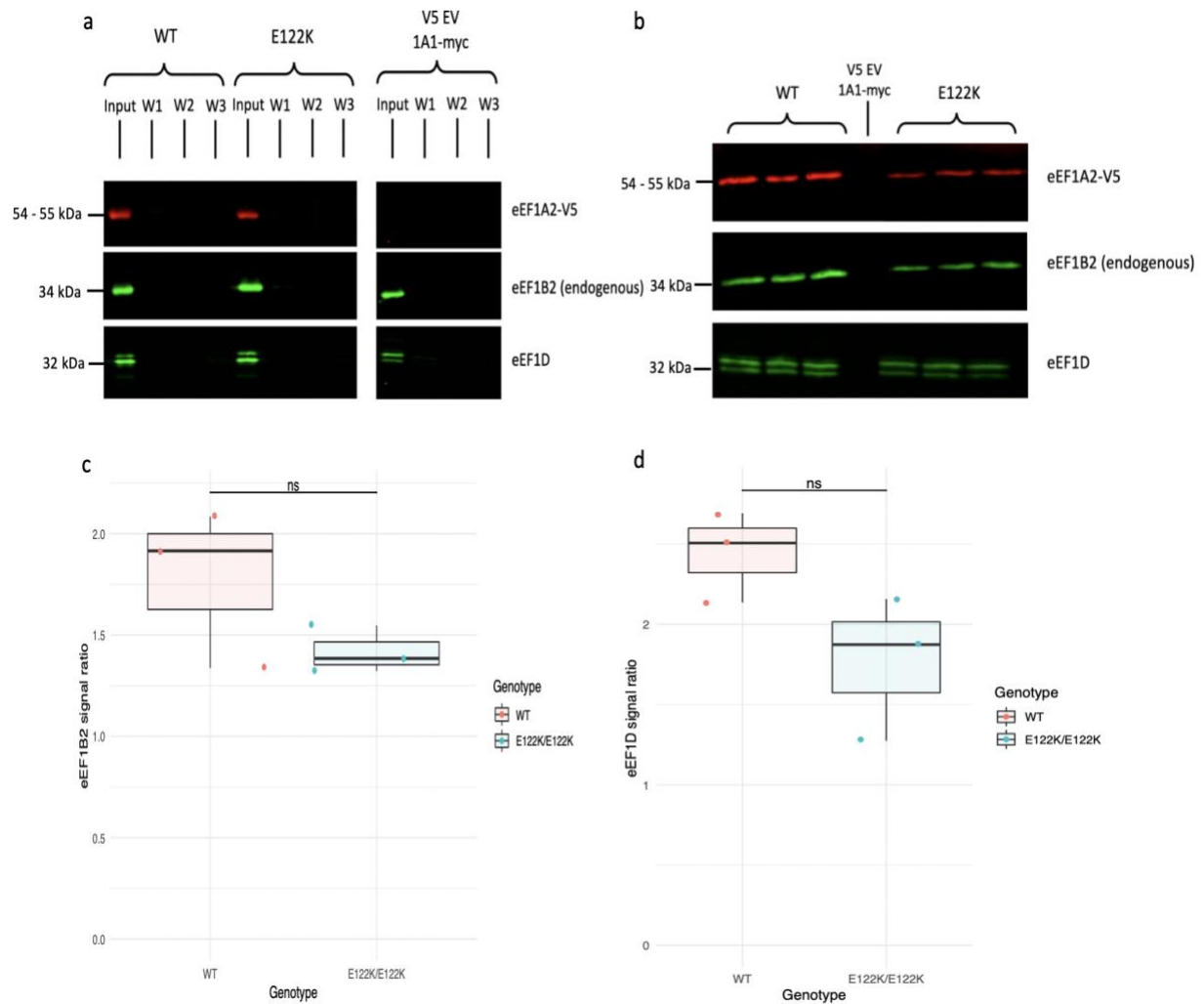
Figure 25: Validating eEF1D and eEF1B2 binding by co-immunoprecipitation in eEF1A2^{E122K} transfected HEK293 cells. *(a) The control inputs and washes prior to co-immunoprecipitation to ensure that enough protein was present in eEF1A2^{E122K} transfected HEK293T samples. (b) shows a comparison of the binding strength of eEF1A2-V5, eEF1B2, and eEF1D following co-immunoprecipitation in E122K and WT samples. (c) western blot quantification of eEF1B2 found reduced binding in E122K mutants, but there was no statistical significance (Wilcoxon: W = 8, p-value = 0.2). (d) eEF1D binding was also decreased in E122K mutants, but the difference relative to WT wasn't statistically significant (Wilcoxon: W = 7, p-value = 0.4). eEF1D (GeneTex, GTX102292) was probed on chemically stripped western blots that had been previously probed for eEF1B2 and eEF1A2-V5. Sample size (n): 6 (3 per genotype). Statistical significance: p ≤ 0.05. The western blot results for eEF1A2-V5 and eEF1B2 (shown in a and b) were taken from Grant Marshall (postdoctoral researcher).*

3.4 A differential expression analysis of the eEF1A2$^{E122K/E122K}$ mouse brain

A differential expression analysis was then conducted on the eEF1A2$^{E122K/E122K}$ mutant mouse brain by label-free quantification LC-MS/MS mass spectrometry (performed by Roopesh Krishnankutty (postdoctoral researcher)) and bioinformatics analysis to identify changes in the mouse brain proteome (*Figure 27*). In the brain, eEF1A1 and eEF1A2 expression is mutually exclusive, with eEF1A2 is expressed exclusively in neurons, whereas eEF1A1 is expressed in glial cells and white matter (Newbery et al., 2007). The aim of identifying changes in the E122K mutant brain proteome was to give insight into the effects of E122K on eEF1A2 stability and function. The mass spectrometry output was run-through the software pipeline DIA/NN for normalized quantification. A 2-sample t-test comparing the means of WT and E122K groups of quantified protein expression was performed to proteins with statistically significant differential expression. Prior to performing the 2-sample t-test, the data had to follow the test's statistical assumptions of random sampling, independence, normal distribution, and homogeneity of variances. The random sampling and independence assumptions in mice and mouse brain samples were handled by Grant Marshall (postdoctoral researcher). A Shapiro-Wilk test of normality found that both WT and E122K protein expression groups were normally distributed, which was also visualized in a Q-Q plot (*Figure 26*). As mentioned above, an F-test determines whether the variances between two groups are equal, and no statistically significant difference in the variances between the average WT and E122K protein expression groups was found (F-test: F = 0.95431, df = 4287, p-value = 0.1258). Therefore, the WT and E122K data was homoscedastic, and all the statistical test assumptions of a t-test were met. The same calculations mentioned above for the interactome analysis were also applied using the average WT and E122K protein expression to generate volcano plots.
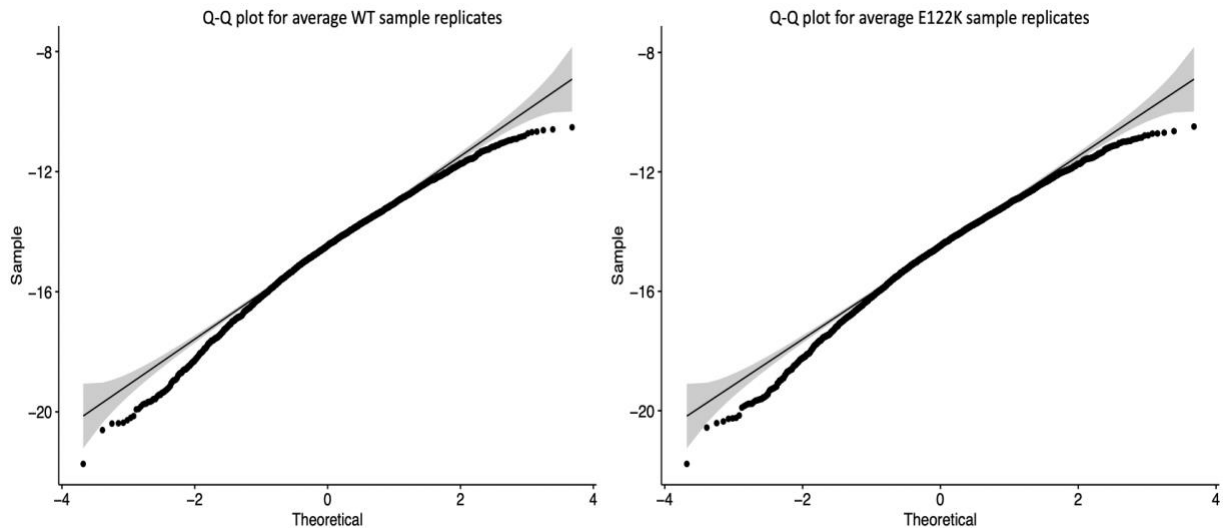
Figure 26: Q-Q-plots to test the normality assumption for a 2-sample t-test. *A Shapiro-Wilk test for normality found both the average WT (Shapiro-Wilk: W = 0.13475, p-value < 2.2 x 10^{-16}) and E122K (Shapiro-Wilk: W = 0.1305, p-value < 2.2 x 10^{-16}) quantified protein expression groups were normally distributed.*

A lower log2 fold change significance threshold of +/- 0.05 on the volcano plots was considered suitable due to the low range of fold change across all differentially expressed proteins (*Figures 27, 29, and 30*). The biological relevance was also considered when deciding the fold change significance threshold. eEF1A2 is known to be significantly downregulated in mutants; therefore, the fold change significance threshold could not be above eEF1A2's fold change. The main functions of each significant differentially expressed gene was summarized to give an overview of the altered eEF1A2$^{E122K/E122K}$ mouse brain proteome (*Table 5*). A comparison of the differentially expressed proteins across sex found that female mice had fewer differentially expressed proteins compared to male mice (*Figures 29 and 30*). Then, a STRING and GO analysis were performed to identify functional protein interactions, and the most enriched biological pathways, respectively. STRING found the major clusters of proteins are involved in protein translation, neuronal regulation, and chromatin modifications (*Figures 28*). Similarly, the GO analysis found the most enriched biological pathways involved chromatin regulation and modifications (*Figure 31*).

3.4.1 Translation regulation is most likely affected in the eEF1A2^{E122K/E122K} mouse brain proteome

The results of differential expression analysis found that the p-value with the highest significant p-value was eEIF5, a translation initiation factor, which is a highly conserved and essential protein involved in protein translation. Studies found that eEIF5A interacts with eEF1A and the 80S ribosome (*Figure 27*)(Zanelli et al., 2006). Furthermore, eIF5A's association to the ribosome is dependent on active protein synthesis, and its function is sensitive to protein synthesis inhibitors, suggesting that eIF5A has a role in translation (Dias et al., 2012; Zanelli et al., 2006). Therefore, eIF5A could be a potential indicator of protein synthesis function in eEF1A2 mutants, but further studies would be required to elucidate the molecular mechanism. Another important differentially expressed gene involved in translation was eEF2, which is an elongation factor protein that regulates the translocation of the polypeptide chain from the A-site to the P-site of the 80S ribosome. Phosphorylation inhibits its regulatory function in translation (Kaul et al., 2011). The differential expression analysis found regulatory proteins involved in protein translation elongation were the most significantly affected in the mouse E122K.eEF1A2 brain proteome. However, it's surprising that there aren't more significantly downregulated proteins considering that translation capacity was one of the most significantly affected functions.

***Figure 27: Volcano plot of differentially expressed proteins in the mouse eEF1A2^{E122K/E122K}
brain.*** *Each datapoint in the volcano plot represents a protein that was detected by LC-MS/MS.
The green datapoints are proteins that were found not to be differentially expressed. The
proteins labelled are those which are differentially expressed. Blue = upregulated. Red =
downregulated. Sample size (n) = 10 (5 male and 5 female). Plot was created on Rstudio.
Statistical significance: p ≤ 0.05 and fold changes > +/- 0.5. Image: author's own.*

Table 5: Significant differentially expressed proteins, their corresponding gene names, and functions

Gene	Protein name	Uniprot ID	Differential Expression	Function(s)
Eef2	Elongation factor 2	P58252	UP	Translation elongation
Smim29	Small integral membrane protein 29	A0A338P7F9;A0A338P7F5;Q8R043	UP	Unknown
Shtn1	Shootin-1	Q8K2Q9;Q8K2Q9-2	UP	Cytoskeletal organisation, axon development
Prrc2a	Protein PRRC2A	Q7TSC1	UP	Regulation of pre-mRNA slicing
Zpr1	Zinc finger protein 1	F8WHU9;Q62384	UP	Binds to eEF1A1
Eef2;Eftud2	116 kDa U5 small nuclear ribonucleoprotein component	A2AH85;G3UZ34;G3UXK8;O08810;P58252	UP	Pre-mRNA splicing and ribosome translocation
Rpl3	60S ribosomal protein L3	A0A2R8VHN4;P27659	UP	Component of the 60S ribosome subunit
Btf3	Isoform 2 of Transcription factor BTF3	Q64152;Q64152-2	UP	Transcription initiation
Serbp1	Serpine1 mRNA binding protein 1	A0A0N4SV40	UP	mRNA stability, ribosome binding activity, ubiquitin-like protein SUMO activity
Galk1	Galactokinase	Q9R0N0	UP	Galactose metabolism
Shisa9	Protein shisa-9	E9QN38;Q9CZN4;Q9CZN4-3;Q9CZN4-4	UP	AMPA receptor activity, synaptic plasticity
Mcts1	Malignant T-cell-amplified sequence 1	Q9CQ21;Q9DB27;Q9DB27-2	UP	Cell cycle, translation initiation
Mdga1	MAM domain-containing glycosylphosphatidylinositol anchor protein 1	D3Z499;A0A3Q4EGH1;F7ABV5;Q0PMG2	UP	Cell adhesion, migration, axon guidance, neuronal migration, inhibitory synapse formation
H1-4	Histone H1.4	P43274	UP	Chromatin compaction, transcription regulation
H1-1;H1-2;H1-4	Histone H1.2	P43275;P43274;P43277;P15864	UP	Transcription regulation
H1-5	Histone H1.5	P43276	UP	Chromatin compaction, transcription regulation
H1-1	Histone H1.1	P43275	UP	Chromatin compaction, transcription regulation
Arl6ip4	ADP-ribosylation factor-like protein 6-interacting protein 4	D3YWC2;D3Z6F1;Q9JM93	UP	RNA splicing and mRNA processing.
Ctcf	Transcriptional repressor CTCF	Q61164	UP	Transcription regulation, chromatin remodelling
Mrpl45	39S ribosomal protein L45, mitochondrial	F6QAU7;Q9D0Q7	UP	Mitochondrial translation
Mob1a;Mob1b	MOB kinase activator 1B	Q3UDM0;Q921Y0;Q921Y0-2;Q8BPB0	UP	Microtubule stability during cytokinesis

Eif5	Eukaryotic translation initiation factor 5	A0A1Y7VKT5;P59325	DOWN	Protein translation
Myl4	Myosin light chain 4	A0A0G2JDM3;Q9CZ19;A2A6Q8;A0A0G2JDW2;P09541;P09542	DOWN	Actin binding, cytoskeleton
Eef1a2	Elongation factor 1-alpha 2	P62631	DOWN	Translation elongation
Kif5a	Kinesin heavy chain isoform 5a	P33175	DOWN	Axonal transport
Lyrm9	LYR motif-containing protein 9	E9PX24;Q3UN90	DOWN	Unknown
Pls1;Pls3	Plastin-1	B1AX58;A0A1C7CYV0;Q99K51;Q3V0K9	DOWN	Osteoblast differentiation
Scn8a	Sodium channel protein type 8 subunit alpha	F7D6K4;F6U329;A0A0J9YUW5;A0A0J9YTW4;F7D6J5;A0A0J9YTW2;Q9WTU3;Q9WTU3-3;Q9WTU3-4;Q9WTU3-5	DOWN	Membrane depolarisation for the generation of action potentials in excitable neurons
Gc	Vitamin D-binding protein	P21614	DOWN	Vitamin D binding and transport
C3	Complement C3	P01027	DOWN	Complement activation, inflammatory response,
Serpina3k	Serine protease inhibitor A3K	E9Q499;A0A0R4J0I1;G3X8T9;F2Z405;Q5I2A0;Q91WP6;P29621;P07759;Q03734	DOWN	Trypsin-like protease inhibition
Hpx	Hemopexin	A0A1B0GS57;Q91X72	DOWN	Transport heme to the liver
Aldoart1	Fructose-bisphosphate aldoase	Q9CPQ9;A6ZI46	DOWN	Glycolysis
Plp1	Myelin proteolipid protein	P60202;P60202-2	DOWN	Myelination, maintenance of myelin
Cadps	Isoform 2 of Calcium-dependent secretion activator 1	A0A286YDH6;Q80TJ1-2	DOWN	Protein transport, exocytosis
Serpinb1a	Leukocyte elastase inhibitor A	Q9D154	DOWN	Unknown
Tspan2	Tetraspanin 2	Q9D1X8;A0A0G2JDX4;A0A0G2JEZ7;Q922J6	DOWN	Stabilise the mature myelin sheath, oligodendrocyte signalling

Note: The functions of each protein are reported from UNIPROT (Wang et al., 2021) and The Human Gene Database (Safran et al., 2021) . Only differentially expressed proteins were included in the table above.

3.4.2 Clusters of protein interactions highlight eEF1A2 function and translation regulation
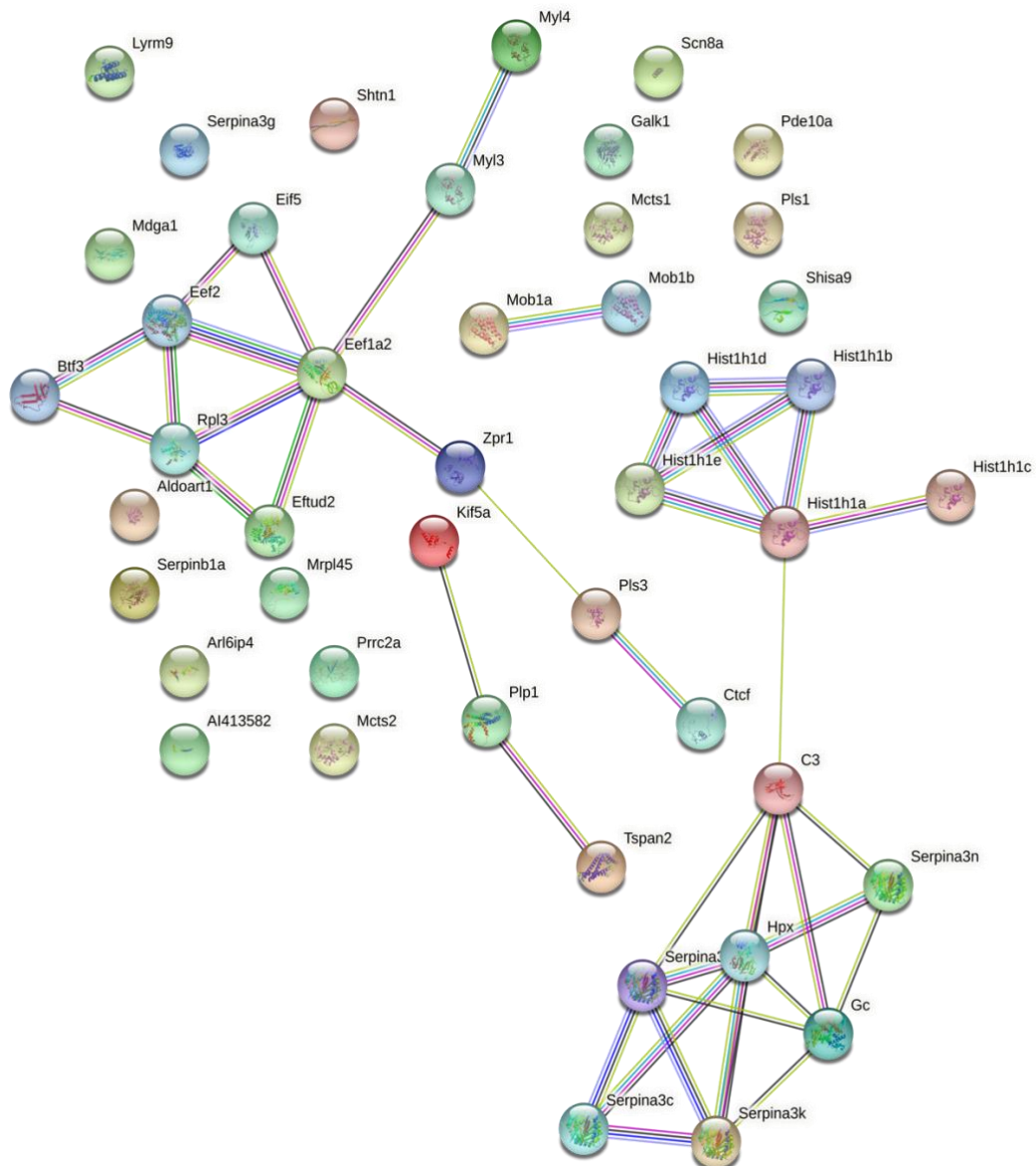
Figure 28: STRING network analysis of differential expression in the mouse eEF1A2^{E122K/E122K} brain. *A network of predicted functional interactions between significantly differentially expressed proteins in mouse eEF1A2^{E122K/E122K} brain (plotted by their mouse gene names) shows some clustering. The colour-coded connectors represent how the functional association between genes was determined. Dark green = gene neighbourhood, light green = textmining, red = gene fusions, dark blue = gene co-occurrence, black = co-expression, pink = experimentally determined, light blue = from curated databases, and violet = protein homology. Image is author's own and was created on STRING (https://string-db.org/).*

Three major clusters of protein interactions were identified in the STRING analysis of differentially expressed proteins in the eEF1A2$^{E122K/E122K}$ brain (*Figure 28*). The largest cluster consists of eEF1A2 interactors, such as EEF2, EIF5, and ZPR1. Zinc protein-like finger (ZPR1) is an essential protein that interacts with eEF1A and survival motor neuron (smn) protein, whereby mutations in SMN cause the motor neuron degenerative disease, spinal muscular atrophy (SMA). ZPR1 competes with eEF1B2 to bind to eEF1A, and the ZPR1-eEF1 complex is required for normal cell cycle progression. In addition, heterozygous mutant ZPR1 mice exhibited motor neuron degeneration bearing similarities to *wst* affected spinal cords (Doran et al., 2006; Mishra et al., 2007). Therefore, the neurodegenerative phenotype may be partly the result of the ZPR1 interaction to eEF1A and could be investigated further to determine whether ZPR1 contributes to the motor delays and defects observed in children affected by mutations in eEF1A2. As previously mentioned, eEF2 and eIF5 also have regulatory roles in protein translation, and ribosomal protein 3 (RPL3) is a component of the 60S ribosome. A functional interaction between eEF2 and eIF5 during translation elongation was discovered in yeast in which protein synthesis defects in eIF5A mutants were ameliorated by a high-copy of eEF2, which suppressed the eIF5A mutant (Dias et al., 2012). More recently, a study found eEF2 and eIF5A bind to the 80S ribosome during translation elongation, and eEF2 binding to the ribosome reduces eIF5A binding affinity to the ribosome in yeast suggestive of mutually exclusive binding to the 80S ribosome. Furthermore, eIF5A$^{Q22H/L93F}$ mutants, which don't have altered binding affinity to the ribosome in the presence of eEF2, exhibited impaired translation elongation due to eEF2 overexpression. Therefore, regulation of eEF2 and eIF5A binding to the ribosome is important for the normal functioning of translation elongation (Rossi et al., 2016). Thus, this cluster highlights the regulation of translation is likely affected in the eEF1A2$^{E122K/E122K}$ mouse brain.

Another extensive cluster of interacting proteins are involved in the inflammatory response, including histones and complement 3 (C3). Within this network, several Serpina protease inhibitors closely interact with hemopexin (HPX). Hemopexin binds and transports heme groups to the liver, but it was also found that it is involved in oligodendrocyte differentiation. Loss of hemopexin in mice resulted in a motor defects and impaired myelination, and it was concluded that it could potentially have a role in the pathogenesis of neurodegenerative disorders. In addition, protease inhibitors have been implicated in the maintenance of myelin,

and Serpina-3 has been implicated in neurodegeneration (Morello et al., 2011; Soman and Asha Nair, 2022). These findings suggest that several affected proteins in the eEF1A2$^{E122K/E122K}$ brain proteome could contribute to the neurodegenerative phenotype observed in E122K mutant mice.

The small network cluster generated on STRING consisting of KIF5A, which interacts with PLP, and PLP interacts with TSPAN2 (*Figure 28*). These proteins were all significantly downregulated in the eEF1A2$^{E122K/E122K}$ mouse brain and are implicated in neurodevelopmental disorders (*Figure 27*). TSPAN2 is the protein tetraspanin, which stabilizes the mature myelin sheath and is involved in oligodrendogenesis. Tetraspanin interacts with proteolipid protein (PLP), the predominant myelin protein in the CNS that causes axonal degeneration when mutated. A study found that tetraspanin and proteolipid protein have potentially overlapping functions in regulating neuroinflammation (de Monasterio-Schrader et al., 2013). KIF5A is a kinesin expressed in neurons that functions as a molecular motor in the transport of proteins and organelles (Hirokawa et al., 2009). Figure 27 shows that KIF5A expression is one of the most significantly downregulated proteins in the eEF1A2$^{E122K/E122K}$ mouse brain. Interestingly, reports have shown that mutations in KIF5A may cause amyotrophic lateral sclerosis (ALS), and patients carrying mutations in eEF1A2 have motor defects and delays, such as walking (Brenner et al., 2018; Kaneko et al., 2021). Loss of KIF5A has also been attributed to epilepsy by affecting GABA trafficking (Gambino et al., 2022). KIF5A knockdown resembles the phenotype of loss of eEF1A2 expression (i.e., wasted brain), which results in motor neuron degeneration in mice. Targeting this molecular network for future studies could give insight into the neurological defects caused by the E122K mutation in eEF1A2. Although eEF1A2 is only expressed in neurons in the brain, missense mutations in eEF1A2 may affect other cell types that do not express eEF1A2, such as oligodendrocytes, via functional interactions. Overall, the STRING analysis has provided an overview of protein interactions and its potential roles in the eEF1A2$^{E122K/E122K}$ degenerative phenotype in mice.

3.4.3 Sex differences in the E122K.EF1A2 mouse brain proteome

The differentially expressed proteins in male and female eEF1A2$^{E122K/E122K}$ mouse brains were compared to identify any sex-specific differences that could correlate to differences in phenotype severity as the eEF1A2$^{D252H/D252H}$ and eEF1A2$^{E122K/E122K}$ male mice had more severe phenotypes (Davies et al., 2020; Marshall, 2022). Interestingly, fewer proteins were found to be differentially expressed in females in comparison to male mice. Different statistically significant proteins were also identified in both sexes (*Figures 29 and 30*). For example, MAPRE1/MAPRE2 and TACC2 are microtubule-interacting and/or microtubule-regulating proteins which were differentially expressed in the female mouse eEF1A2$^{E122K/E122K}$ brain (Gergely et al., 2000; Su and Qi, 2001). In contrast, the differentially expressed proteins in males largely resembled the volcano plot in *Figure 26*, with the exception of a few proteins, including CAMK2, which are Ca^{2+}/calmodulin-dependent protein kinases involved in synaptic plasticity (Lucchesi et al., 2011). Due to the small sample sizes of each sex in the proteomic analysis, western blotting of more samples was conducted to observe whether differences in differential expression could also be detected across sex. Figure 34a shows the results of a western blot for FKBP3, a protein found differentially expressed in females, but not in the E122K.eEF1A2 male mouse brain. FKBP3 was selected for western blotting analysis because it had the highest p-value; therefore, any differences in expression could be easier to detect by western blotting. However, there were no differences in FKBP3 expression in E122K.eEF1A2 mutants compared to wildtype (*Figures 34a, and 34b*). Thus, further experiments would be needed to determine whether sex phenotypic differences in mutant mice correlate with differences in differential expression in the mouse brain.

Figure 29: Differential expression analysis of female mouse eEF1A2$^{E122K/E122K}$ brain. *Samples from female mice were statistically analyzed to compare differentially expressed proteins to the male mouse brain proteome. Statistical significance: p ≤ 0.05 and fold changes > +/- 0.5. Sample size (n): 4 (2 WT and 2* eEF1A2$^{E122K/E122K}$*). Image: author's own.*
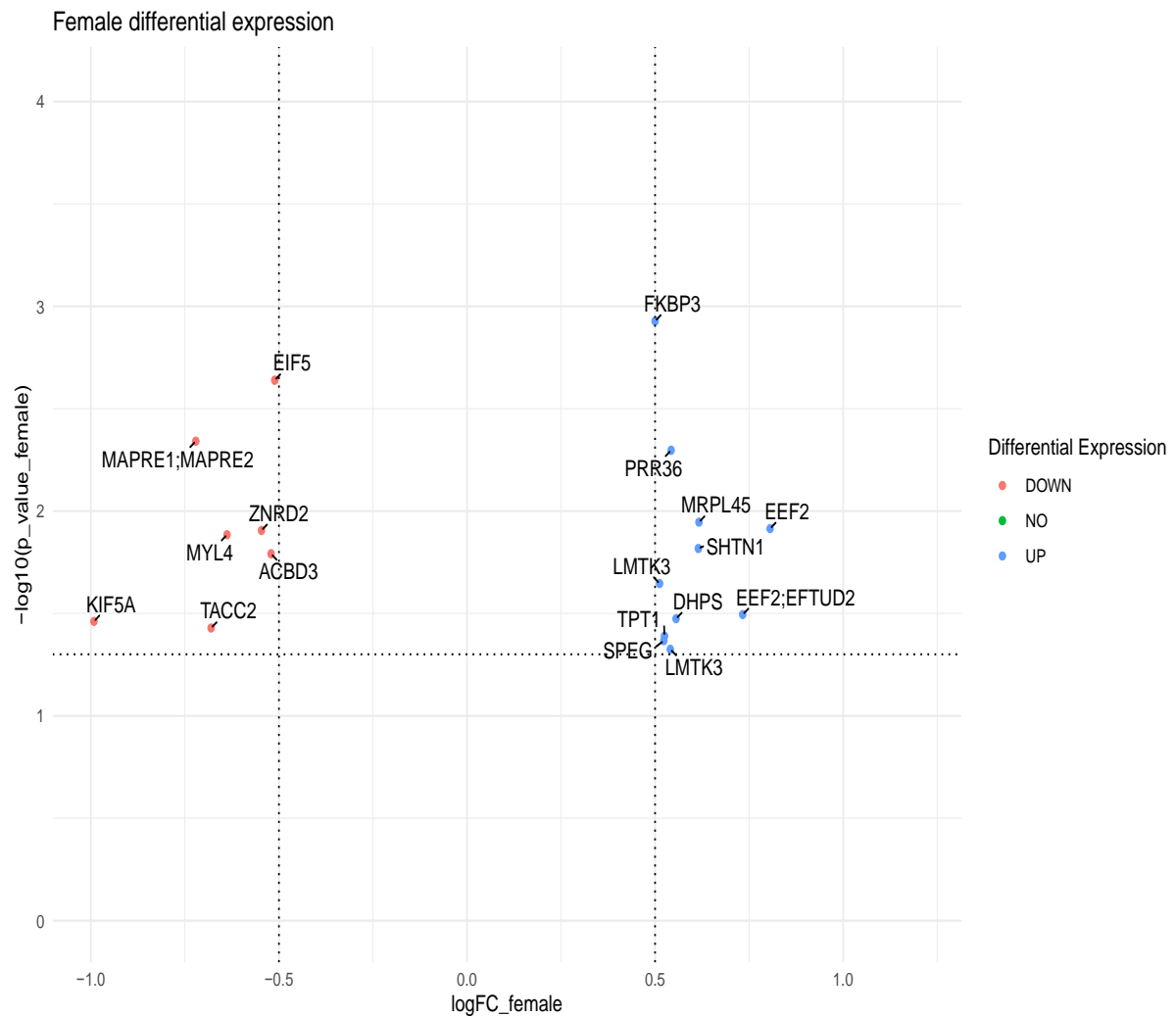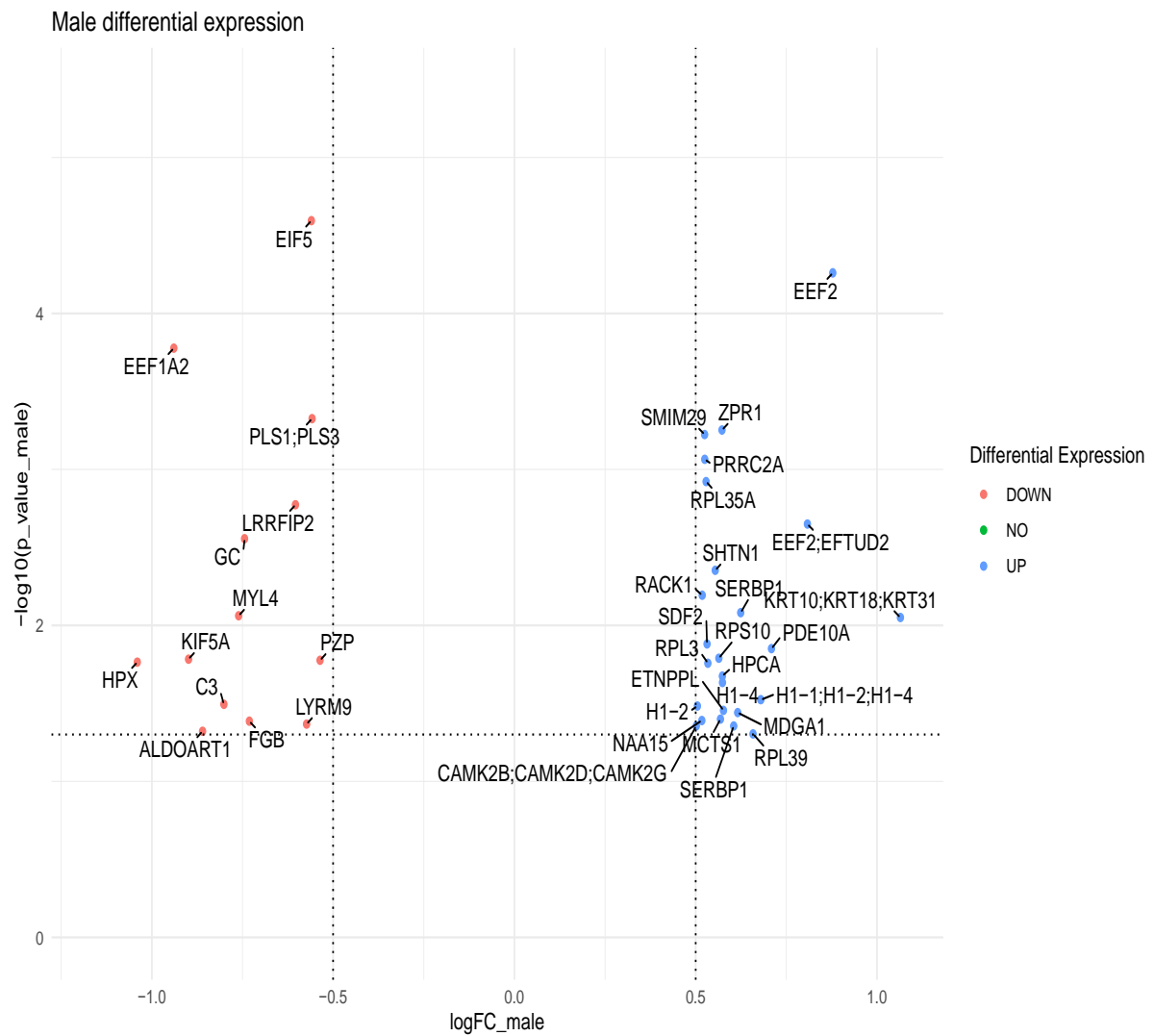
Figure 30: Differential expression analysis in male mouse eEF1A2$^{E122K/E122K}$ brain. *Samples from male mice were statistically analyzed to compare differentially expressed proteins to the female mouse brain proteome. Statistical significance: p ≤ +/- 0.05. Sample size (n): 6 (3 WT and 3* eEF1A2$^{E122K/E122K}$). *Image: author's own.*

3.4.4 The most enriched biological pathways in the eEF1A2$^{E122K/E122K}$ mouse brain involve chromatin remodelling

Following the STRING analysis, a GO analysis was conducted of the 20 most enriched biological pathways in the altered eEF1A2$^{E122K/E122K}$ mouse brain. Interestingly, the packaging of DNA into nucleosomes and higher order chromatin were the most prominent biological pathways, which is surprising considering eEF1A2 is a cytosolic protein that hasn't been reported to enter the nucleus (*Figure 31*). A wide range of neurodevelopmental disorders, such as autism and intellectual disability-related disorders, have altered chromatin modifiers. For example, CTCF, a chromatin organizer, pathogenic variants were identified in individuals with highly heterogenous neurodevelopmental disorders characterized by intellectual disability, minor facial dimorphisms, and mild seizures. Overexpression of CTCF in drosophila impaired neurological function, and the differential expression analysis found CTCF was upregulated in mice (Konrad et al., 2019). In addition, epigenetic changes, in particular methylation, have also been attributed to neurodevelopmental disorders (LaSalle, 2013; Mossink et al., 2021). These findings suggest the eEF1A2$^{E122K/E122K}$ mouse brain shares similar characteristics to other heterogeneous neurodevelopmental disorders. It is not fully understood how chromatin and epigenetic changes are attributed to neurodevelopmental disorders and eEF1A2 function. These enriched pathways could be indirectly linked to eEF1A2 or be arquefactual; therefore, more studies are needed to confirm these findings.
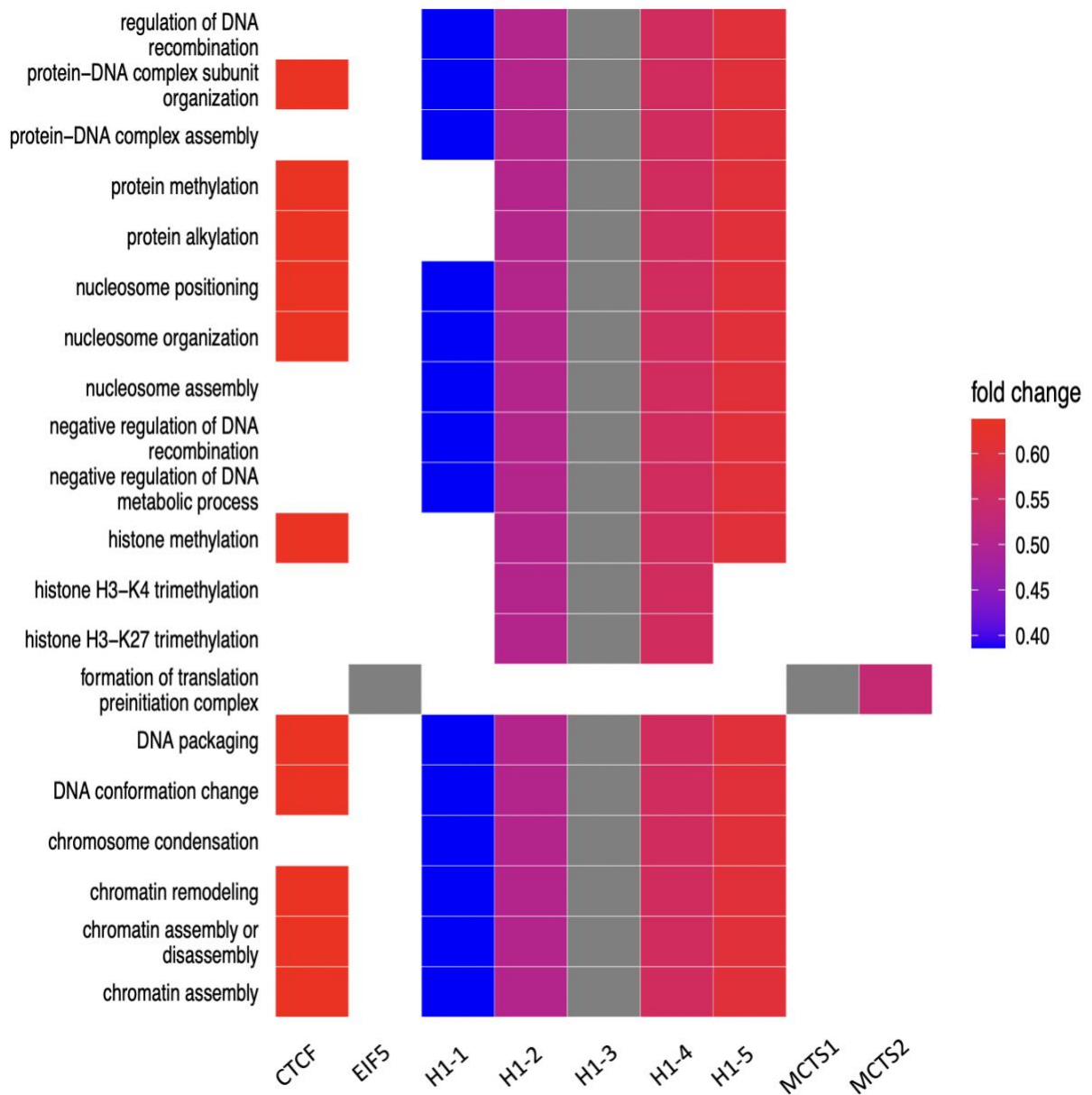
Figure 31: GO analysis of enriched biological pathways in the eEF1A2^E122K/E122K mouse brain. *The heatmap shows the 20 most enriched biological pathways from the differentially expressed proteins found in eEF1A2^E122K/E122K mouse brain proteome. The fold change indicates whether the protein is upregulated or downregulated. The grey-coloured squares indicate that the fold change is not significant. The heatmap was created on Rstudio using the enrichplot package. Image: author's own.*

3.4.5 Validating the eEF1A2$^{E122K/E122K}$ differential expression analysis by Western blotting

Following the bioinformatics analysis of the mass spectrometry data, the same eEF1A2$^{E122K/E122K}$ mouse brain samples were analysed by western blotting to determine whether the same changes in protein expression were observed. The proteins selected for western blotting were some of the most significantly altered and relevant to eEF1A2 function. The proteins KIF5A, SHTN1, and eEF2 showed the same differential expression patterns as the results observed from mass spectrometry (*Figure 27*).

Phosphorylated eEF2 was analysed on western blotting because phosphorylation by eEF2 kinase (eEF2K) on the Thr-56 residue inhibits eEF2 activity, resulting in the suppression of protein synthesis (Sutton et al., 2007). A comparison of eEF2 and phospho-eEF2 expression levels in the eEF1A2$^{E122K/E122K}$ mouse brain could be an indication of whether protein synthesis is reduced in mutants. The western blot results showed a significant increase in eEF2 expression in mutants, but no difference in phospho-eEF2 expression was observed compared to wildtype (*Figure 32*).

Other proteins for which validation by western blotting was attempted were Shootin1 (SHTN1), KIF5A, and FKBP3. Shootin1 and KIF5A expression in western blotting resembled the mass spectrometry findings with significantly increased and decreased expression in eEF1A2$^{E122K/E122K}$ mutants, respectively (*Figure 33*). As previously mentioned, mutations in KIF5A have been implicated in neurodevelopmental disorders, such as ALS. Shootin1 functions in axonal maturation and neurite extension during development and interacts in a common molecular pathway with the gene X-linked cyclin-dependent kinase-like 5 (CDKL5), whereby mutations cause epileptic encephalopathies (Nawaz et al., 2016). FKBP3 was identified in mass spectrometry as significantly upregulated in the female eEF1A2$^{E122K/E122K}$ mouse brain; however, no significant difference in expression was found across all mutants compared to wildtype. There was also no significant difference across all mouse brain mutants, irrespective of sex (*Figures 34a and 34b*). FKBP3 encodes a protein in the FKBP family and their functions include acting as chaperones in protein folding and trafficking (Bonner and Boulianne, 2017). FKBP3 interacts with mTOR and has been implicated in the progression of non-small cell lung cancer (NSCLC) (Zhu et al., 2017). However, there are no studies

reporting SHTN1 or FKBP3 having a role in eEF1A2's known functions or similar neurodevelopmental pathologies.

Overall, the western blot validation found that 3 out of the 5 proteins identified by mass spectrometry followed the same differential expression pattern. ZPR1 showed the opposite pattern of expression in western blotting to mass spectrometry, with decreased expression in E122K mutants (*Figures 34c and 34d*). However, confounding factors, such as high background staining, should be taken into consideration, and the results of the mass spectrometer were considered largely valid.
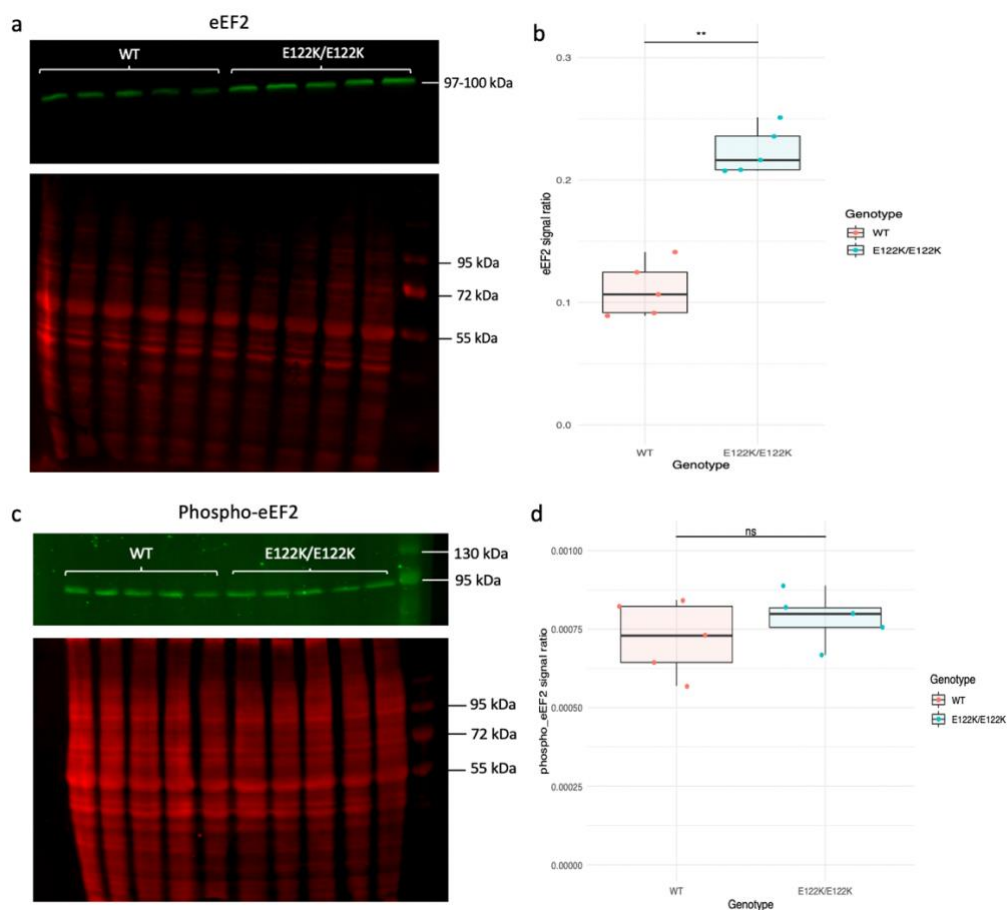
***Figure 32: eEF2 and phospho-eEF2 expression in mouse* eEF1A2$^{E122K/E122K}$ *brain tissue. Sample size (n) = 10 (5 male and 5 female). (a and b) show the western blot results and quantification of eEF2 expression, which was significantly higher in mutant E122K samples compared to wildtype (Wilcoxon test: W = 25, p-value = 0.01). (c and d) found no significant changes in phospho-eEF2 expression compared to wildtype (Wilcoxon test: W = 16, p-value = 0.55). Statistical significance: ns = non-significant,* ** *p ≤ 0.01. Image: author's own.*
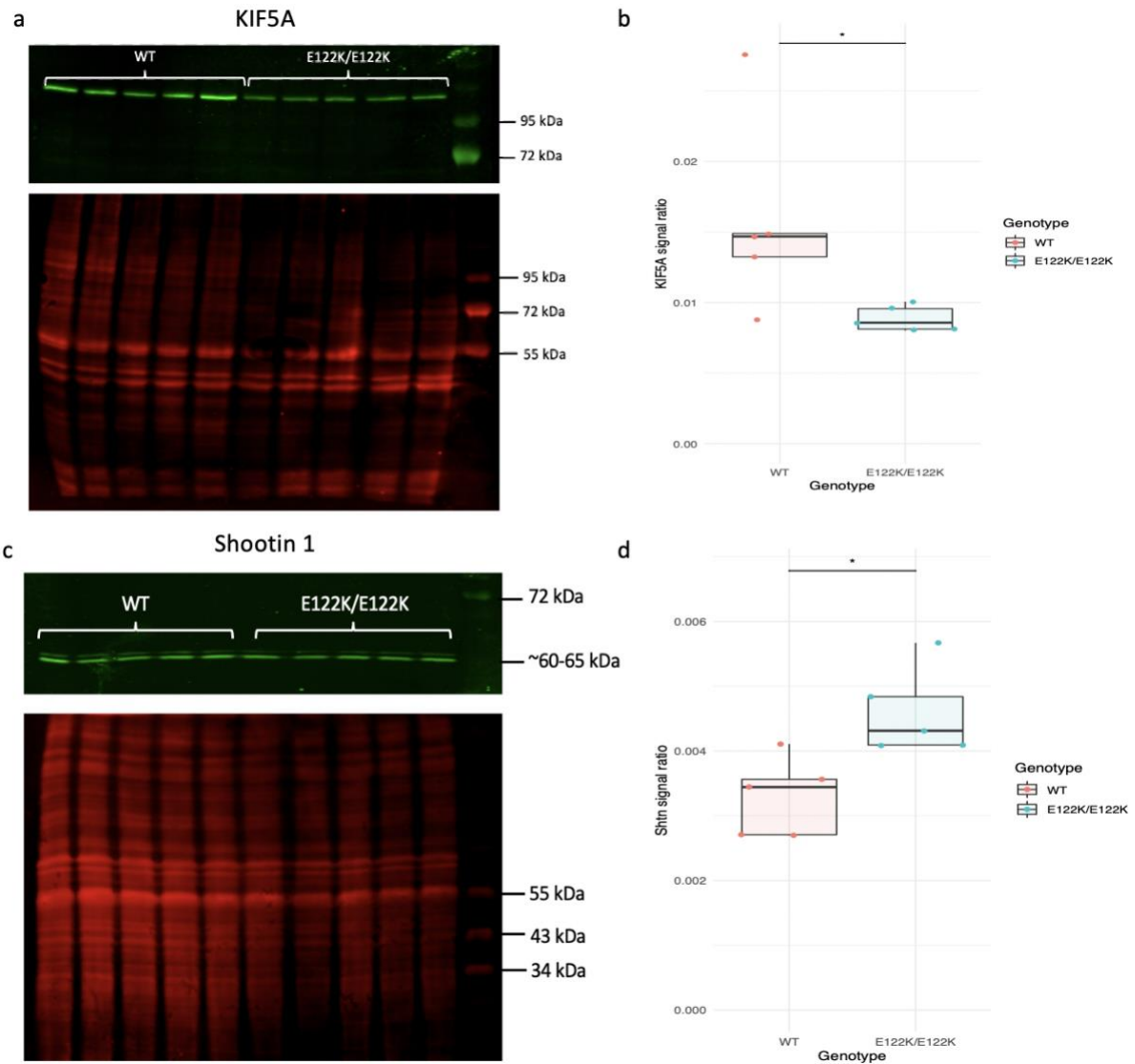
Figure 33: Western blot validation of KIF5A and SHTN 1 expression in eEF1A2$^{E122K/E122K}$ mouse brain tissue. *(a and b) show the western blot results and quantification of KIF5A expression, which was significantly lower eEF1A2$^{E122K/E122K}$ mutant mouse brain tissue compared to WT (Wilcoxon test: W = 2, p-value = 0.03). (c and d) show the western blot results and quantification of SHTN1 expression, which was significantly higher in E122K mutants (Wilcoxon test: W = 23, p-value = 0.03). Sample size (n) = 10 (5 male and 5 female). Statistical significance: ns = non-significant, * p ≤ 0.05. Image: author's own.*
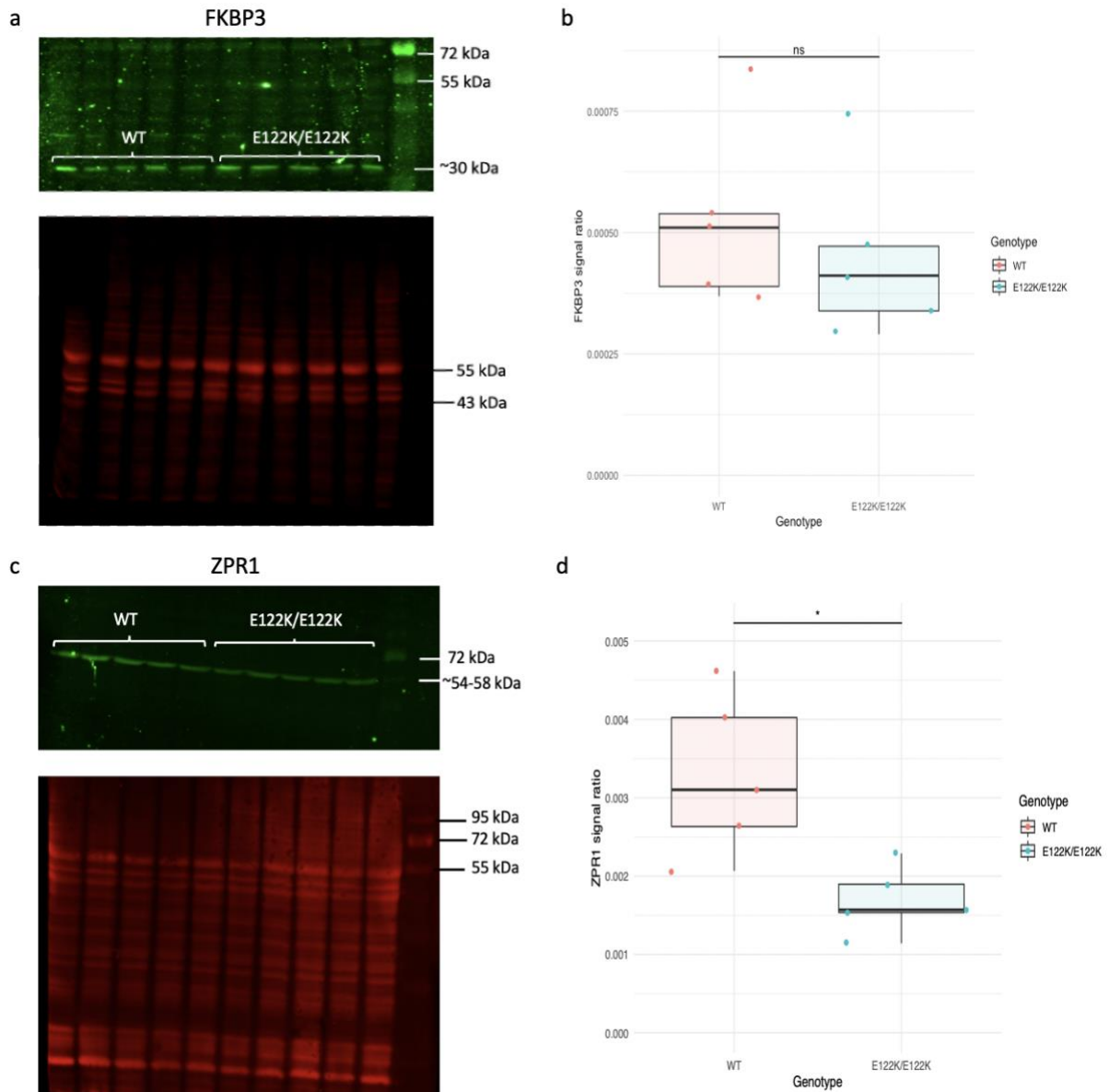
***Figure 34: Western blot validation of FKBP3 and ZPR1 expression in mouse* eEF1A2[E122K/E122K]**
brain tissue. *(a and b) show the western blot results and quantification of FKBP3 expression.*
No differences in expression were found in eEF1A2[E122K/E122K] mouse brain tissue compared to
wildtype (Wilcoxon test: W = 8, p-value = 0.42). (c and d) western blot results and
quantification of ZPR1 expression show that expression was significantly higher in WT samples
compared to E122K homozygotes (Wilcoxon test: W = 1, p-value = 0.02). Sample size (n) = 10
*(5 male and 5 female). Statistical significance: ns = non-significant, * p ≤ 0.05. Image: author's*
own.

Chapter 4: Discussion

4.1 Changes in the interactome could underlie differences in eEF1A2 mutants and tissue-specificity

The mutations D252H and E122K have different relative expression levels in the heart, muscle, and mouse brain suggestive of a tissue-specific interaction. It was also found in HEK293 transfections, that eEF1A2 expression was 61.5% lower in E122K mutants compared to 14.3% in D252H mutants, resembling the expression levels found in the E122K/E122K muscle (skeletal and heart) and the D252H mouse brain, respectively. A total of 30 proteins were significantly altered in the E122K.eEF1A2 interactome, whereas 35 proteins were significantly altered D252H.eEF1A2 interactome. An interactome analysis comparing the D252H.eEF1A2 and E122K.eEF1A2 interactomes found only four significantly altered molecular partners of eEF1A2 in common that all function in the eEF1B-ValRS complex, which as mentioned above, is a GEF for aa-tRNAs during translation elongation. The E122K.eEF1A2 interactome had many more significantly altered ribosomal proteins, which are essential for efficient protein translation. As mentioned above, eEF1Bγ binds to eEF1Bα and eEF1Bβ, and eEF1Bβ forms a stable homotrimer Bondarchuk et al. (2022). Therefore, a defect in one of the subunits could be destabilizing to the whole complex, affecting its function. Mutations in eEF1Bα caused global developmental delay, epilepsy, and intellectual disability that could not be rescued by eEF1Bβ, suggesting that subunits of the complex cannot compensate for each other (Bondarchuk et al., 2022; Larcher et al., 2020). This reflects the findings of the interactome analysis in which all subunits of the eEF1B-ValRS were downregulated. An *in vitro* assay measuring the rates of guanine nucleotide exchange on eEF1A isoforms revealed that eEF1A2 isoform is more dependent on GDP/GTP exchange than eEF1A1, suggesting that the eEF1B-ValRS complex is necessary for translation efficiency neurons, which express eEF1A2 (Trosiuk et al., 2016). Thus, translation efficiency is one of the major biological processes affected in D252H.eEF1A2 and E122K.eEF1A2 mutants. These findings could be interesting to compare to the interactomes of less severe mutants, such as E124K, to determine if proteins encoding the eEF1B-ValRS complex are also affected and contributing to pathogenicity (*Table 1*).

Several studies have reported on eEF1A2's non-canonical functions in regulating actin dynamics. Interestingly, no proteins involved in pathways regulating actin dynamics, such as RhoA, were not identified as significant in the interactome or E122K mutant mouse proteome (Mendoza et al., 2021). However, proteins associated with actin dynamics, such as Shootin1 and MYL4, could indicate that either eEF1A2 interacts with actin indirectly or that actin dynamics are not significantly affected by E122K (*Table 1*).

4.2 Does phenotype severity in mouse models correlate to an altered proteome?

A differential expression analysis was then conducted on the eEF1A2$^{E122K/E122K}$ mouse brain to identify changes in the brain proteome caused by E122K.eEF1A2. Human *EEF1A2* and mouse *eEf1A2* are almost identical and only differ by one amino acid out of 463. The eEF1A2$^{E122K/E122K}$ mouse model has been extensively studied by Grant Marshall in his PhD thesis, which details the E122K mutant mouse extensively, including the body weight, neuroscore, ambulation, and grip strength. Homozygous E122K/E122K mice are postnatal lethal and reach humane endpoints between P27 and P31 (*Figure 35*). The mouse brain samples used in this project were between P28 and P30. As expected, this project found proteins involved in translation elongation had significantly altered expression, but considering how pathogenic and severe these mutations are, it is surprising that these results don't show a higher fold change in expression and/or more proteins altered by the mutation or skewing towards downregulation. Some neurological defects, such as motor defects, appeared to be sex-specific as male mice exhibited ambulation deficits at P10, whereas only female heterozygotes showed increased righting latencies and negative geotaxis latencies at P8 and P10, respectively. As previously mentioned, sex-specific differences in eEF1A2 expression in muscle and brain tissue were also observed in E122K heterozygote and homozygous mouse models, with no significant changes in eEF1A2 expression in female E122K heterozygotes and male E122K heterozygotes exhibiting lower eEF1A2 expression relative to WT (*Tables 8 and 9*). Our comparative analysis of the female and male eEF1A2$^{E122K/E122K}$ brain proteome also found differences in overall differential protein expression, with females showing fewer differentially expressed proteins. However, it is unknown whether sex-specific differences in the mouse proteome could correlate to differences in phenotype severity.
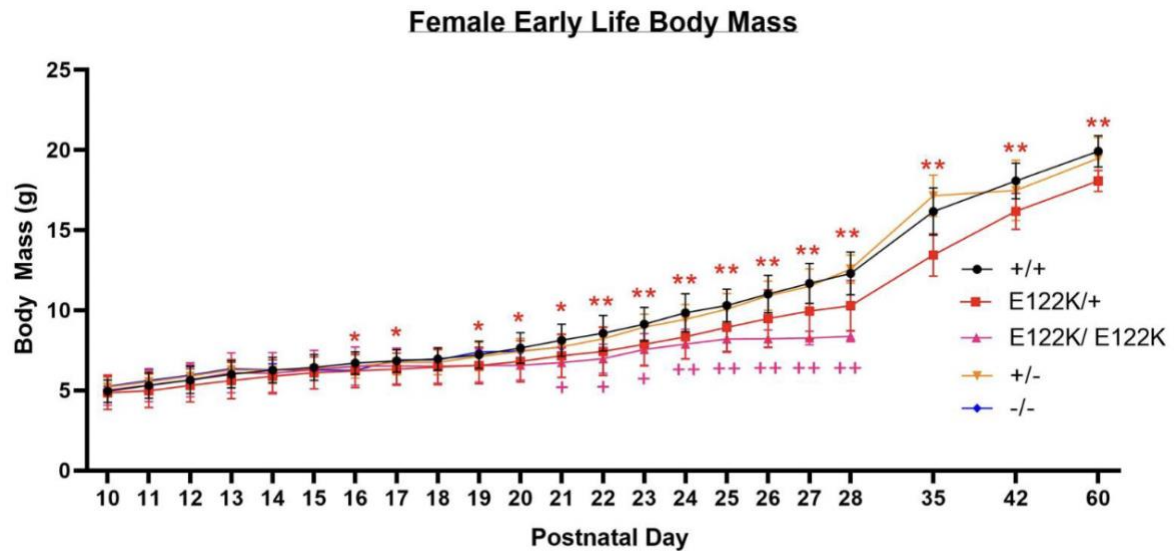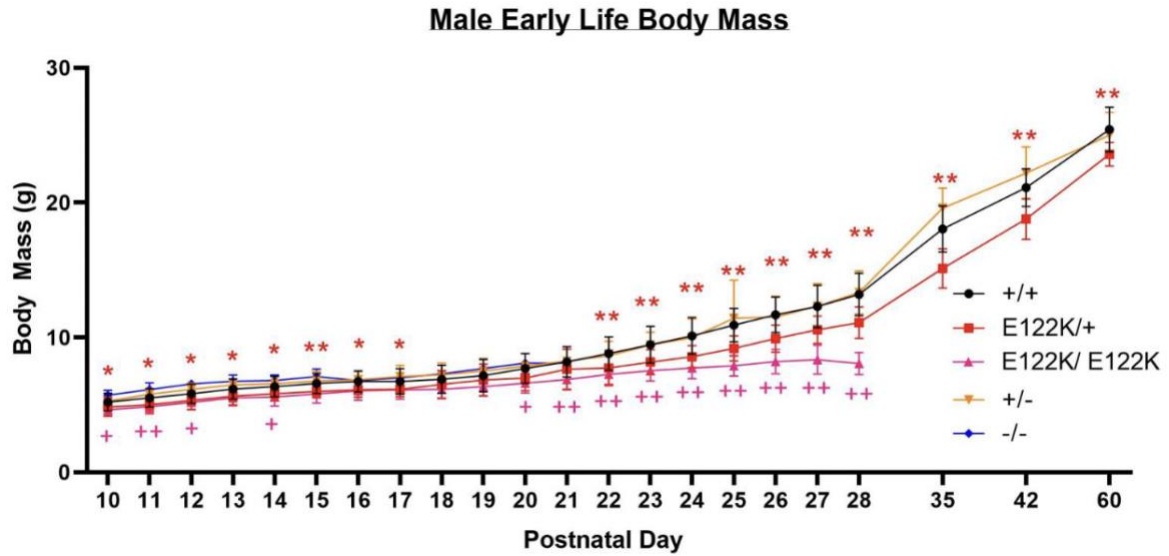
Figure 35: Comparing male and female body mass to heterozygous and homozygous E122K mutants. The + symbol indicates statistical significance in E122K/E122K homozygotes compared to wildtype (+/+). The asterisks (*) show statistical significance comparing body mass in E122K/+ heterozygotes to wildtype (+/+). Figure taken from: (Marshall, 2022).

4.3 Analysis of post-translational modifications (PTMs) in the mouse eEF1A2$^{E122K/E122K}$ brain proteome

As mentioned above, eEF1A2 has multiple sites of phosphorylation, which is an important regulator of canonical and non-canonical functions of the eEF1 complex (Sasikumar et al., 2012). Importantly, many of the predicted phosphosites are specific to eEF1A2 and not shared with eEF1A1 (Mendoza et al., 2021; Soares and Abbott, 2013). The elongation factor, eEF2, is also regulated by phosphorylation and was the most significantly upregulated protein identified in the differential expression analysis. Therefore, a PTM analysis was conducted on the software pipeline, DIA/NN, to identify any relevant PTMs that could alter protein function. Once PTMs were identified by the pipeline, a statistical analysis was conducted to select the statistically significant PTMs in differentially expressed proteins in the mouse eEF1A2$^{E122K/E122K}$ brain. UNIMOD is a database of protein modifications for mass spectrometry, and PTMs were identified by their assigned UNIMOD identifier (Creasy and Cottrell, 2004). The protein eEF2 was of particular interest as its phosphorylation via the EEF2/EEFK pathway has been implicated in epilepsy. A study discovered that genetic and pharmacological inhibition of the eEFK kinase ameliorated symptoms of epilepsy in a Scn1a +/- mouse model of Dravet syndrome. Similar to the pathology of mutated eEF1A2, Dravet syndrome is a childhood disorder characterized by severe epilepsy, intellectual disability, and autism (Beretta et al., 2022). Increased phosphorylation of eEF2 was found in Scn1a +/- mice prior to genetic and pharmacological manipulation, and the same was observed in other diseases, including Alzheimer's disease and Parkinson's disease (Jan et al., 2018, 2017). Western blotting identified the expression of phosphorylated eEF2 in the mouse eEF1A2$^{E122K/E122K}$ brain, but the PTM analysis results did not identify eEF2 phosphorylation. The majority of significant PTMs identified in the differentially expressed proteins in the eEF1A2$^{E122K/E122K}$ brain proteome were carbamidomethylation, a synthetic PTM attached to cysteine residues during sample preparation to prevent side reactions that can affect the proteomic analysis results (Kuznetsova et al., 2020). Moreover, the mouse brain tissue samples weren't enriched for phosphopeptides, so the analysis was considered more of a comparative analysis. Phosphorylation is difficult to detect in mass spectrometry due to its low ionization efficiency and abundance, which is further reduced after proteolytic digestion. Phosphopeptide enrichment of samples prior to mass spectrometry analysis reduces the likelihood of loss of

phosphorylation (Li et al., 2016; Steen et al., 2006). It is likely that some degree of phosphorylation was lost during the preparation and analysis of samples by mass spectrometry as phospho-eEF2 was detected in these mouse brain samples by western blotting (*Figures 32c and d*).

4.4 Are western blotting and mass spectrometry effective research partners?

Western blotting is an effective and low-cost technique for detecting proteins in complex samples of tissue and/or cells. However, the accuracy of protein detection largely depends on antibody specificity. In this project, there were challenges in eEF1A2 antibody specificity because both eEF1A isoforms are very similar structurally and at the amino acid level. Moreover, the molecular weight of both isoforms is almost the same (~ 52 kDa), so it was difficult to distinguish the isoforms on western blotting. However, the use of appropriate controls, WT muscle in mice and wst/wst samples, in western blotting overcame the challenge of distinguishing eEF1A isoforms. Another caveat found in western blotting during this project was that some antibodies failed to detect proteins identified in mass spectrometry. Antibodies for MOB1 and SUPT16H failed to detect its specific proteins for validation of the mass spectrometry and co-immunoprecipitation experiments, respectively. Working positive controls for the MOB1 antibody suggested the issue was that MOB1 has low abundance in the mouse brain, therefore, western blotting may not have been sensitive enough to detect MOB1. Additionally, a preliminary western blot for eEF2 showed no significant difference in expression in western blotting; however, a 50% reduction in the amount of protein loaded onto western blot gels showed the same expression pattern as the results of the mass spectrometry (Figure 32a and b). This observation could be due to oversaturated secondary antibody fluorescence due to high amounts of protein loaded that are outside the linear range of dynamic detection. Due to time limitations, western blots weren't repeated for FKBP3 and ZPR1 to determine if the loaded protein in western blots were also likely outside the linear range of detection (*Figure 34*). Western blotting could also have limited sensitivity, in comparison to mass spectrometry, with small changes in protein expression not as easily detectable on western blotting (Taylor et al., 2013). However, optimization of protein loading and detection prior to analysis can reduce the occurrence of these caveats.

A combination of co-immunoprecipitation and mass spectrometry were effective high-throughput techniques for identifying molecular binding partners altered by E122K mutant eEF1A2. Despite it being more expensive than western blotting, mass spectrometry is much more sensitive at detecting proteins with low abundance in complex samples and can be more informative about peptide structure and PTMs (Domon and Aebersold, 2006). Furthermore, this approach vastly reduces the number of western blots needed for the same type of analysis. However, a caveat of mass spectrometry is that less abundant PTMs, such as phosphorylation, are difficult to detect and are easily degraded without prior enrichment of samples, such as phosphopeptide enrichment (Kim et al., 2011). Future studies could focus on PTMs in eEF1A2 and its binding partners by enriching samples prior to mass spectrometry analysis followed by western blotting with antibodies specific for phosphorylated eEF1A2 to validate the findings.

In this project, both the standard and robot co-immunoprecipitation experiments were performed. The challenges of standard co-immunoprecipitation were antibody detection and specificity, as multiple bands were detected for a specific protein and some blots failed to detect the desired protein at all. Due to time limitations, the co-immunoprecipitation experiments could not be repeated, but the approach was an effective and cheaper method of validating the interactome analysis findings in the neuronal cell line, SH-SY5Y, as well as other samples of HEK293T cells. These findings did not detect any differences across the SH-SY5Y and HEK293T cell lines, suggesting both cell lines are appropriate models to study the interactome of mutant eEF1A2, at least for ubiquitously expressed protein binding partners.

4.5 Molecular pathways interconnect neurodevelopmental disorders and cancer

Neurodevelopmental disorders and cancer share common affected genes and have converging molecular pathways (Nussinov et al., 2022a). It was reasoned that some molecular binding partners of eEF1A2 could be associated with cancer as eEF1A2 was identified as an oncogene which is overexpressed in ovarian cancer, resulting in increased cell proliferation (Lee, 2003). Therefore, a disease enrichment analysis was conducted to determine which significantly affected proteins in the E122K.eEF1A2 interactome were also associated with cancer. Multiple proteins were found associated with a broad range of enriched cancers, including oligodendrogliomas and gliosarcomas (*Figure 36*). Comparably, the differential expression analysis of the mutant mouse brain proteomes found altered proteins involved in chromatin remodelling, which is also associated with cancer (*Figure 31*) (Nussinov et al., 2022b). Thus, future research and treatment of eEF1A2-related neurodevelopmental disorders should arguably consider the link to cancer for potential drug repurposing. Metarrestin was identified as a potential anti-cancer drug that targets metastasis by inhibiting the perinucleolar compartment (PNC), a subcellular body located next to the nucleolus that is detected in cancer cells. PNC prevalence in cancer cells and tissues correlate with disease progression and inversely correlate with patient outcomes in cancers, such as breast cancer (Frankowski et al., 2018; Kamath et al., 2005). A study found metarrestin binds to eEF1A2, and a reduction of *eEF1A2* disrupted PNC structure, which resembled metarrestin treated human prostate cancer cells (PC3M) (Frankowski et al., 2018). However, a study assessing the safety of metarrestin treatment in dogs revealed side effects, including behavioural changes, ataxia, and seizure-like symptoms, which were suggested to be caused by eEF1A2 inhibition (Bourdi et al., 2020). Nevertheless, analysis of the E122K.eEF1A2 interactome identified multiple proteins that are also associated with cancer, which could be potential targets for drug research.

Figure 36: The E122K.eEF1A2 interactome is associated with cancer. *A disease enrichment analysis showed all the significantly altered proteins in the E122K.eEF1A2 interactome associated with the 35 most enriched cancers. The adjusted p-value shows the significance level of the protein clusters. Image is author's own and was created on R studio using the DOSE package.*

4.6 A hypothesis-generating approach to targeting complex neurodevelopmental disorders

Differentially expressed proteins in the mouse eEF1A2$^{E122K/E122K}$ brain proteome could be potential biomarkers for mechanism-targeting research that aims to rescue or ameliorate disease phenotypes in animal models of epilepsy and/or neurodevelopmental disorders resembling eEF1A2-related disorders. For example, as mentioned above, in the Scn1a +/- mouse model of Dravet syndrome researchers pharmacologically and genetically manipulated eEF2K, a regulator of eEF2, which ameliorated the disease phenotype (Beretta et al., 2022). Therefore, eEF2 could be a potential biomarker for Dravet syndrome.

Mutations in cyclin-dependent-like kinase 5 (CDKL5) cause infantile epileptic encephalopathies, and knockout (KO) Cdkl mouse models exhibit many of the same disease symptoms, including deficits in learning, motor control, and sociability (Zhou et al., 2020). A study found that Shootin1 interacts with CDKL5 in a complex in yeast, and both act in the same molecular pathway (Nawaz et al., 2016). Therefore, targeting Shootin1 in Cdkl KO mouse models could give more mechanistic insights into CDKL disorder.

TSPAN2 was one of the most downregulated proteins in the eEF1A2$^{E122K/E122K}$ mouse brain and had previously been found to be differentially expressed in the dentate granule cell layer in the hippocampus of rat seizure models which is typically resistant to seizure-induced damage (Borges et al., 2007). The aim of the study was to identify the mechanisms of neuroprotective effects in preconditioned seizures against status epilepticus damage. Therefore, TSPAN2 could be a potential biomarker for epilepsy, but further studies would be required to ensure that the findings were a neuroprotective effect and not just the result of preconditioning. Alternatively, TSPAN2 could be a marker for assessing correction of the E122K phenotype in animal models.

Therefore, the significantly differentially expressed proteins found in the eEF1A2$^{E122K/E122K}$ mouse brain could be considered a hypothesis-generating approach to identifying potential biomarkers for other complex neurodevelopmental disorders.

Chapter 5: Conclusion

This project aimed to improve current understanding of how mutations affect eEF1A2 function by implementing a hypothesis-generating approach using high-throughput proteomics experiments and bioinformatics. An interactome analysis was performed to identify altered eEF1A2 binding proteins resulting from the E122K mutation. Some of most significantly altered proteins were subunits of the eEF1B-ValRS complex, a GEF that facilitates the GTP-dependent delivery of aa-tRNAs during translation elongation. A comparative analysis of mutant eEF1A2 interactomes revealed the eEF1B-ValRS complex was also significantly downregulated in the D252H.eEF1A2 interactome. Mutations in eEF1A2 were suggested to cause a conformational change in eEF1A2 that affects its ability to bind to molecular binding partners (Carvill et al., 2020; Davies et al., 2020). Therefore, we can infer that E122K most likely induces a conformational change in eEF1A2, causing altered binding to molecular partners.

GO and STRING analyses categorised significantly altered proteins into their enriched biological pathways and predicted functional associations, respectively, as a strategy for grouping altered eEF1A2 molecular partners by common functions and biological pathways. Multiple ribosomal subunits that form the 80S ribosome were found altered in the E122K.eEF1A2 interactome, and translation elongation was one of the most enriched biological pathways, suggesting multiple proteins involved in protein translation regulation and quality control are altered in the E122K.eEF1A2 interactome and likely reduce translation efficiency. Comparing the interactome of eEF1A2 affected by different missense mutations could highlight common molecular pathways that could be manipulated in future experiments and give insight into why there is such a broad range of disease severity across different mutations and/or identify proteins that ameliorate the mutant phenotype in animal models. However, applying the same proteomics techniques of AP-MS might prove challenging for mutations, such as P333L, which were shown to be unstable in western blot analyses of E122K.eEF1A2 HEK293T transfections. A caveat of AP-MS is that unstable proteins are less likely to maintain protein–protein interactions resistant to the lysis and purification conditions, which are necessary for AP-MS protein detection (Gingras et al., 2007).

This project found D252H and E122K mutant eEF1A2 expression levels in mouse heart tissue resembled those found in mutant mouse muscle. HEK293T transfections of D252H, P333L, and E122K eEF1A2 constructs found significantly decreased expression in mutants relative to WT, suggesting mutation may alter eEF1A2 stability. Mutant eEF1A2 expression in HEK293T cells didn't resemble the expression levels found across different mouse tissues, validating previous findings suggesting a tissue-specific interaction across different mutations in eEF1A2.

A differential expression analysis of the eEF1A2$^{E122K/E122K}$ mouse brain proteome revealed proteins involved in translation elongation were downregulated that suggested altered regulation of translation. Other altered proteins were linked to other neurodevelopmental disorders and cancer, which may prove advantageous for future research targeting of eEF1A2-causing neurodevelopmental disorders in animal models. Alternatively, the differential expression analysis results could be potential biomarkers for future studies targeting the affected phenotype in mutant eEF1A2 animal models. Some of the limitations of this project included antibody specificity and detection in western blotting validation experiments that required several rounds of optimization but were limited by time constraints. The GO analysis results could be another potential limitation as several identified enriched pathways are localized in the nucleus and eEF1A2 is a cytosolic protein. Therefore, future experiments are required to validate these findings.

Overall, this project provides avenues for further research in examining the role of eEF1A2 mutations, how they affect its function, and cause neurodevelopmental disorders.

References

Amor, D.J., Stephenson, S.E.M., Mustapha, M., Mensah, M.A., Ockeloen, C.W., Lee, W.S., Tankard, R.M., Phelan, D.G., Shinawi, M., de Brouwer, A.P.M., Pfundt, R., Dowling, C., Toler, T.L., Sutton, V.R., Agolini, E., Rinelli, M., Capolino, R., Martinelli, D., Zampino, G., Dumić, M., Reardon, W., Shaw-Smith, C., Leventer, R.J., Delatycki, M.B., Kleefstra, T., Mundlos, S., Mortier, G., Bahlo, M., Allen, N.J., Lockhart, P.J., 2019. Pathogenic Variants in GPC4 Cause Keipert Syndrome. The American Journal of Human Genetics 104, 914–924. https://doi.org/10.1016/j.ajhg.2019.02.026

Andersen, G.R., Valente, L., Pedersen, L., Kinzy, T.G., Nyborg, J., 2001. Crystal structures of nucleotide exchange intermediates in the eEF1A–eEF1Bα complex. Nat. Struct Biol. 8, 531–534. https://doi.org/10.1038/88598

Bec, G., Kerjan, P., Waller, J.P., 1994. Reconstitution in vitro of the valyl-tRNA synthetase-elongation factor (EF) 1 beta gamma delta complex. Essential roles of the NH2-terminal extension of valyl-tRNA synthetase and of the EF-1 delta subunit in complex formation. Journal of Biological Chemistry 269, 2086–2092. https://doi.org/10.1016/S0021-9258(17)42139-9

Beretta, S., Gritti, L., Ponzoni, L., Scalmani, P., Mantegazza, M., Sala, M., Verpelli, C., Sala, C., 2022. Rescuing epileptic and behavioral alterations in a Dravet syndrome mouse model by inhibiting eukaryotic elongation factor 2 kinase (eEF2K). Molecular Autism 13, 1. https://doi.org/10.1186/s13229-021-00484-0

Bina, R., Matalon, D., Fregeau, B., Tarsitano, J.J., Aukrust, I., Houge, G., Bend, R., Warren, H., Stevenson, R.E., Stuurman, K.E., Barkovich, A.J., Sherr, E.H., 2020. De novo variants in *SUPT16H* cause neurodevelopmental disorders associated with corpus callosum abnormalities. J Med Genet 57, 461–465. https://doi.org/10.1136/jmedgenet-2019-106193

Bondarchuk, T.V., Shalak, V.F., Lozhko, D.M., Fatalska, A., Szczepanowski, R.H., Liudkovska, V., Tsuvariev, O.Y., Dadlez, M., El'skaya, A.V., Negrutskii, B.S., 2022. Quaternary organization of the human eEF1B complex reveals unique multi-GEF domain assembly. Nucleic Acids Research gkac685. https://doi.org/10.1093/nar/gkac685

Bonner, J.M., Boulianne, G.L., 2017. Diverse structures, functions and uses of FK506 binding proteins. Cellular Signalling 38, 97–105. https://doi.org/10.1016/j.cellsig.2017.06.013

Borges, K., Shaw, R., Dingledine, R., 2007. Gene expression changes after seizure preconditioning in the three major hippocampal cell layers. Neurobiology of Disease 26, 66–77. https://doi.org/10.1016/j.nbd.2006.12.001

Bourdi, M., Rudloff, U., Patnaik, S., Marugan, J., Terse, P.S., 2020. Safety assessment of metarrestin in dogs: A clinical candidate targeting a subnuclear structure unique to metastatic cancer cells. Regulatory Toxicology and Pharmacology 116, 104716. https://doi.org/10.1016/j.yrtph.2020.104716

Brenner, D., Yilmaz, R., Müller, K., Grehl, T., Petri, S., Meyer, T., Grosskreutz, J., Weydt, P., Ruf, W., Neuwirth, C., Weber, M., Pinto, S., Claeys, K.G., Schrank, B., Jordan, B., Knehr, A., Günther, K., Hübers, A., Zeller, D., Kubisch, C., Jablonka, S., Sendtner, M., Klopstock, T., de Carvalho, M., Sperfeld, A., Borck, G., Volk, A.E., Dorst, J., Weis, J., Otto, M., Schuster, J., Del Tredici, K., Braak, H., Danzer, K.M., Freischmidt, A., Meitinger, T., Strom, T.M., Ludolph, A.C., Andersen, P.M., Weishaupt, J.H., The German ALS network MND-NET, Weyen, U., Hermann, A., Hagenacker, T., Koch, J.C., Lingor, P., Göricke, B., Zierz, S., Baum, P., Wolf, J., Winkler, A., Young, P., Bogdahn, U., Prudlo, J., Kassubek, J., 2018. Hot-spot KIF5A mutations cause familial ALS. Brain 141, 688–697. https://doi.org/10.1093/brain/awx370

Cao, S., Smith, L.L., Padilla-Lopez, S.R., Guida, B.S., Blume, E., Shi, J., Morton, S.U., Brownstein, C.A., Beggs, A.H., Kruer, M.C., Agrawal, P.B., 2017. Homozygous EEF1A2 mutation causes dilated cardiomyopathy, failure to thrive, global developmental delay, epilepsy and early death. Human Molecular Genetics 26, 3545–3552. https://doi.org/10.1093/hmg/ddx239

Cao, Y., Portela, M., Janikiewicz, J., Doig, J., Abbott, C.M., 2014. Characterisation of Translation Elongation Factor eEF1B Subunit Expression in Mammalian Cells and Tissues and Co-Localisation with eEF1A2. PLoS ONE 9, e114117. https://doi.org/10.1371/journal.pone.0114117

Carriles, A.A., Mills, A., Muñoz-Alonso, M., Gutiérrez, D., Domínguez, J.M., Hermoso, J.A., Gago, F., 2021. Structural Cues for Understanding eEF1A2 Moonlighting. ChemBioChem 22, 374–391. https://doi.org/10.1002/cbic.202000516

Carvill, G.L., Helbig, K.L., Myers, C.T., Scala, M., Huether, R., Lewis, S., Kruer, T.N., Guida, B.S., Bakhtiari, S., Sebe, J., Tang, S., Stickney, H., Oktay, S.U., Bhandiwad, A.A., Ramsey, K., Narayanan, V., Feyma, T., Rohena, L.O., Accogli, A., Severino, M., Hollingsworth, G., Gill, D., Depienne, C., Nava, C., Sadleir, L.G., Caruso, P.A., Lin, A.E., Jansen, F.E., Koeleman, B., Brilstra, E., Willemsen, M.H., Kleefstra, T., Sa, J., Mathieu, M.-L., Perrin, L., Lesca, G., Striano, P., Casari, G., Scheffer, I.E., Raible, D., Sattlegger, E., Capra, V., Padilla-Lopez, S., Mefford, H.C., Kruer, M.C., 2020. Damaging de novo missense variants in EEF1A2 lead to a developmental and degenerative epileptic-dyskinetic encephalopathy. Hum Mutat 41, 1263–1279. https://doi.org/10.1002/humu.24015

Chambers, D.M., Peters, J., Abbott, C.M., 1998. The lethal mutation of the mouse wasted (wst) is a deletion that abolishes expression of a tissue-specific isoform of translation elongation factor 1 , encoded by the Eef1a2 gene. Proceedings of the National Academy of Sciences 95, 4463–4468. https://doi.org/10.1073/pnas.95.8.4463

Chuang, S.-M., Chen, L., Lambertson, D., Anand, M., Kinzy, T.G., Madura, K., 2005. Proteasome-Mediated Degradation of Cotranslationally Damaged Proteins Involves Translation Elongation Factor 1A. Mol Cell Biol 25, 403–413. https://doi.org/10.1128/MCB.25.1.403-413.2005

Creasy, D.M., Cottrell, J.S., 2004. Unimod: Protein modifications for mass spectrometry. Proteomics 4, 1534–1536. https://doi.org/10.1002/pmic.200300744

Davies, F.C.J., Hope, J.E., McLachlan, F., Marshall, G.F., Kaminioti-Dumont, L., Qarkaxhija, V., Nunez, F., Dando, O., Smith, C., Wood, E., MacDonald, J., Hardt, O., Abbott, C.M., 2020. Recapitulation of the EEF1A2 D252H neurodevelopmental disorder-causing missense mutation in mice reveals a toxic gain of function. Human Molecular Genetics 29, 1592–1606. https://doi.org/10.1093/hmg/ddaa042

de Monasterio-Schrader, P., Patzig, J., Möbius, W., Barrette, B., Wagner, T.L., Kusch, K., Edgar, J.M., Brophy, P.J., Werner, H.B., 2013. Uncoupling of neuroinflammation from axonal degeneration in mice lacking the myelin protein tetraspanin-2: Tspan2-Deficient Myelin Induces Neuroinflammation. Glia 61, 1832–1847. https://doi.org/10.1002/glia.22561

De Rinaldis, M., Giorda, R., Trabacca, A., 2020. Mild epileptic phenotype associates with de novo eef1a2 mutation: Case report and review. Brain and Development 42, 77–82. https://doi.org/10.1016/j.braindev.2019.08.001

Dias, C.A.O., Gregio, A.P.B., Rossi, D., Galvão, F.C., Watanabe, T.F., Park, M.H., Valentini, S.R., Zanelli, C.F., 2012. eIF5A interacts functionally with eEF2. Amino Acids 42, 697–702. https://doi.org/10.1007/s00726-011-0985-0

Domon, B., Aebersold, R., 2006. Mass Spectrometry and Protein Analysis. Science 312, 212–217. https://doi.org/10.1126/science.1124619

Doran, B., Gherbesi, N., Hendricks, G., Flavell, R.A., Davis, R.J., Gangwani, L., 2006. Deficiency of the zinc finger protein ZPR1 causes neurodegeneration. Proc. Natl. Acad. Sci. U.S.A. 103, 7471–7475. https://doi.org/10.1073/pnas.0602057103

Dunham, W.H., Mullin, M., Gingras, A.-C., 2012. Affinity-purification coupled to mass spectrometry: Basic principles and strategies. Proteomics 12, 1576–1590. https://doi.org/10.1002/pmic.201100523

Fagerland, M.W., 2012. t-tests, non-parametric tests, and large studies—a paradox of statistical practice? BMC Med Res Methodol 12, 78. https://doi.org/10.1186/1471-2288-12-78

Fan, A., Zhao, Xiaojuan, Liu, H., Li, D., Guo, T., Zhang, J., Duan, L., Cheng, H., Nie, Y., Fan, D., Zhao, Xiaodi, Lu, Y., 2022. eEF1A1 promotes colorectal cancer progression and predicts poor prognosis of patients. Cancer Medicine cam4.4848. https://doi.org/10.1002/cam4.4848

Frankowski, K.J., Wang, C., Patnaik, S., Schoenen, F.J., Southall, N., Li, D., Teper, Y., Sun, W., Kandela, I., Hu, D., Dextras, C., Knotts, Z., Bian, Y., Norton, J., Titus, S., Lewandowska, M.A., Wen, Y., Farley, K.I., Griner, L.M., Sultan, J., Meng, Z., Zhou, M., Vilimas, T., Powers, A.S., Kozlov, S., Nagashima, K., Quadri, H.S., Fang, M., Long, C., Khanolkar, O., Chen, W., Kang, J., Huang, H., Chow, E., Goldberg, E., Feldman, C., Xi, R., Kim, H.R., Sahagian, G., Baserga, S.J., Mazar, A., Ferrer, M., Zheng, W., Shilatifard, A., Aubé, J., Rudloff, U., Marugan, J.J., Huang, S., 2018. Metarrestin, a perinucleolar compartment inhibitor, effectively suppresses metastasis. Sci. Transl. Med. 10, eaap8307. https://doi.org/10.1126/scitranslmed.aap8307

Gambino, G., Rizzo, V., Giglia, G., Ferraro, G., Sardo, P., 2022. Microtubule Dynamics and Neuronal Excitability: Advances on Cytoskeletal Components Implicated in Epileptic Phenomena. Cell Mol Neurobiol 42, 533–543. https://doi.org/10.1007/s10571-020-00963-7

Gergely, F., Karlsson, C., Still, I., Cowell, J., Kilmartin, J., Raff, J.W., 2000. The TACC domain identifies a family of centrosomal proteins that can interact with microtubules. Proc. Natl. Acad. Sci. U.S.A. 97, 14352–14357. https://doi.org/10.1073/pnas.97.26.14352

Gingras, A.-C., Gstaiger, M., Raught, B., Aebersold, R., 2007. Analysis of protein complexes using mass spectrometry. Nat Rev Mol Cell Biol 8, 645–654. https://doi.org/10.1038/nrm2208

Griffiths, L.A., Doig, J., Churchhouse, A.M.D., Davies, F.C.J., Squires, C.E., Newbery, H.J., Abbott, C.M., 2012. Haploinsufficiency for Translation Elongation Factor eEF1A2 in Aged Mouse Muscle and Neurons Is Compatible with Normal Function. PLoS ONE 7, e41917. https://doi.org/10.1371/journal.pone.0041917

Gross, S.R., Kinzy, T.G., 2007. Improper Organization of the Actin Cytoskeleton Affects Protein Synthesis at Initiation. Mol Cell Biol 27, 1974–1989. https://doi.org/10.1128/MCB.00832-06

Gross, S.R., Kinzy, T.G., 2005. Translation elongation factor 1A is essential for regulation of the actin cytoskeleton and cell morphology. Nat Struct Mol Biol 12, 772–778. https://doi.org/10.1038/nsmb979

Hirokawa, N., Noda, Y., Tanaka, Y., Niwa, S., 2009. Kinesin superfamily motor proteins and intracellular transport. Nat Rev Mol Cell Biol 10, 682–696. https://doi.org/10.1038/nrm2774

Inui, T., Kobayashi, S., Ashikari, Y., Sato, R., Endo, W., Uematsu, M., Oba, H., Saitsu, H., Matsumoto, N., Kure, S., Haginoya, K., 2016. Two cases of early-onset myoclonic seizures with continuous parietal delta activity caused by EEF1A2 mutations. Brain and Development 38, 520–524. https://doi.org/10.1016/j.braindev.2015.11.003

Jan, A., Jansonius, B., Delaidelli, A., Bhanshali, F., An, Y.A., Ferreira, N., Smits, L.M., Negri, G.L., Schwamborn, J.C., Jensen, P.H., Mackenzie, I.R., Taubert, S., Sorensen, P.H., 2018. Activity of translation regulator eukaryotic elongation factor-2 kinase is

increased in Parkinson disease brain and its inhibition reduces alpha synuclein toxicity. acta neuropathol commun 6, 54. https://doi.org/10.1186/s40478-018-0554-9

Jan, A., Jansonius, B., Delaidelli, A., Somasekharan, S.P., Bhanshali, F., Vandal, M., Negri, G.L., Moerman, D., MacKenzie, I., Calon, F., Hayden, M.R., Taubert, S., Sorensen, P.H., 2017. eEF2K inhibition blocks Aβ42 neurotoxicity by promoting an NRF2 antioxidant response. Acta Neuropathol 133, 101–119. https://doi.org/10.1007/s00401-016-1634-1

Kahns, S., Lund, A., Kristensen, P., Knudsen, C.R., Clark, B.F., Cavallius, J., Merrick, W.C., 1998. The elongation factor 1 A-2 isoform from rabbit: cloning of the cDNA and characterization of the protein. Nucleic Acids Res 26, 1884–1890. https://doi.org/10.1093/nar/26.8.1884

Kaitsuka, T., Kiyonari, H., Shiraishi, A., Tomizawa, K., Matsushita, M., 2018. Deletion of Long Isoform of Eukaryotic Elongation Factor 1Bδ Leads to Audiogenic Seizures and Aversive Stimulus-Induced Long-Lasting Activity Suppression in Mice. Front. Mol. Neurosci. 11, 358. https://doi.org/10.3389/fnmol.2018.00358

Kaitsuka, T., Matsushita, M., 2015. Regulation of Translation Factor EEF1D Gene Function by Alternative Splicing. IJMS 16, 3970–3979. https://doi.org/10.3390/ijms16023970

Kamath, R.V., Thor, A.D., Wang, C., Edgerton, S.M., Slusarczyk, A., Leary, D.J., Wang, J., Wiley, E.L., Jovanovic, B., Wu, Q., Nayar, R., Kovarik, P., Shi, F., Huang, S., 2005. Perinucleolar Compartment Prevalence Has an Independent Prognostic Value for Breast Cancer. Cancer Research 65, 246–253. https://doi.org/10.1158/0008-5472.246.65.1

Kaneko, M., Rosser, T., Raca, G., 2021. Dilated cardiomyopathy in a patient with autosomal dominant EEF1A2-related neurodevelopmental disorder. European Journal of Medical Genetics 64, 104121. https://doi.org/10.1016/j.ejmg.2020.104121

Kaul, G., Pattan, G., Rafeequi, T., 2011. Eukaryotic elongation factor-2 (eEF2): its regulation and peptide chain elongation. Cell Biochem. Funct. 29, 227–234. https://doi.org/10.1002/cbf.1740

Khalyfa, A., Bourbeau, D., Chen, E., Petroulakis, E., Pan, J., Xu, S., Wang, E., 2001. Characterization of Elongation Factor-1A (eEF1A-1) and eEF1A-2/S1 Protein Expression in Normal and wasted Mice. Journal of Biological Chemistry 276, 22915–22922. https://doi.org/10.1074/jbc.M101011200

Kim, J.-S., Kim, J., Oh, J.M., Kim, H.-J., 2011. Tandem mass spectrometric method for definitive localization of phosphorylation sites using bromine signature. Analytical Biochemistry 414, 294–296. https://doi.org/10.1016/j.ab.2011.03.032

Kjaer, S., Wind, T., Ravn, P., Østergaard, M., Clark, B.F.C., Nissim, A., 2001. Generation and epitope mapping of high-affinity scFv to eukaryotic elongation factor 1A by dual application of phage display: Mapping of scFv to isoforms of elongation factor 1A. European Journal of Biochemistry 268, 3407–3415. https://doi.org/10.1046/j.1432-1327.2001.02240.x

Knudsen, S.M., Frydenberg, J., Clark, B.F.C., Leffers, H., 1993. Tissue-dependent variation in the expression of elongation factor-1alpha isoforms: Isolation and characterisation of a cDNA encoding a novel variant of human elongation-factor 1alpha. Eur J Biochem 215, 549–554. https://doi.org/10.1111/j.1432-1033.1993.tb18064.x

Konrad, E.D.H., Nardini, N., Caliebe, A., Nagel, I., Young, D., Horvath, G., Santoro, S.L., Shuss, C., Ziegler, A., Bonneau, D., Kempers, M., Pfundt, R., Legius, E., Bouman, A., Stuurman, K.E., Õunap, K., Pajusalu, S., Wojcik, M.H., Vasileiou, G., Le Guyader, G., Schnelle, H.M., Berland, S., Zonneveld-Huijssoon, E., Kersten, S., Gupta, A., Blackburn, P.R., Ellingson, M.S., Ferber, M.J., Dhamija, R., Klee, E.W., McEntagart, M., Lichtenbelt, K.D., Kenney, A., Vergano, S.A., Abou Jamra, R., Platzer, K., Ella Pierpont, M., Khattar, D., Hopkin, R.J., Martin, R.J., Jongmans, M.C.J., Chang, V.Y., Martinez-Agosto, J.A., Kuismin, O., Kurki, M.I., Pietiläinen, O., Palotie, A., Maarup, T.J., Johnson, D.S., Venborg Pedersen, K., Laulund, L.W., Lynch, S.A., Blyth, M., Prescott, K., Canham, N., Ibitoye, R., Brilstra, E.H., Shinawi, M., Fassi, E., Sticht, H., Gregor, A., Van Esch, H., Zweier, C., 2019. CTCF variants in 39 individuals with a variable neurodevelopmental disorder broaden the mutational and clinical spectrum. Genetics in Medicine 21, 2723–2733. https://doi.org/10.1038/s41436-019-0585-z

Kuznetsova, K.G., Solovyeva, E.M., Kuzikov, A.V., Gorshkov, M.V., Moshkovskii, S.A., 2020. Modification of Cysteine Residues for Mass Spectrometry-Based Proteomic Analysis: Facts and Artifacts. Biochem. Moscow Suppl. Ser. B 14, 204–215. https://doi.org/10.1134/S1990750820030087

Lam, W.W.K., Millichap, J.J., Soares, D.C., Chin, R., McLellan, A., FitzPatrick, D.R., Elmslie, F., Lees, M.M., Schaefer, G.B., DDD study, Abbott, C.M., 2016. Novel de novo EEF1A2 missense mutations causing epilepsy and intellectual disability. Mol Genet Genomic Med 4, 465–474. https://doi.org/10.1002/mgg3.219

Larcher, L., Buratti, J., Héron-Longe, B., Benzacken, B., Pipiras, E., Keren, B., Delahaye-Duriez, A., 2020. New evidence that biallelic loss of function in EEF1B2 gene leads to intellectual disability. Clin Genet 97, 639–643. https://doi.org/10.1111/cge.13688

LaSalle, J., 2013. Autism genes keep turning up chromatin. OA Autism 1. https://doi.org/10.13172/2052-7810-1-2-610

le Cessie, S., Goeman, J.J., Dekkers, O.M., 2020. Who is afraid of non-normal data? Choosing between parametric and non-parametric tests. European Journal of Endocrinology 182, E1–E3. https://doi.org/10.1530/EJE-19-0922

Lee, D.H., Goldberg, A.L., 1998. Proteasome inhibitors: valuable new tools for cell biologists. Trends in Cell Biology 8, 397–403. https://doi.org/10.1016/S0962-8924(98)01346-4

Lee, J.M., 2003. The role of protein elongation factor eEF1A2 in ovarian cancer. Reprod Biol Endocrinol 1, 69. https://doi.org/10.1186/1477-7827-1-69

Li, X.-S., Yuan, B.-F., Feng, Y.-Q., 2016. Recent advances in phosphopeptide enrichment: Strategies and techniques. TrAC Trends in Analytical Chemistry 78, 70–83. https://doi.org/10.1016/j.trac.2015.11.001

Long, K., Wang, H., Song, Z., Yin, X., Wang, Y., 2020. EEF1A2 mutations in epileptic encephalopathy/intellectual disability: Understanding the potential mechanism of phenotypic variation. Epilepsy & Behavior 105, 106955. https://doi.org/10.1016/j.yebeh.2020.106955

Lucchesi, W., Mizuno, K., Giese, K.P., 2011. Novel insights into CaMKII function and regulation during memory formation. Brain Research Bulletin 85, 2–8. https://doi.org/10.1016/j.brainresbull.2010.10.009

Marshall, G.F., 2022. Generation and validation of mouse models of neurodevelopmental disorders. https://doi.org/10.7488/ERA/2283

Marshall, G.F., Gonzalez-Sulser, A., Abbott, C.M., 2021. Modelling epilepsy in the mouse: challenges and solutions. Disease Models & Mechanisms 14, dmm047449. https://doi.org/10.1242/dmm.047449

McLachlan, F., 2020. Investigating the role of eukaryotic translation elongation factor eEF1A2 in autism, epilepsy and intellectual disability. https://doi.org/10.7488/ERA/75

McLachlan, F., Sires, A.M., Abbott, C.M., 2019. The role of translation elongation factor eEF1 subunits in neurodevelopmental disorders. Human Mutation 40, 131–141. https://doi.org/10.1002/humu.23677

Mendoza, M.B., Gutierrez, S., Ortiz, R., Moreno, D.F., Dermit, M., Dodel, M., Rebollo, E., Bosch, M., Mardakheh, F.K., Gallego, C., 2021. The elongation factor eEF1A2 controls translation and actin dynamics in dendritic spines. Sci. Signal. 14, eabf5594. https://doi.org/10.1126/scisignal.abf5594

Mills, A., Gago, F., 2021. On the Need to Tell Apart Fraternal Twins eEF1A1 and eEF1A2, and Their Respective Outfits. IJMS 22, 6973. https://doi.org/10.3390/ijms22136973

Mishra, A.K., Gangwani, L., Davis, R.J., Lambright, D.G., 2007. Structural insights into the interaction of the evolutionarily conserved ZPR1 domain tandem with eukaryotic EF1A, receptors, and SMN complexes. Proc. Natl. Acad. Sci. U.S.A. 104, 13930–13935. https://doi.org/10.1073/pnas.0704915104

Mohamoud, H.S., Ahmed, S., Jelani, M., Alrayes, N., Childs, K., Vadgama, N., Almramhi, M.M., Al-Aama, J.Y., Goodbourn, S., Nasir, J., 2018. A missense mutation in TRAPPC6A leads to build-up of the protein, in patients with a neurodevelopmental syndrome and dysmorphic features. Sci Rep 8, 2053. https://doi.org/10.1038/s41598-018-20658-w

Morello, N., Bianchi, F.T., Marmiroli, P., Tonoli, E., Rodriguez Menendez, V., Silengo, L., Cavaletti, G., Vercelli, A., Altruda, F., Tolosano, E., 2011. A Role for Hemopexin in Oligodendrocyte Differentiation and Myelin Formation. PLoS ONE 6, e20173. https://doi.org/10.1371/journal.pone.0020173

Mossink, B., Negwer, M., Schubert, D., Nadif Kasri, N., 2021. The emerging role of chromatin remodelers in neurodevelopmental disorders: a developmental perspective. Cell. Mol. Life Sci. 78, 2517–2563. https://doi.org/10.1007/s00018-020-03714-5

Nakajima, J., Okamoto, N., Tohyama, J., Kato, M., Arai, H., Funahashi, O., Tsurusaki, Y., Nakashima, M., Kawashima, H., Saitsu, H., Matsumoto, N., Miyake, N., 2015. *De novo EEF1A2* mutations in patients with characteristic facial features, intellectual disability, autistic behaviors and epilepsy: *De novo EEF1A2* mutations in patients. Clin Genet 87, 356–361. https://doi.org/10.1111/cge.12394

Nawaz, M.S., Giarda, E., Bedogni, F., La Montanara, P., Ricciardi, S., Ciceri, D., Alberio, T., Landsberger, N., Rusconi, L., Kilstrup-Nielsen, C., 2016. CDKL5 and Shootin1 Interact and Concur in Regulating Neuronal Polarization. PLoS ONE 11, e0148634. https://doi.org/10.1371/journal.pone.0148634

Negrutskii, B.S., Novosylna, O.V., Porubleva, L.V., Vislovukh, A.A., 2018. Control of the amount and functionality of the eEF1A1 and eEF1A2 isoforms in mammalian cells. Biopolym. Cell 34, 411–425. https://doi.org/10.7124/bc.00098C

Newbery, H.J., Loh, D.H., O'Donoghue, J.E., Tomlinson, V.A.L., Chau, Y.-Y., Boyd, J.A., Bergmann, J.H., Brownstein, D., Abbott, C.M., 2007. Translation Elongation Factor eEF1A2 Is Essential for Post-weaning Survival in Mice. Journal of Biological Chemistry 282, 28951–28959. https://doi.org/10.1074/jbc.M703962200

Novosylna, O., Doyle, A., Vlasenko, D., Murphy, M., Negrutskii, B., El'skaya, A., 2017. Comparison of the ability of mammalian eEF1A1 and its oncogenic variant eEF1A2 to interact with actin and calmodulin. Biol Chem 398, 113–124. https://doi.org/10.1515/hsz-2016-0172

Nussinov, R., Tsai, C.-J., Jang, H., 2022a. How can same-gene mutations promote both cancer and developmental disorders? Sci. Adv. 8, eabm2059. https://doi.org/10.1126/sciadv.abm2059

Nussinov, R., Tsai, C.-J., Jang, H., 2022b. Neurodevelopmental disorders, immunity, and cancer are connected. iScience 25, 104492. https://doi.org/10.1016/j.isci.2022.104492

Rossi, D., Barbosa, N.M., Galvão, F.C., Boldrin, P.E.G., Hershey, J.W.B., Zanelli, C.F., Fraser, C.S., Valentini, S.R., 2016. Evidence for a Negative Cooperativity between eIF5A and eEF2 on Binding to the Ribosome. PLoS ONE 11, e0154205. https://doi.org/10.1371/journal.pone.0154205

Ruest, L.-B., Marcotte, R., Wang, E., 2002. Peptide Elongation Factor eEF1A-2/S1 Expression in Cultured Differentiated Myotubes and Its Protective Effect against Caspase- 3-mediated Apoptosis. Journal of Biological Chemistry 277, 5418–5425. https://doi.org/10.1074/jbc.M110685200

Safran, M., Rosen, N., Twik, M., BarShir, R., Stein, T.I., Dahary, D., Fishilevich, S., Lancet, D., 2021. The GeneCards Suite, in: Abugessaisa, I., Kasukawa, T. (Eds.), Practical Guide to Life Science Databases. Springer Nature Singapore, Singapore, pp. 27–56. https://doi.org/10.1007/978-981-16-5812-9_2

Samocha, K.E., Robinson, E.B., Sanders, S.J., Stevens, C., Sabo, A., McGrath, L.M., Kosmicki, J.A., Rehnström, K., Mallick, S., Kirby, A., Wall, D.P., MacArthur, D.G., Gabriel, S.B., DePristo, M., Purcell, S.M., Palotie, A., Boerwinkle, E., Buxbaum, J.D., Cook, E.H., Gibbs, R.A., Schellenberg, G.D., Sutcliffe, J.S., Devlin, B., Roeder, K., Neale, B.M., Daly, M.J., 2014. A framework for the interpretation of de novo mutation in human disease. Nat Genet 46, 944–950. https://doi.org/10.1038/ng.3050

Sarmiere, P.D., Bamburg, J.R., 2004. Regulation of the neuronal actin cytoskeleton by ADF/cofilin. J. Neurobiol. 58, 103–117. https://doi.org/10.1002/neu.10267

Sasikumar, A.N., Perez, W.B., Kinzy, T.G., 2012. The many roles of the eukaryotic elongation factor 1 complex: The many roles of the eukaryotic elongation factor 1 complex. WIREs RNA 3, 543–555. https://doi.org/10.1002/wrna.1118

Sedgwick, P., 2015. A comparison of parametric and non-parametric statistical tests. BMJ 350, h2053–h2053. https://doi.org/10.1136/bmj.h2053

Soares, D.C., Abbott, C.M., 2013. Highly homologous eEF1A1 and eEF1A2 exhibit differential post-translationalmodification with significant enrichment around localised sites of sequence variation. Biol Direct 8, 29. https://doi.org/10.1186/1745-6150-8-29

Soares, D.C., Barlow, P.N., Newbery, H.J., Porteous, D.J., Abbott, C.M., 2009. Structural Models of Human eEF1A1 and eEF1A2 Reveal Two Distinct Surface Clusters of Sequence Variation and Potential Differences in Phosphorylation. PLoS ONE 4, e6315. https://doi.org/10.1371/journal.pone.0006315

Soman, A., Asha Nair, S., 2022. Unfolding the cascade of SERPINA3: Inflammation to cancer. Biochimica et Biophysica Acta (BBA) - Reviews on Cancer 1877, 188760. https://doi.org/10.1016/j.bbcan.2022.188760

Steen, H., Jebanathirajah, J.A., Rush, J., Morrice, N., Kirschner, M.W., 2006. Phosphorylation Analysis by Mass Spectrometry. Molecular & Cellular Proteomics 5, 172–181. https://doi.org/10.1074/mcp.M500135-MCP200

Su, L.-K., Qi, Y., 2001. Characterization of Human MAPRE Genes and Their Proteins. Genomics 71, 142–149. https://doi.org/10.1006/geno.2000.6428

Sutton, M.A., Taylor, A.M., Ito, H.T., Pham, A., Schuman, E.M., 2007. Postsynaptic Decoding of Neural Activity: eEF2 as a Biochemical Sensor Coupling Miniature Synaptic Transmission to Local Protein Synthesis. Neuron 55, 648–661. https://doi.org/10.1016/j.neuron.2007.07.030

Szklarczyk, D., Franceschini, A., Kuhn, M., Simonovic, M., Roth, A., Minguez, P., Doerks, T., Stark, M., Muller, J., Bork, P., Jensen, L.J., Mering, C. v., 2011. The STRING database in 2011: functional interaction networks of proteins, globally integrated and scored. Nucleic Acids Research 39, D561–D568. https://doi.org/10.1093/nar/gkq973

Szklarczyk, D., Gable, A.L., Nastou, K.C., Lyon, D., Kirsch, R., Pyysalo, S., Doncheva, N.T., Legeay, M., Fang, T., Bork, P., Jensen, L.J., von Mering, C., 2021. The STRING database in 2021: customizable protein–protein networks, and functional characterization of user-uploaded gene/measurement sets. Nucleic Acids Research 49, D605–D612. https://doi.org/10.1093/nar/gkaa1074

Taylor, S.C., Berkelman, T., Yadav, G., Hammond, M., 2013. A Defined Methodology for Reliable Quantification of Western Blot Data. Mol Biotechnol 55, 217–226. https://doi.org/10.1007/s12033-013-9672-6

Thomas, P., Smart, T.G., 2005. HEK293 cell line: A vehicle for the expression of recombinant proteins. Journal of Pharmacological and Toxicological Methods 51, 187–200. https://doi.org/10.1016/j.vascn.2004.08.014

Thornton, S., Anand, N., Purcell, D., Lee, J., 2003. Not just for housekeeping: protein initiation and elongation factors in cell growth and tumorigenesis. Journal of Molecular Medicine 81, 536–548. https://doi.org/10.1007/s00109-003-0461-8

Tomlinson, V.A., Newbery, H.J., Wray, N.R., Jackson, J., Larionov, A., Miller, W.R., Dixon, J.M., Abbott, C.M., 2005. Translation elongation factor eEF1A2 is a potential oncoprotein that is overexpressed in two-thirds of breast tumours. BMC Cancer 5, 113. https://doi.org/10.1186/1471-2407-5-113

Trosiuk, T.V., Shalak, V.F., Szczepanowski, R.H., Negrutskii, B.S., El'skaya, A.V., 2016. A non-catalytic N-terminal domain negatively influences the nucleotide exchange activity of translation elongation factor 1Bα. FEBS J 283, 484–497. https://doi.org/10.1111/febs.13599

Wang, Y., Wang, Q., Huang, H., Huang, W., Chen, Y., McGarvey, P.B., Wu, C.H., Arighi, C.N., on behalf of the UniProt Consortium, 2021. A crowdsourcing open platform for literature curation in UniProt. PLoS Biol 19, e3001464. https://doi.org/10.1371/journal.pbio.3001464

Woo, J.-A.A., Liu, T., Fang, C.C., Cazzaro, S., Kee, T., LePochat, P., Yrigoin, K., Penn, C., Zhao, X., Wang, X., Liggett, S.B., Kang, D.E., 2019. Activated cofilin exacerbates tau

pathology by impairing tau-mediated microtubule dynamics. Commun Biol 2, 112. https://doi.org/10.1038/s42003-019-0359-9

Yen, H.-C.S., Xu, Q., Chou, D.M., Zhao, Z., Elledge, S.J., 2008. Global Protein Stability Profiling in Mammalian Cells. Science 322, 918–923. https://doi.org/10.1126/science.1160489

Zanelli, C.F., Maragno, A.L.C., Gregio, A.P.B., Komili, S., Pandolfi, J.R., Mestriner, C.A., Lustri, W.R., Valentini, S.R., 2006. eIF5A binds to translational machinery components and affects translation in yeast. Biochemical and Biophysical Research Communications 348, 1358–1366. https://doi.org/10.1016/j.bbrc.2006.07.195

Zhou, H., Meng, J., Malerba, A., Catapano, F., Sintusek, P., Jarmin, S., Feng, L., Lu-Nguyen, N., Sun, L., Mariot, V., Dumonceaux, J., Morgan, J.E., Gissen, P., Dickson, G., Muntoni, F., 2020. Myostatin inhibition in combination with antisense oligonucleotide therapy improves outcomes in spinal muscular atrophy. Journal of Cachexia, Sarcopenia and Muscle 11, 768–782. https://doi.org/10.1002/jcsm.12542

Zhu, W., Li, Z., Xiong, L., Yu, X., Chen, X., Lin, Q., 2017. FKBP3 Promotes Proliferation of Non-Small Cell Lung Cancer Cells through Regulating Sp1/HDAC2/p27. Theranostics 7, 3078–3089. https://doi.org/10.7150/thno.18067

Zhu, W., Smith, J.W., Huang, C.-M., 2010. Mass Spectrometry-Based Label-Free Quantitative Proteomics. Journal of Biomedicine and Biotechnology 2010, 1–6. https://doi.org/10.1155/2010/840518

Zilka, N., Korenova, M., Novak, M., 2009. Misfolded tau protein and disease modifying pathways in transgenic rodent models of human tauopathies. Acta Neuropathol 118, 71–86. https://doi.org/10.1007/s00401-009-0499-y